EXPERIMENTAL AND NUMERICAL INVESTIGATIONS ON WOOD ACCUMULATION AT BRIDGE PIERS WITH DIFFERENT SHAPES

Dissertation

submitted to and approved by the

Department of Architecture, Civil Engineering and Environmental Sciences

University of Braunschweig – Institute of Technology

and the

Department of Civil and Environmental Engineering

University of Florence

in candidacy for the degree of a

Dottore di Ricerca in Civil and Environmental Engineering

by

Pina Nicoletta De Cicco

born 28/11/1985

from Foggia, Italy

Submitted on	28.02.2017
Oral examination on	09.05.2017
Professorial advisors	Prof. Luca Solari
	Prof. Hans Matthias Schöniger

2017

Experimental and numerical investigations on wood accumulation at bridge piers with different shapes

De Cicco Pina Nicoletta (Ph.D. Candidate)

Tutors:
Prof. Luca Solari
Prof. Hans Matthias Schöniger

Co-tutors:
Prof. Enio Paris
Ph.D. Virginia Ruiz-Villanueva

Abstract

The awareness of in-channel wood transport in rivers changed significantly with the historical contest. In 18th century logs were transported from forests to sawmills and pulp mills by the natural streamflow of the waterways. Later the waterways were substituted with the railroads and the in-channel wood became only a natural river component. In last decades, the increasing abandonment of rural lands has caused significant growth in the total volume of available wood to be transported by the flow, especially during flood events. In-channel wood has become an additional component in potential hazard evaluation, in particular when it leads to the obstruction of hydraulic structures, e.g. the bridges.

Wood accumulation at bridges exerts additional forces to the structures and aggravates local scouring around piers, which may result to bridge failure. Moreover, it may considerably reduce the flow opening causing higher flow levels and inundation of nearby areas.

On the other hand, increasing awareness of the importance of the ecological role of wood in rivers calls for a compromise between the preservation of river ecosystems and in-channel wood management strategies for the prevention of wood-related hazards.

The present PhD research aims to enhance the knowledge on the process of interaction between wood and bridge piers. The two main objectives were first to find the wood accumulation probability (here called "blockage probability") as a function of the bridge pier geometry (with a focus on non-standard pier shapes typical of historical cities), hydraulic conditions of the approaching flow, and wood transport regime, second to assess the capability of 2D and 3D numerical models in reproducing the interaction between wood and structures (i.e. the bridge pier). The combined experimental and numerical research approach is used.

The thesis first presents a review of recent advances in research on wood accumulations at bridges that highlights main gaps in knowledge. Secondly, the formulation of the blockage probability function based on the analysis of the main variables that controls wood accumulation at a single-pier. Lastly, the experimental and numerical results are analysed and discussed.

The experiments were done at the hydraulic laboratory of the Department of Civil and Environmental Engineering of the University of Firenze aimed at investigating the

most critical conditions for wood accumulation at a single-pier for a combination of different pier shapes, wood transport regimes and Froude numbers (in sub-critical conditions). The numerical simulations were carried out both with 2D and 3D models. In particular, the 2D model was aimed at reproducing the experimental findings and to assess its strengths and weaknesses. The 3D model was applied to investigate the 3D character of the interaction between wood and bridge pier and at reproducing the 3D secondary flow field.

The results showed that blockage probability at the flatter pier shape is three times greater than the triangular shaped piers, in congested wood transport regime (logs move as a single mass and are unable to move independently of each other) and at high Froude number (in this case Fr=0.5). In case of Ogival pier, zero blockage probability was found for both cases of Froude numbers. Potential flow analysis indicated that the lower curvature of the streamlines at the rounded pier favours the log sliding the pier.

The comparison between experimental and 2D numerical simulations revealed strengths and weaknesses. Despite the capability of the 2D model in reproducing the log transport the discrepancy between experimental and the 2D numerical results showed the two-dimensional numerical model cannot correctly capture the complicated log travel path and thus the log blockage probability at the pier. The problem is related to inability of modelling the important secondary flows and the log-pier interactions. In the straight rectangular flume, in addition to the Reynolds number, stronger secondary currents occur due to the different roughness between the side-walls and the bed. The secondary flow strength is greater towards the walls or the centreline according to the ratio between the channel width and water depth. This means that the logs may move differently in the cross section affecting the probability to touch and stop at the central pier. Further aspects to be improved are the elastic collision between logs, the smooth surface of logs and the constant drag coefficient, the superposition of logs.

The 3D confirmed the action of secondary currents on log motion. Furthermore, the 3D modelling allowed to reproduce the 3D character of the wood-pier interaction process as the logs that move along the vertical upstream face of the pier, the non-elastic collision between logs and between logs and the pier, and the skin friction of logs.

Finally, one of the main novelties of the current research in the estimation of blockage probability represented by the definition of a new pier hydraulic-shape coefficient (c_{pier}) that takes into account the shape of the pier and the 2D velocity flow field upstream of the pier. The flatter is the pier shape, the higher is c_{pier}. The probability of logs blockage at the pier increases with increasing c_{pier}. These results suggest that the pier shape has an important effect on the flow field upstream of the pier and thus on the log motion and its blockage.

The thesis was also successful in defining the joint blockage probability at a bridge pier for the prevailing variables used in the study. The concept should find applications both in research and practical situation. It is highly desirable and useful to state the total probability of log blockage at a bridge pier given a set of flow, log, and pier variables.

To investigate log transport in rivers the thesis suggests a twostep approach. Step one is the use of a relevant 2D model as a good starting point that should give a general understanding of log transport combination. The main advantages are the robustness and the limited required CPU power. In the second step, a 3D log transport model could be applied to study the specific features and to explore the deviations between the two models. The latter results could sever for calibration of selected the 2D. The models used in the present study (Wood-*Iber & Flow3D*) showed promising results within the constraints of the model applicabilities

Acknowledgements

v

Summary

List of Figures

List of Tables

List of Symbols

A_{LFV}	Low flow velocity area upstream of the pier	m^2
A_{sub}	Submerged area of the log	m^2
a_{log}	Log acceleration	$m \cdot s^{-2}$
B	Blockage function	-
Bl	Blockage ratio	-
C	Transport inhibition parameter	-
C_d	Drag coefficient	-
c_{pier}	Pier hydraulic shape coefficient	-
D	Pier diameter	m
D_d	Debris raft length parallel to the flow	m
D_e	Effective pier diameter	m
D_{log}	Log diameter	m
d_s	Scour depth at pier	m
d_{sub}	Submerged diameter of the log	m
e	Restitution coefficient	-
EA	Effective Accumulation	-
F_d	Drag force acting on a log	$Kg \cdot m \cdot s^{-2}$
F_g	Gravitational force acting on a log	$Kg \cdot m \cdot s^{-2}$
F_f	Frictional force acting on a log	$Kg \cdot m \cdot s^{-2}$
Fr	Froude number	-
F_n	Normal force	$Kg \cdot m \cdot s^{-2}$
g	Acceleration due to gravity	$m \cdot s^{-2}$
T_d	Debris raft depth	m
h	Water depth	m
L_{EFF}	The width of the pier bounded by the arc of the isovel $i = 0.6 \cdot U_\infty$	m
L_{log}	Log length	m
L_p	Pier length	m
m_i	Mass of log i	Kg
PA	Potential Accumulation	-
Q_{flow}	Flow discharge	$m^3 \cdot s^{-1}$
Q_{log}	Volumetric log input rate	$m^3 \cdot s^{-1}$
Re_b	Reynolds number for bed	-
Re_w	Reynolds number for walls	-
r_b	Hydraulic radius of the bed	m
r_w	Hydraulic radius of the walls	m
T_d	Thickness of wood accumulation	m
U	Flow velocity	$m \cdot s^{-1}$
U_{lim}	Threshold velocity for wood incipient motion	$m \cdot s^{-1}$
U_{log}	Log velocity	$m \cdot s^{-1}$
U_r	Relative flow velocity	$m \cdot s^{-1}$
U_∞	Undisturbed free stream velocity	$m \cdot s^{-1}$
$u^{1,2}$	Flow velocity at log ends	$m \cdot s^{-1}$

u^{cm}	Flow velocity at the log centre	m· s^{-1}
u^{cm}_{log}	Log centre velocity in flow direction	m· s^{-1}
$x^{1,2}_{log}$	Position of log extremities	m
x^{cm}_{log}	Position of log centre (vector)	m
w	Channel width	m
W_{eff}	Effective weight force of the log	Kg· m· s^{-2}
W_{log}	Weight force of the log	Kg· m· s^{-2}
w_p	Pier width	m

Greek letters

α	Angle of the bed channel	°
θ	Inclination of the log relative to the flow direction	°
μ	Dynamic viscosity of the fluid	Kg ·m^{-1}·s^{-1}
μ_{bed}	Coefficient of the friction between log and the river bed	-
ρ	Density of the fluid	Kg· m^{-3}
ρ_{log}	Density of wood	Kg· m^{-3}
σ	Incidence angle between the log and the boundaries	rad
σ_{cr}	Threshold value of incidence angle between the log the and boundaries	rad
τ_0	Bed shear stress	Kg· m^{-1}·s^{-2}
τ_c	Critical bed shear stress	Kg· m^{-1}·s^{-2}
$\tau_{wood,i}$	Shear stress due to log presence	Kg· m^{-1}·s^{-2}
Φ	Velocity potential function	m^2·s
ψ	Stream function	m^2·s
ω	Vorticity	s^{-1}

List of Abbreviations

C	Congested wood transport
CFD	Computational Fluid Dynamic
DOF	Degrees of freedom
EA	Effective Accumulation
FAVOR^{TM}	Fractional Area/Volume Obstacle Representation
FVM	Finite Volume Method
GMO	General Moving Object
LW	Large Wood
MW	Medium Wood
PA	Potential Accumulation
RANS	Reynolds Averaged Navier-Stokes
RNG	Re-Normalization Group method
SW	Small Wood
U	Uncongested wood transport

_____

1 Introduction

1.1 Motivation

The presence of wood in river ecosystem provides habitat diversity and food for invertebrates, fishes, and other vertebrates (Benke and Wallace, 2003; Harmon et al., 1986). In particular, wood accumulations create storage areas for organic material and this together with the decomposition of wood itself, provide a rich nutrient source for aquatic species (see e.g. Gurnell et al., 2002).

However, the natural afforestation in most of the European catchments due to the abandonment of agricultural lands occurred in the last decades, has most likely determined a rising amount of in-channel wood in rivers (e.g. Comiti, 2012).

The perception of the presence of wood in river ecosystems have changed significantly during years. With the Industrial Revolution in the 18th century and the development of sawmills and pulp mills in the 19th century in United States, a new transportation method, called "log driving", developed to transport wood from forests to industries. In Europe, the timber transport in rivers is much older: the Romans started to build a system of streams and rivers for logs transportation, from the second century BC (Comiti, 2012).

The trunks 5 meters long were transported by the natural streamflow of the waterways by the "log drivers". The latter were responsible for the dislocation of the floating logs to avoid the formation of potential wood jams with dangerous consequences on the rising water levels. Any straight and uniform stream with no bridges and no piers was considered a floatable stream for logs. In other cases, the river morphology was altered and "improved" (e.g. channel widening, scouring) to favour log passing, with negative consequences on the natural river bed equilibrium and the aquatic ecosystem (Rosholt, 1980). With the development of railroads, in the mid-19th century, the waterways came increasingly substituted and the presence of wood in rivers occurs only as a natural process.

Despite the importance of large wood in fluvial ecosystems, the transport of large quantities of wood during floods may imply potential hazards for humans and infrastructures. Figure 1.1 shows photographs of bridge clogging and induced failure in Italy, Spain, US and Japan.

Wood accumulation at bridge piers has been identified as one of the most frequent causes of bridge failures in the Unites States (Diehl, 1997), and many damages to infrastructures were observed during several recent flood events in Europe (e.g. the Magra river basin in north-western Italy and the Emme catchment in Switzerland; Comiti et al., 2016).

In case of historical bridges or anyhow where no modifications to decrease or even eliminate their potential wood trapping role are allowed, catchment-scale preventive measures are the only alternatives. Thus, the prevention of hazards related to in-channel wood and in-channel wood management strategies become not only fundamental, but also more complex. In some cases, the installation of retention structures can provide a good compromise, as it preserves the river ecosystems upstream of the structures and reduces bridge clogging and related hazards.

Wood dynamics have been extensively investigated in rivers of different size and morphology, as well as the effects of wood accumulation at bridge structures on pier scour. On the other hand, there is still the need for a better understanding of the effects and interactions of in-stream wood logs and bridges.

In recent years, an increasing number of researchers have focused on the blockage probability of logs at bridges and on their effects on the backwater rise. In most cases, flume experiments are used to study the various aspects of log transport.

The current research aims to contribute to progress the knowledge in wood-pier interaction as specified in the research questions, aims and methodology described below.

A B

C D

E
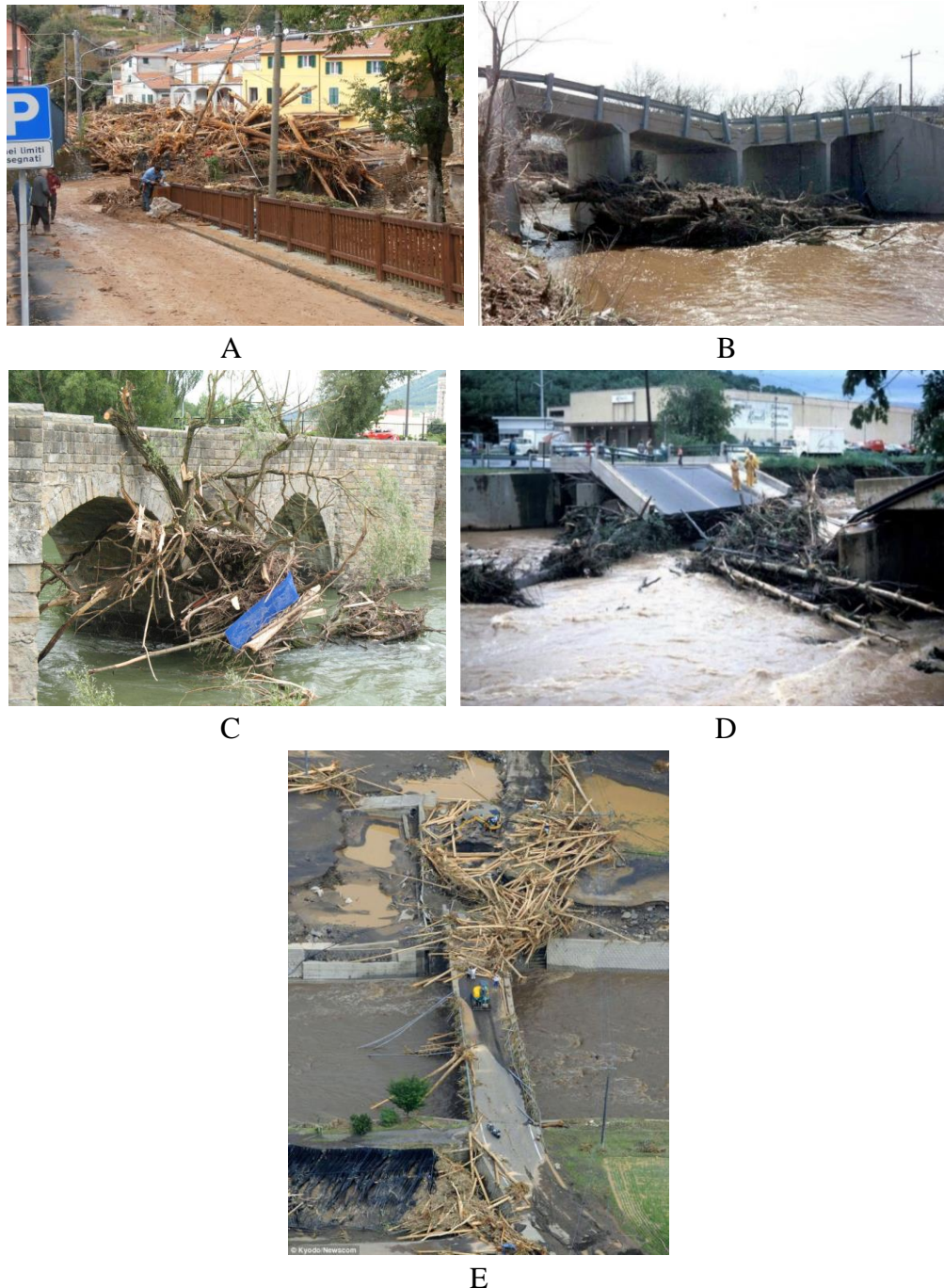
Figure 1.1 Cases of wood accumulation at bridges during a flood: A) La Spezia, Italy, 2011 (picture from Comiti F.); B) bridge failure by wood Oklahoma, USA (picture from Bradley et al., 2005); C) Pamplona, Spain, 2013 (picture courtesy of Virginia Ruiz-Villanueva); D) bridge failure by wood, New York, USA (picture from Bradley et al., 2005); E) Kyushu, Japan, 2012.

_____

1.2 Objectives and methodology

The current research has two main objectives: i) to analyse the blockage probability of wood accumulation at bridge piers and how it is affected by pier shape, wood transport regime, flow velocity and water depth i.e., Froude number; ii) to assess the capability of 2D and 3D numerical models in reproducing the interaction between wood and structures (as the bridge pier). The more specific objectives are:

1. to find the most critical conditions (the ratio between wood discharge and flow discharge Q_{log}/Q_{flow}, the ratio between the log length and pier width L_{log}/w_p, and the Froude number Fr) in the case of different pier shapes for blockage probability;
2. to analyse the most critical pier shapes for wood accumulation in subcritical flow conditions (Fr<1), and thus, to define a pier hydraulic-shape coefficient c_{pier} that characterizes each pier shape hydraulically and geometrically in order to find the relation between the blockage probability and the pier shape;
3. *to reproduce the experimental tests with the 2D numerical model (Iber-Wood; Ruiz-Villanueva et al., 2014a) and to highlight the strengths and weaknesses of the model;*
4. *to reproduce the log transport and the log-pier interaction with the 3D numerical model Flow 3D (Flow Science, Inc., 2014) and to analyse the 3D log paths and the relation between drag coefficient and log orientation for semi-submerged logs.*

In order to reach the goals described before, three different methodologies are used as detailed below.

1) Experimental analysis

Flume experiments on wood accumulation at different bridge piers having different shapes were carried out. The wood transport is reproduced in a straight rectangular flume under steady state flow conditions and fixed flume bed. Cylindrical dowels with no branches and no roots are used to reproduce wood logs. The main objective of the flume experiments is to find the most critical hydraulic and geometric conditions $(\frac{L_{log}}{w_p}; \frac{Q_{log}}{Q_{flow}}; Fr)$ for wood blockage at the bridge pier.

2) The 2D numerical modelling

The second step concerns the modelling of the experimental tests with a 2D hydrodynamic model that implements the log motion and the interaction between the logs and between the logs and the boundaries.

3) The 3D numerical modelling

The last step is the 3D modelling of wood-pier that can fully account for 3D interaction of the flow with the logs and the effects of the increasing number of logs on the blockage and the log path and orientation.

The main objectives (research questions) aims and the methodology are illustrated in Figure 1.2 and summarized in *Table 1.1*.

DEFINITION OF THE BLOCKAGE PROBABILITY
AND THE MAIN INFLUENCING FACTORS

EXPERIMENTAL AND 2-D NUMERICAL
INVESTIGATIONS

3-D NUMERICAL
INVESTIGATION ON THE 3-D
CHARACTER OF THE WOOD-
PIER INTERACTION PROCESS

$$B = f\left(\frac{Q_{log}}{Q_{flow}}; \frac{L_{log}}{w_p}; Fr; c_{pier}\right)$$

NEW
COEFFICIENT

Identification of blockage probabilities

$$B_1 = f_1\left(\frac{Q_{log}}{Q_{flow}}\right)$$

$$B_2 = f_2\left(\frac{L_{log}}{w_p}\right)$$

$$B_3 = f_3\left(Fr\right)$$

Identification of
blockage probability
and pier shape

$$B_4 = f_4(c_{pier})$$

3D character of
the wood-pier
interaction

2D

3D

FLUME EXPERIMENTS   →   **NUMERICAL MODELLING**

Figure 1.2 Graphical summary of the main goals and the methodology of the current research.

Table 1.1 Scheme of the main research questions, aims and the methodology of the current research.

Research question	Aim	Methodology

▪ How does
  - Q_{log}/Q_{flow}
  - L_{log}/w_p
  - Fr
  influence the blockage probability
  at bridge pier by wood?
	To find the most critical pier shapes and conditions for wood accumulation at the bridge pier.	Flume experiments with different pier shape, wood transport regimes, Froude numbers.

▪ Which is the relationship between the blockage probability and the pier hydraulic-shape coefficient c_{pier}? ▪ Which are the strengths and weakness of the 2D numerical model in reproducing the interaction wood-pier?	To test the 2D model for wood-pier interaction. To find the relation between the blockage probability and the pier shape. To propose improvements and modification of the 2D numerical model.	Simulation of flume experiments with the 2D hydrodynamic model *Iber-Wood.*
▪ How does the 3D character of the flow affect the log movement upstream of the pier and then the interaction with the structure? ▪ How does the drag coefficient change with log orientation with respect to the flow and in semi-submerged conditions?	To simulate the interaction wood-pier with a 3D numerical model to highlight the effects of the 3D component on the log movement close to the pier	Simulation of one test case from flume experiments with the 3D numerical model Flow 3D

1.3   Thesis structure

The thesis is organized in seven main Chapters detailed below and schematized in Figure 1.3:

- literature review (Chapter 2);
- theoretical background (Chapter 3);
- methodological approach (Chapter 4);
- experimental and numerical results (Chapter 5)
- discussion and comparison of the results (Chapter 6);
- conclusions (Chapters 7);
- future works (Chapters 8).

Chapter 2 is a review of the published work concerning the interactions between in-channel wood and bridges. It provides a comprehensive summary of the recent advances describing and quantifying:

(i)   the types and shapes of wood accumulations at bridges;
(ii)   the main factors influencing wood accumulation (e.g. channel width, logs length, wood amount, wood transport regime…);
(iii)   the physical effects of wood accumulation at bridges (influence on pier scour and upstream water levels…);

(iv)   the different approaches to analyse wood-bridge interactions (i.e., flume experiments and numerical modelling).

Results from different studies and geographical regions are presented. Finally, we also highlight areas of research importance and their likely future trajectories (Paragraph 2.5).

The Chapter 3 provides the theoretical basis for understanding the mechanisms and influential parameters for the probability of wood accumulation at a single pier.

The Chapter 4 shows the methodology and approach used to reach the aim of the current research. The experimental and numerical set-up, as well as the boundary conditions and the variables selected are described for both 2D and 3D numerical modelling.

In the Chapter 5 the main experimental and numerical results are presented while the discussion of the study assumptions and limitations is presented in Chapter 6.

The last two chapters (7-8) contain the main conclusions and the future challenges.
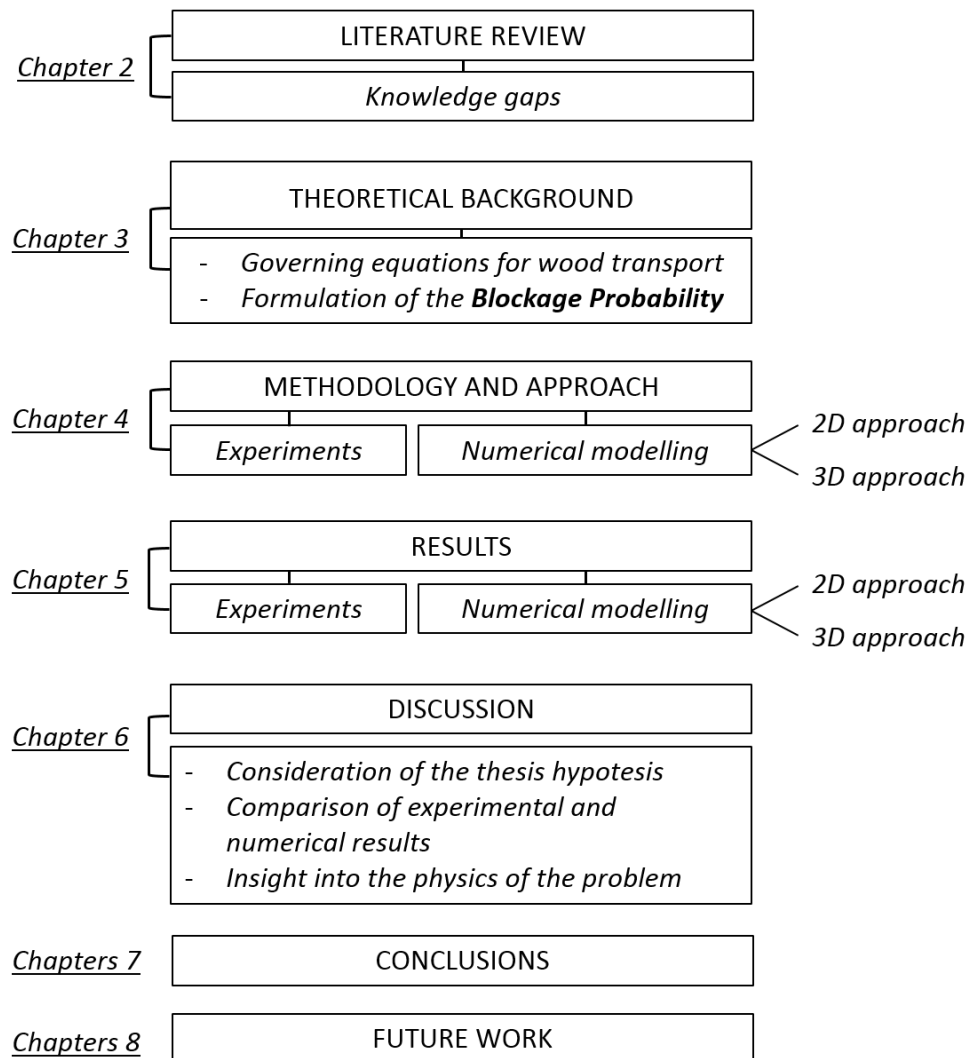
Figure 1.3 The thesis outline.

_____

2 Literature review

Over the last decades, the transport and accumulation of in-channel wood has received increasing interest among river scientists recognizing its significance as a functional component of fluvial ecosystems (Gurnell et al., 2002; Gurnell 2013; Gurnell et al., 2012; Wohl et al., 2010; Wohl, 2011, 2013; Le Lay et al., 2013; Solari et al., 2015; Ruiz-Villanueva et al., 2016b). Nevertheless, its perception - at least in Europe and in other densely urbanized countries - is mostly linked to flood hazard or unsafe recreational use of rivers, which then commonly results in indiscriminate wood removal from watercourses (Mutz et al., 2006; Piegay et al., 2005; Chin et al., 2008 and 2012; Wohl, 2014).

In-channel wood (also called large woody debris, but preferably referred to as wood or instream wood; Gregory et al., 2003) is usually referred to as logs longer than 1 m and with a minimum diameter of 0.1 m falling into the stream and that can be transported by a flow (Wohl et al., 2010).

In-channel wood enters rivers by a multitude of different recruitment processes along the fluvial corridor or from the hillslopes (Benda and Sias, 2003). These processes vary based on regional climatic, lithological, geomorphological and hydrological characteristics, such as the duration and frequency of precipitation (Comiti et al., 2006; Mazzorana, 2009; Seo and Nakamura, 2009; Lucía et al., 2014; Ruiz-Villanueva et al., 2014c; Fremier et al., 2014; Seo et al., 2015). In small basins of temperate climate regions, where intense, but short-lived rainstorms are frequent in summer and may cause flash floods and debris flow, thereby acting as the main recruitment processes (Comiti et al., 2006). In coastal areas, by contrast, the main factor controlling wood input is wind (Benda and Sias, 2003).

The other source is through bank erosion, landslides, and other types of mass movements may occur in most of the regions and basins (Benda, 2003; Piégay, 1993). Bank erosion is the main source of in-channel wood during floods (for unconfined rivers), but recruitment here depends on the erodibility of banks, flood frequency, and stand density index (Benda and Sias, 2003). Recruited trees can be transported by the flow over long distances and until they are deposited in a wood jam or trapped by banks, natural obstacles (i.e., boulders) or hydraulic structures (e.g., dams, bridges) (Wallerstein and Thorne, 1997; Bradley et al., 2005; Abbe and Montgomery, 1996; Jochner et al., 2015).

2.1   Wood accumulation at bridges

2.1.1   *Wood jam formation*

Wood accumulation formation initiates by falling tree into the river and provided its two extremities, or both, are stuck into the riverbanks or into the bed, such that it can trap, smaller logs floating from upstream into the obstacle (Wallerstein and Thorne, 1997; Bradley et al., 2005). Alternatively, wood jams can also occur in case of large logs (i.e. larger than channel width) break into smaller pieces, thereby entrapping the upcoming logs (Nakamura and Swanson, 1993). The element starting wood jam formation is known as "key member", the smaller pieces are known as "racked members", and the pieces that occupy the interstitial areas are generally called "loose members" (Abbe and Montgomery, 2003; Curran, 2010; Wallerstein and Thorne, 1997).

Some falling trees are transported by the flow until they are hindered by a hydraulic structure such as a bridge pier or deck. They then become "key members" for the floating

_____

pieces of wood that are coming from upstream. One of the first and most relevant contributions to the knowledge of wood accumulation at bridges was presented by Diehl (1997), which was based on work done at the United States Geological Survey (USGS) from 1992 to 1995, in cooperation with the Federal Highway Administration. This study included a review of published literature on in-channel wood, analysis of data from 2,577 reported wood accumulations at bridges, and field investigations of 144 wood jams. The result of this pioneering work was a useful collection of guidelines and flow charts to determine the potential of wood accumulation at bridges. Based on the collected data, Diehl (1997) identified different areas along a stream with high, medium, and low potential for in-channel wood delivery and transport which was then combined with additional information on bridge characteristics (i.e., bridge opening, pier shape and size) to finally determine the likelihood of blockage at bridges.

Other important contributions are the studies by Lyn et al. (2003, 2007) and the Hydraulic Engineering Circular (HEC 9) published by Bradley et al. (2005) on wood control structures and countermeasures. The experimental analysis on wood accumulation at a square pier with rounded nose and the field monitoring at bridges with video recording by Lyn et al., (2003, 2007) proved that (i) smaller velocity and flow depth favour the accumulation of wood at bridges (in case of rounded pier shape); (ii) in-channel wood delivery tends to be more like a succession of impulses than a continuous release; and that (iii) the in-channel wood is more prone to stop at the pier located within the channel than close to the banks.

2.1.2 *Type, shape and geometry of wood accumulation at bridges*

Depending on log length and upstream channel width, Diehl (1997) identified two different mechanisms of wood accumulations at bridge piers, namely the *single-pier accumulation* and the *span-blockage accumulation* (see Figure 2.1, b). The former occurs when the effective opening between bridge piers (i.e., the distance between piers perpendicular to the flow direction that passes through the nose of each pier (see Figure 2.1, a) is greater than the maximum length of logs. In this case, wood accumulations usually start as soon as woods hit the pier perpendicularly to the flow direction. In the latter case, the effective opening between bridge piers is less than the maximum length of logs and the wood is entrapped between two piers (*pier-to-pier accumulation*), or between a pier and a bank, or other obstacles (e.g. an existing bar).

Depending on the number and dimensions of wood that accumulates at the bridge, Lagasse et al., (2010) made a distinction between (i) single-log accumulation formed by one or two logs entrapped at a bridge pier or between spans; (ii) multiple-log accumulation characterized by connected logs that form a jam or raft without fragments or sediments in the interstices; as well as (iii) the mass of logs accumulation formed by connected logs and small logs with sediments and detritus filling interstitial voids.

Floating logs tend to accumulate at the bridge pier at the water surface level. If water level increases, upcoming logs will pile up on existing wood jams (partially submerged accumulation), whereas if the water depth decreases, the accumulated logs will slide down to the bottom of the pier. If logs are not removed, the upcoming flood can fully submerge the accumulation (Diehl, 1997; Lagasse et al., 2010).

Lagasse et al. (2010) collected a great number field data, both photographs and field surveys, from the South Platte River in Colorado to identify typical geometries of wood accumulation at bridges. They noted that the most common forms of single-pier accumulation are the triangular plan with a conical profile and the rectangular plan with a rectangular profile. The triangular planform may originate as an inverted conical profile

_____

when the wood accumulation slides down after the first flood and remains against the pier, flood after flood. The types of wood accumulation are reported in Table 2.1.
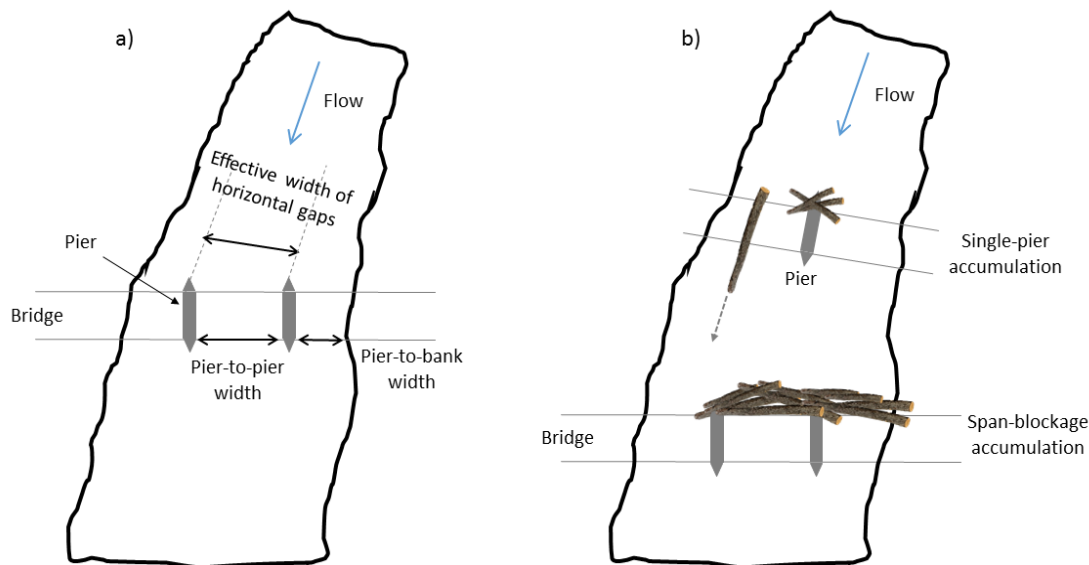
Figure 2.1 Plan view scheme of the effective opening between bridge piers (a) and of the types of wood accumulation at bridges (b).

Table 2.1 Classification of in-channel wood accumulation at bridges.

Classification criteria	Type of wood accumulation	Key references
Log length and bridge opening	- Single-pier accumulation - Span-blockage accumulation	*Diehl* [1997];
Amount of logs	- Single-log - Multiple-logs - Mass of logs	*Lagasse et al.* [2010];
Water level	- Partially submerged - Fully submerged	*Diehl* [1997]; *Lagasse et al.* [2010];
Wood accumulation planform	- Triangular - Rectangular	*Lagasse et al.* [2010];
Wood accumulation profile geometry	- Rectangular - Conical - Inverted-conical	*Lagasse et al.* [2010];

In the case of pier to pier accumulation, the "key-member" of the jam stops perpendicular to the flow direction, as well as upcoming logs. Due to the lateral hydraulic forces, the final shape will be in the form of an accumulation with a curved upstream tip.

_____

The dimensions of the wood accumulation depends on the floods frequency, the amount of wood and the frequency or absence of wood removal, and in-channel wood management activities (Diehl, 1997).

2.2   Factors influencing wood accumulation at bridges

The probability of wood entrapment at bridge piers or potential bridge clogging depends on many factors, such as (i) the size and volume of the approaching wood, (ii) the transport regime that can be uncongested or congested, as defined by Braudrick et al. (1996), (ii) the approaching flow characteristics (i.e., flow depth and Froude number), and (iii) the geometry of the bridge (see Figure 2.2).
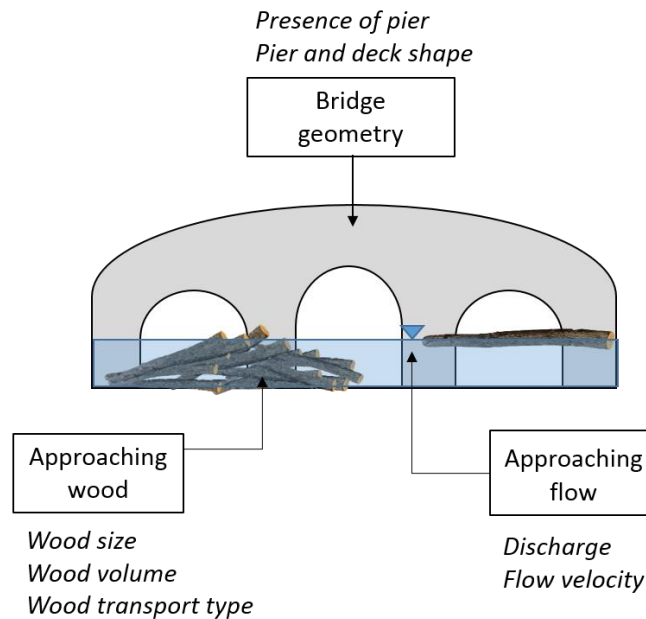
Figure 2.2 Factors influencing wood accumulation at bridges.

Concerning the "approaching wood", the length of the longest piece of wood entrapped at the bridge determines the width of drift accumulation that does not necessary coincides with the height of trees recruited by bank erosion (Diehl, 1997). The trees falling into the channel from banks can be fragmented before encountering a hydraulic structure as a bridge. Diehl (1997) introduced the definition of "design log length" that represents "*a length above which logs are insufficiently strong throughout their full length, to produce drift accumulations equal to their length*".

The mobilization of in-channel wood, that may stop at an obstacle causing blockage, is also determined by flow characteristics (i.e., discharge, velocity; Braudrick & Grant, 2000; Braudrick & Grant, 2001). The volume of the wood accumulation is related to the ratio between the volumetric log input rate (Q_{log}) and flow discharge (Q_{flow}) (Braudrick et al., 1997). Using this ratio, three different in-channel wood transport regimes can be defined, namely congested ($Q_{log}/ Q_{flow} = 0.07 \div 0.2$), uncongested ($Q_{log}/ Q_{flow} \approx 0.015$), and semi-congested ($Q_{log}/ Q_{flow} = 0.015 \div 0.06$) (see Figure 2.3). Recent studies based on videos of wood transport (Macvicar and Piégay, 2012), monitoring based on repeat photography (Kramer & Wohl, 2014), wood tracking with radio frequency transmitters (Schenk et al., 2014) and numerical modelling (Ruiz-Villanueva et al., 2016c) all show that wood flux or wood discharge is higher during the rising limb of the hydrograph and lower during the falling limb. This is valid when the main source is in-channel wood or bank erosion, while in mountainous basins debris flow and

landslides can inject huge amounts also during the falling limb. Higher wood discharge in the present work implies higher blockage probability (Gschnitzer et al., 2013; Ruiz-Villanueva et al., 2016a).
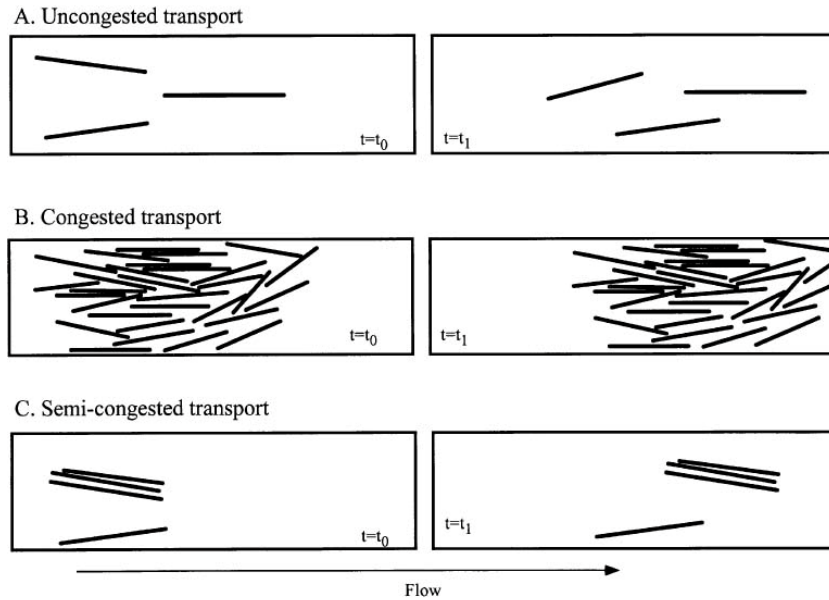
Figure 2.3 Wood transport regimes. Logs at the initial time (left) and at a later time (right). (Picture from Braudrick et al., 1997).

The prediction of wood fluxes during flood events is still challenging and subject to limitations due to the lack of data and the uncertainties in the evaluation of widening processes in channels with vegetated floodplains and even more uncertain is the estimation of landslide inputs (Comiti et al., 2016; Lucía et al., 2015; Ruiz-Villanueva et al., 2016b).

Moreover, bridge structure characteristics, such as piers, abutments, decks and their position and shape will control in-channel wood blockage (according to the channel curvature upstream of the bridge). Some bridge characteristics exist for which wood entrapment is more likely, such as, for example, multiple, closely-spaced piers or pile groups, exposed pier footing piles, open truss superstructures, superstructures with open parapets of pillars, and/or rails (Bradley et al., 2005; Schmocker and Hager, 2011). A smooth structure like a baffle bridge will favour passage of logs, in particular at higher Froude numbers, because of the combination of the baffle smooth shape, which usually accelerates the flow, and high flow velocities (Schmocker et al., 2011).

In the case of straight channels, logs tend to move in the middle of the stream because of the higher flow velocities and the occurrence of secondary circulation which will create a double longitudinal vortex forming by convergence of flow at the surface and a divergence of flow at the bed, with both coinciding typically with the thalweg (Diehl, 1997). The presence of piers will increase in-channel wood accumulation: a central pier is more prone to entrap logs than piers on the banks in a straight stream. The piers on the banks will have a high trapping potential if their distance from the banks is less than the maximum log length and if the reach upstream to the bridge is a long curve (Diehl, 1997; Lyn et al., 2007).

By contrast to the rather extensive works on pier arrangement, little is known about the importance of pier shape on wood accumulation at bridges. Lyn et al. (2003) and

_____

Gschnitzer et al. (2013) reproduced rounded pier shapes in a flume, but other shapes have not yet been considered. The aim of their tests was to analyse how flow depth and velocity affect wood accumulation in the presence of a central pier. The main findings of these studies will be described in section 5.1. Field observations showed that in-channel floating wood tended to stop against the flat surface of the pier, whereas round-nosed piers tended to induce rotation of the log (Lagasse et al., 2010).

2.3   Impacts of wood accumulation at bridges

Wood accumulation at bridges may reduce the effective flow area and thereby decrease the discharge capacity. It can also deflect the flow and increase local scouring (Kattell and Eriksson, 1998). The latter can cause bridge failure by additional hydrodynamic forces generated in proximity of the wood accumulation and the increased blockage of frontal area and lower porosity (Parola, 2000; Manners et al., 2007). The impacts of wood accumulation at bridges may be classified according to their effects on the morphology e.g., bed profiles and on flow hydraulics (i.e., water profile). In the former case, (i) scour at the bridge pier is the main consequence, whereas in the latter case (ii) backwater effect will be dominant.

Pioneering studies on pier local scouring driven by wood presence were done by Laursen and Toch (1956), Dongol (1989) and Melville and Dongol (1992). The earlier studies assessed scouring at a pier with sandy bed found that wood caused scour at a bridge pier except when the accumulation was at the base of the pier (Eqs. (2-1),(2-2),(2-3)). Melville and Dongol (1992) studied three different shapes of wood accumulation at the pier (cylindrical, conical and elliptical shape) in flume experiments and identified the cylindrical pier as being the one causing the maximum scour. They also introduced the concept of the "effective pier diameter" (D_e, in Eqs.(2-1) (2-2) (2-3)) for the evaluation of mass located on a circular pier (Figure 2.4).
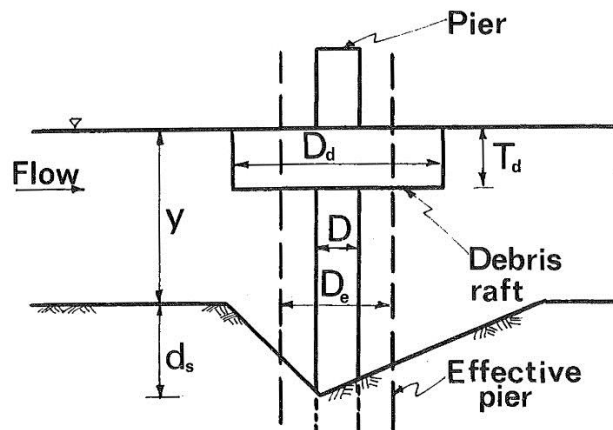
Figure 2.4 Debris mass at the water surface on a single circular pier and effective pier diameter (Melville and Dongol, 1992) (in the figure y=h=water depth).

Dongol (1989) analysed scour around a cylindrical pier using a debris raft around the pier, and the maximum scour depth identified was 2.3 times the effective pier width. His results were later confirmed by Pagliara and Carnacina (2010; 2011), who found that scour may increase to up to 2.4 times of the effective pier width (i.e., the pier diameter including the wood mass around the pier), and up to 3 times the effective pier width in case of cylindrical piers. Equations (2-1),(2-2),(2-3) are as follows:

_____

$$\frac{d_s}{D_e} = 1.872 \left(\frac{h}{D_e}\right)^{0.255} \qquad \left(\frac{h}{D_e}\right) < 2.6$$

$$(2\text{-}1)$$

$$\frac{d_s}{D_e} = 2.4 \qquad \left(\frac{h}{D_e}\right) \geq 2.6$$

$$(2\text{-}2)$$

$$D_e = \frac{0.52 T_d \cdot D_d + (h - 0.52 T_d) D}{h}$$

$$(2\text{-}3)$$

in which d_s is the scour depth, h the water depth, D_e the effective diameter of the pier with wood accumulation, D_d and T_d are respectively, the diameter and thickness of wood accumulation, respectively and D is the pier diameter.

The outer shape of wood accumulation influences scour depth as well. Lagasse et al., (2010) demonstrated that the triangular profile of the wood jam was the most critical factor because of its larger thickness at the frontal pier face. Furthermore, the scour originated when the prolongation of the wood accumulation upstream of the pier was approximately equal to the flow depth.

Wood accumulation at bridges may not only change the bed profile but also the water surface profile. For cases in which wood spans the bridge the upstream water level will increase, causing severe consequences for areas adjacent to the river (Schmocker and Hager, 2010). The backwater effect or afflux due to the bridge clogging may induce more frequent floods than in the absence of a wood clogging. Thus, the impact of a lower return period flood in presence of wood may be the same as of a higher return period flood in absence of wood (Ruiz-Villanueva et al., 2013b; 2014b; 2016c). This is the reason why Ruiz-Villanueva et al. (2013b) suggested the introduction of the equivalent return period in the flood hazard evaluation. They defined the equivalent return period as being "the recurrence interval for an event of a given magnitude that in the presence of any obstruction (i.e., wood) is equivalent to an event of greater magnitude".

Gippel et al. (1992) proposed an equation to calculate the afflux generated by the presence of wood accumulation in rivers, depending on the Froude number, drag coefficient (C_d) and blockage ratio Bl (i.e. the cross-sectional area of flow occupied by wood divided by the cross-sectional area of the flow):

$$\Delta h = \frac{h_3 \left[(Fr_3{}^2 - 1) + \sqrt{(Fr_3^2 - 1)^2 + 3 C_d Bl\, Fr_3^2} \right]}{3}$$

$$(2\text{-}4)$$

where $\Delta y = h_1 - h_3$ is the afflux (h_1 and h_3 are respectively the water level upstream and downstream of wood accumulation), Fr_3 is the Froude number at the downstream section of wood.

Laboratory tests done by Schmocker and Hager (2013) and Schalko et al. (2016) showed that the water level upstream of the wood jam, and at the level of a debris rack, increased during the jam formation phase for higher Froude number and lower porosity. If wood accumulation was compacted and the upcoming logs formed a wood covered surface, the impact on backwater was minor.

_____

The dimensions of logs will also affect the backwater. Tight and long logs filled the interstices of wood accumulations cause higher flow resistance that will increase the upstream water level (Schmocker et al., 2015).

2.4 Recent advances in flume experiments and numerical models on wood accumulation at bridges

This section presents a review of the main approaches (i.e., laboratory tests and numerical models) to analyse interactions between in-channel wood and bridges.

2.4.1 *Flume experiments*

Most of the flume experiments of wood in rivers aimed at investigating wood transport regime, incipient log motion, interactions between in-channel wood and morphodynamics or at validating numerical models (Braudrick and Grant, 2000; Braudrick and Grant, 2001; Bocchiola et al., 2006; Crosato et al, 2013; Bertoldi et al., 2014; Braudrick et al., 1997; Ruiz-Villanueva et al., 2014a).

A growing interest has been recently observed on the interaction between wood and hydraulic structures.

One of the first experiments on wood accumulation at bridges consisted in the reproduction of wood accumulation at a single pier, two adjacent piers, and at a bridge deck, with the aim to measure drag forces induced by wood (Parola et al., 2000). The aim was to investigate the drag forces generated by wood accumulation against a structure. Parola et al. (2000) supported the theory proposed by Koch et al. (1926) based on the partition of the total force acting on an obstruction into drag and hydrostatic components. He demonstrated that an obstruction caused by wood might substantially change the drag coefficient. The results of this study also showed that the drag coefficient of the force exerted by wood on bridges decreased for higher blockage ratios.

Lyn et al. (2003) carried out a series of flume tests on wood accumulation at a single rounded pier positioned in the middle of a channel (Figure 2.5), demonstrating that smaller velocities and smaller flow depths favoured wood deposition at the pier.

Figure 2.5 Wood accumulation at a rounded single pier in laboratory tests from Lyn et al. (2003).

A few years later, and possibly reflecting the growing concern about bridge collapse and the role that wood accumulations are playing, researchers started to explore impacts of wood accumulations on bridge pier scour. Presumably Lagasse et al. (2010) provided one of the most important contributions to this research question; the study also became a reference for its theoretical approach as described in the previous sections. The

_____

main goal of the flume tests presented by Lagasse et al. (2010) was to investigate the influence of wood accumulation shape, porosity, and position on bridge pier scour. Three different shapes (i.e., rectangular, cubic, and triangular) were reproduced with a steel frame filled with logs which was then positioned at the square, multiple column and wall pier, at three different heights relative to the pier. In most cases, the scour at the pier was more pronounced in the presence of wood. The authors also observed that scour was related to the thickness of the wood accumulation at the pier face: the greater is the thickness of the wood accumulation, the deeper the scour depth, larger the scour hole. In addition, it was shown that the triangular wood accumulation profile produced more scour at the pier face, as wood accumulation thickness was also larger here.

Interestingly most recent flume experiments on bridge clogging were done in Switzerland and Austria. In fact, in August 2005, severe flood events were hitting large areas of the Alps and a great amount of wood was transported by the flood flow, resulting in the clogging of bridges and, in a few cases, their collapse. Schmocker and Hager (2011) analysed the blockage probability of a bridge deck structure to entrap wood to improve bridge design and to favour wood outflow in the proximity of the structure. They modelled four different types of bridge decks (i.e., bridge roadway, truss bridge, railing bridge, and baffle bridge) and wood with natural logs both with and without roots. The results from the flume tests encouraged adopting a smoother bridge deck design. Schmocker and Hager (2011) also observed that the probability of wood to be stopped at the bridge was increasing with flow depth. According to their experiments, the baffle bridge showed the best capability to facilitate the passage of wood as opposed to the truss or railing bridges.

Gschnitzer et al. (2013) tested the effects of a central pier on blockage probability through a series of experiments carried out in a rectangular flume under different hydraulic conditions, slope, and with and without a pier in the middle of the flow. They found that high water levels, the presence of a central pier and congested transport of branched logs were the conditions for the highest blockage probability at bridges (Figure 2.6).
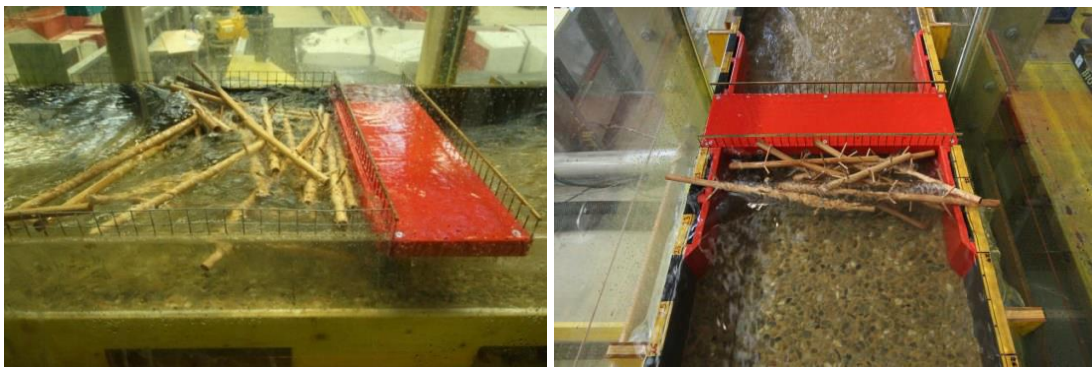
Figure 2.6 Accumulation of logs at a bridge with no pier in the flume experiments from Gschnitzer et al. (2013). Picture from WWR2015 (International Conference on Wood in World Rivers, 2015).

Laboratory experiments on wood accumulation at a structure were recently done by Schmocker and Hager (2011), Schmocker et al. (2015), and Schalko et al. (2016). The structure in this case was not a bridge but a retention wall in the form of a rack. However, an analogy can be found between the distance between piers or between a pier and a river bank, and the distance between the cylindrical elements of the rack. In these experiments,

logs were reproduced with three dimension classes of both natural and small wood sticks without branches, and the backwater levels were measured before and during jamming process. The tests primarily illustrated how backwater effects changed with the wood accumulation over time: during the first phase of jam formation, the backwater rise was faster and larger, as soon as the logs spanned the entire rack, the upcoming logs formed a debris carpet and the effect on the backwater rise was minor (Schmocker and Hager 2011). The presence of organic fine material in the interstices between logs accumulated against a structure was also shown to increase backwater levels (Schalko et al., 2015).

Schmocker et al., (2015) find that the water level upstream of the wood accumulation rises almost linearly with increasing Froude number and decreasing porosity, with the latter being affected by the size and assortment of logs.

Rusyda (2015) done flume tests on wood accumulation at two different model bridges (with and without pier) and steadily increased the number of released logs. He showed that wood accumulation at bridges increases with the number of transported logs and the frontal area of the bridge perpendicular to the flow direction ("shaded area"). The characteristics of the main flume experiments on wood accumulation at bridges are listed in Table 2.2.

Table 2.2 Characteristics of the main flume experiments on wood accumulation at bridge.

Effects	Bridge/pier shape	Wood model description	Wood model dimensions: log length L_{log} (m) and diameter D_{log} (m)	Froude number	Bed type; D_{50} (mm)	Key references
Drag forces generated by wood accumulation against a structure	- Rectangular pier - Two column with a rectangular cap - Bridge deck	natural twigs (no roots, no branches)	L_{log} = 0.61 D_{log}= 0.0127÷0.0254	0.4 ÷ 0.6	Fixed bed	*Parola et al.* [2000]
Flow depth and velocity variation at a wood jam	- Single rounded pier	natural twigs (no roots, no branches)	L_{log} = 0.116 D_{log} = 0.0058	0.2 ÷ 0.4	Fixed smooth bed	*Lyn et al.* [2003]
Wood shape accumulation on bridge pier scour	- Square pier - Multiple column pier - Wall pier	Cylindrical dowels in a rolled steel (cubic, rectangular, triangular shape)	L_{log} = 0.05 ÷ 0.30 D_{log} = 0.006 ÷ 0.05	0.3	Sand bed D_{50} = 0.7	*Lagasse et al.* [2010]

Table 2.3 (continued)

Wood blockage probability at bridge deck	- Roadway bridge - Truss bridge - Railway bridge - Baffle bridge	Cylindrical dowels (with and without branches, no roots)	$L_{log} = 0.15 \div 0.90$ $D_{log} = 0.015 \div 0.02$	$0.3 \div 1.2$	Fixed bed	*Schmocker and Hager* [2011]
Wood blockage with and without pier	- Single rounded pier - Bridge deck with no pier	Cylindrical dowels (with and without branches, no roots)	$L_{log} = 0.24 \div 0.72$ $D_{log} = 0.015$	$0.6 \div 1.2$	Fixed gravel bed (grain size $= 8 \div 16$)	*Gschnitzer et al.* [2013]
Wood accumulation at bridges with and without pier	- Bridge deck with no pier - Bridge with a central rectangular pier	Cylindrical dowels with no branches and no roots	$L_{log} = 0.07$ $D_{log} = 0.002$	NA	Movable + fixed bed $D_{50} = 3.6$	*Rusyda* [2015]
Wood accumulation at bridge piers	- Five different pier shapes	Cylindrical dowels with no branches and no roots	$L_{log} = 0.06 \div 0.15$ $D_{log} = 0.002 \div 0.006$	0.3; 0.5	Fixed bed $D_{50} = 6.8$	*De Cicco et al.* [2016]

Structure

Backwater effect caused by woodaccumulation	- Debris rack - Two "bar-racks"	Natural logs (no roots, no branches)	$L_{log} = 0.047 \div 0.40$ $D_{log} = 0.002 \div 0.15$	$0.3 \div 1.4$	Fixed bed	*Schmocker et al.* [2015]
Backwater effect caused by the accumulation of wood andorganic fine material	- Debris rack - Two "bar-racks"	Natural logs (no roots, no branches) + plastic fir tree	$L_{log} = NA$ $D_{log} = 0.006 \div 0.014$	$0.2 \div 1.4$	Fixed bed	*Schalko et al.*[2016]

_____

2.4.2   *Numerical models*

The use of numerical modelling to analyse wood accumulations in rivers is a recent development. The main difference in existing numerical models is the implemented method for the simulation of log motion.

The one-dimensional numerical models described below cannot be used to simulate the incipient motion of logs, but are only suitable to reproduce the effects of wood accumulation that are caused by the reduction of the cross-sectional area (Parola, 2000; Bradley et al., 2005; Lagasse et al., 2010).

Some of these studies used the output hydraulic parameters of existing two-dimensional models to calculate the forces acting on a piece of wood in a water course (Mazzorana et al., 2011). Ruiz-Villanueva et al. (2014a) presented the first 2D numerical model that implicitly reproduces the motion of rigid cylindrical logs using a Lagrangian approach and fully coupled with hydrodynamics.

2.4.2.1   *1D numerical models*

Parola et al. (2000) simulated in-channel wood bridge clogging using the numerical 1-D hydraulic model HEC-RAS of the Hydrologic Engineering Center of the United States Army Corps of Engineers. Based on flume experiments, they reproduced the single pier accumulation and the span blockage between two piers, increasing the width of the pier and removing the flow area from downstream cross sections outlining an ineffective triangular flow area downstream of the pier beyond 92 m (4:1 expansion rate) (Figure 2.7). The output of hydraulic parameters and characteristics were used to calculate the drag force exerted by in-channel wood. The latter was done through the implementation of the force-prediction methodology suggested by Koch (1926). Their data from numerical simulations combined with the theoretical analysis confirmed the experimental results.
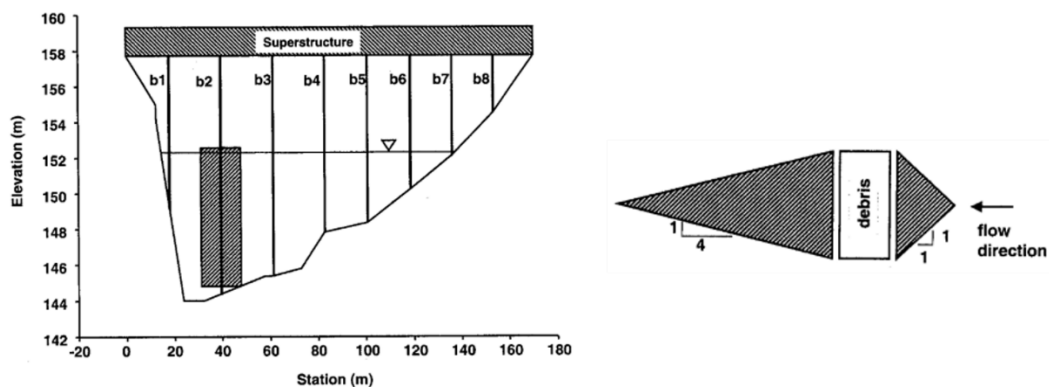
Figure 2.7 Model wood accumulation upstream of the bridge piers (on left) and ineffective flow areas for wood accumulated at the bridge pier (on right) (Source: Parola et al., 2000).

Bradley et al. (2005) and Lagasse et al. (2010) proposed new studies on bridge clogging using the 1-D model HEC-RAS. They adopted two distinct methodologies. Two possibilities to reproduce wood accumulation at bridges, either by (i) acting on the contraction and expansion losses parameters on the bridge structure; or by (ii) creating an extended cross-section downstream of the obstruction. The second method utilized the "Floating Pier Debris" tool of HEC-RAS which allows reproduction of wood as a

_____

continuous blockage with assigned sizes. The "wood block" moves along the vertical direction depending on water level, and may be included in the computation of losses through the bridge as an affective flow area in the energy equations or in the drag force of piers in momentum balance equations.

Ruiz-Villanueva et al. (2013b) proposed a procedure to reconstruct clogging curves – defined here as "the ratio between the percentage of occlusion and the water level for a given discharge" – at the bridge cross-section occluded by wood, thereby reproducing bridge clogging with the reduction of the bridge opening in the 1D hydraulic model HEC-RAS.

2.4.2.2 2D numerical models

Mazzorana et al. (2011) proposed the first 2-D modelling approach for wood transport in rivers using a raster-based data model implemented in ArcGIS (Esri). The hydraulic outputs of the 2-D hydrodynamic simulations were used as input data into GIS, where calculations at each cell determined log incipient motion and transport. After determining the flow direction in each cell, logs were positioned perpendicular to the flow direction and their movement is determined by a simplified force balance equation (Braudrick and Grant, 2000; Haga et al., 2002). The model also reproduces log deposition at obstacles (e.g., a bridge). Polygonal objects reproduce obstacles, each of them being defined by a retention probability (i.e. "the probability of the colliding logs to get entrapped at the considered obstacle") and obstacle height (i.e. "the height of the lower chord obstacle above the initial water level").

In case of single pier accumulation, the log trajectory intersects an obstacle and it deposits, whereas in case of span blockage, log length will determine log deposition. The approach proposed by Mazzorana et al. (2011) provided important results in terms of the amount of potential "movable" wood and critical sections in terms of blockage.

The practice to combine hydraulic data from numerical models with geographical data can help the formulation of strategies for wood management in rivers, as shown by Comiti et al. (2012). They did a detailed study in the Rienz River (Italy) to identify optimal sites for wood retention structures. For this purpose, they used the output from 2D hydraulic and morphodynamics modelling with the visual identification of potential wood input areas in LiDAR data.

More recently, Bladé et al., (2012) simulated individual pieces of wood (by using a discrete element or Lagrangian framework) coupled to an existing 2D hydrodynamic model. The log incipient motion was computed by a force balance and additional drag terms were added to the 2D Shallow Water Equations to account for the presence of wood (Ruiz-Villanueva et al., 2013a, 2014a, see Appendix A). The *Iber-Wood* model solves the hydrodynamic equations with the finite volume method. The logs are modelled as cylindrical elements without roots and branches and may collide between them or with the river boundaries. The position and velocity of the log centre and both its extremities are known at each time step. After testing and validating the numerical model through a series of flume experiments, the model was applied to reproduce wood transport under real conditions and for the case of a flash flood event occurred in 1997 in the Arroyo Cabrera catchment of the Sierra de Gredos (Central Spain). The bridge clogging caused by in-channel wood during this flash flood was well reproduced by the model, as was the depositional wood areas. Interesting recent application of *Iber-Wood* model is the study of the Czarny Dunajec River in Southern Poland, in which the interaction between wood and bridges has been simulated showing some limitation and difficulties in reproducing the log stopping at the single pier (Ruiz-Villanueva et al., 2015; 2016c). The

Iber-Wood model well reproduces the wood transport, the pier-to-pier accumulation but it needs more improvements in reproducing the single-pier accumulation. This aspect will be described in detailed in the current research.

Starting from the approach presented by Ruiz-Villanueva et al. (2014a), a recent 2D numerical model for wood transport was developed by Persi et al. (2016). The log motion in their approach was implemented in the 2D hydrodynamic model (ORSA2D) by using a dynamic approach (Petaccia et al., 2010). Here, the log is divided in four cells and the resultant forces calculated for the centre of each cell. The preliminary numerical and experimental results produced by ORSA2D highlight the necessity to investigate and implement numerically the drag coefficient on partial submerged cylindrical bodies and the variability of the drag with log orientation.

The main characteristics of the numerical models described above are listed in Table 2.4.

Table 2.4 Characteristics of the 1D and 2D numerical models on wood accumulation at bridges.

Model effects	Model dimension	Software	Key references
Blockage: - Increasing the pier width - Creating an ineffective flow area downstream of the wood accumulation	1D	HEC-RAS	*Parola et al.* [2000]
Blockage: - Acting on the contraction and expansion losses parameters - Creating an extended cross section downstream of the wood accumulation	1D	HEC-RAS	*Bradley et al.* [2005]
Blockage: - With the tool "Floating Pier Debris"	1D	HEC-RAS	*Lagasse et al.* [2010]
Blockage: - Reducing bridge opening	1D	HEC-RAS	*Ruiz-Villanueva et al.* [2013b]
Transport: - Using the output hydraulic parameters of numerical simulation into the force balance equation for log movement	2D + raster data	SOBEK rural ArcGIS Esri	*Mazzorana et al.* [2011]

Table 2.5 (continued)

Blockage: - The blockage starts when the path line of the log crosses an obstacle			
Wood deposition: - Using the output hydraulic and morphodinamic parameters of numerical simulation to identify optimal sites where to place wood retention structures	2D	FLO-2D	_Comiti et al._ [2012]
Transport: - Force balance equation and additional drag term implemented into the 2D Shallow Water Equations (Finite Volume Method with II order Roe scheme) - Log motion: both kinematic and dynamic method Blockage: - Interaction between logs and river geometry and between logs and structures	2D	Iber-Wood	_Ruiz-Villanueva et al._ [2014a]
Transport - Force balance equation into the 2D Shallow Water Equations (Finite Volume Method with I order Roe scheme) - Log motion: dynamic method - Interaction between logs and boundaries and between logs	2D	ORSA2D	_Persi et al._ [2016]

_____

2.5   Knowledge gaps

Despite the uncertainty in estimating wood supply and transport upstream of bridges and the effectiveness of the structural countermeasures during flood events, the scientific community has made good progress and now provides invaluable tools for the river managers.

Wood accumulation at bridges is a very complex process that depends on the geometry of the bridge and the logs, the river morphology, hydraulics and morphodynamics and on wood supply processes. The bridge structure may favor wood entrapment but the boundary conditions determine the log incipient motion, the track, and the orientation as well as the log transport regime.

The previous research provided a great contribute to the knowledge of how the log moves in waterstream, the forces exerted by water on the log surface and how they change with log orientation. After analyzing the basic mechanisms of wood transport, the next step is to explore the interaction between the logs and hydraulic obstacles.

The flume experiments done emphasize the most favorable bridge deck for wood transit or the effects of clogging caused by in-channel wood on the water and the mobile bed profile. Most of the experiments on wood accumulation at a single pier aimed to study the correlation between the shape of the wood accumulation and the pier scour or the blockage probability in presence of the pier. These studies stress the main problems related to the wood accumulation at bridges but neglect further aspects concerning the hydraulics of the problem. The flow field acts on the log motion as well as the presence of the pier produces a distorted flow field around the obstacle that affects the motion of the approaching logs. The shape of the pier plays here a determinant role combined with water depth and flow velocity.

A single piece of wood may rest against the pier or it may flows away depending on the hydrodynamic forces acting on the log, the resultant moment of the forces, the position of the log centre when it bump into the pier, the skin friction at the contact point between the log surface and the pier surface. All the listed aspects need to be deeply investigated both experimentally and numerically. For example, the drag force has been measured experimentally only for submerged logs. The floating logs are partially submerged in the water and thus the force exerted by flow on the logs changes and consequently the drag coefficient. More experimental measures of drag-force on semi-submerged logs in water are required.

Further aspects should be considered, however, in the future, such as the presence of logs with roots and branches (and not only cylinders), the number of piers, the influence of movable bed on wood transport, or the effects of different river morphologies, such as in the case of meandering rivers.

Most of the flume experiments dealing with wood transport and the presence of an obstacle in the middle of the cross-section were carried out in straight channels and with fixed bed conditions. Recent flume experiments performed on wood transport in a braided river system including a movable bed clearly underlined the great influence of morphodynamics processes on the remobilization of logs and on the formation of potential depositional areas for wood (Bertoldi et al., 2014). The combination of more complex processes, such as sediment transport or growing vegetation, that could be potentially influencing factors of wood transport and accumulation, is still and most critically needed.

In relation to log shape, the generalized used of cylindrical, smooth logs without roots and branches of course represents the main simplification of numerical models. As

Ruiz-Villanueva et al. (2013a) already highlighted, and even if many authors (Braudrick et al., 1997; Bocchiola et al., 2008) agree with this hypothesis, a more irregular log shape is likely to increase clogging probability.

The research in numerical modelling of wood transport has made great progress. The existing 2D numerical models allow to reproduce the log incipient motion, transport and deposition of logs on the river banks, as well as the collision between logs and between the logs and the boundaries. But there is still much work to be done.

The future way to improve numerical modeling should also include the use of logs with roots and branches, even in a schematic way (e.g., with a disk as suggested by Braudrick and Grant, 2000) and the combination of wood transport and deposition with more complex hydrodynamic and morphodynamics processes such as bank erosion (Solari et al., 2015).

Numerical models may provide a valuable tool to analyze possible flood hazard scenarios related to the presence of wood in rivers. They will also allow inclusion of effects related to backwater rise and the presence of the cross-sectional obstruction by wood in hazard delineation (Mazzorana et al., 2011; Ruiz-Villanueva et al., 2013b). However, more experimental and field data are required to further reduce uncertainty in the modelling approaches and to validate numerical models (Bladè et al., 2016).

The main remaining research issues are summarized in Table 2.6.

Table 2.6 Remaining research issues in the fields of wood transport and entrapment for future research.

	Issues	*Key references*
Field	- localization of potential sites for wood recruitment; - quantification of recruitable wood flux;	*Comiti et al.,* (2008) *Mao et al.,*(2013) *Mazzorana et al.,* (2009)
Flume experiments	- tests on wood accumulation at different pier shapes; - tests on "pier-to-pier" accumulation; - wood accumulation at bridges in a curved channel; - wood transport combined with morphodynamics processes;	*Ruiz-Villanueva et al.* (2013a) *Schmocker and Hager* (2010) *Solari et al.* (2015) *Bertoldi et al.* (2014)
Numerical modelling	- numerical modelling of interaction between logs and structures (e.g. the piers); - validation with field data; - reproduction of real trees with roots and branches; - wood transport and sediment transport; - 3D modelling of logs;	*Ruiz-Villanueva et al.* (2014a) *Bladè et al.* (2016)

3 Theoretical background

The physics of wood log transport in open waters and jamming at bridge crossings is complicated by the dynamic forces that act on the logs and the interaction of different logs through collision and repulsion. The forces comprise of drag forces and buoyancy that are caused by the flow as well as additional drag force induced by the wind. The complex interacting forces drive the logs to divert from the main flow streamlines. An additional mechanism is the rotation of a single log that depends on the spatial positions of the centres of gravity and resultant forces on the log. The following section provides an overview of the system of forces and controlling parameters for log transport with the focus on a single, straight wooden log.

3.1 The governing equations for wood transport

"Wood transport" refers to the study of wood dynamics and thus the forces acting on a piece of wood floating in a river, the incipient motion conditions and the wood transport regimes. A tree that falls into the river is mobilized depending on flow regime and on wood characteristics and on channel morphology. The incipient motion of a piece of wood is determined analysing the forces acting on the trunk as suggested by Braudrick and Grant (2000).

Considering a wooden cylindrical log (with no roots and branches) in a uniform flow, the acting forces are listed below (illustrated in Figure 3.1):

- *Effective weight of the log (W_{eff})*

The effective weight of the log is the weight force (W) minus buoyant force (B) which is given by equation 3.1:

$$W_{eff} = g \cdot \rho_{log} \cdot L_{log} \cdot \frac{\pi D_{log}^2}{4} - g \cdot \rho \cdot L_{log} \cdot A_{sub} \qquad (3\text{-}1)$$

in which L_{log} is the length of the piece of wood, ρ_{log} and ρ are the density of wood and water, D_{log} is the diameter of log piece, g is the gravity, A_{sub} is the submerged area of the log perpendicular to the length of piece. For a right-circular cylinder A_{sub} depends on diameter of piece (D_{log}) and submerged log diameter (d_{sub}):

$$A_{sub} = \left\{ 2 \cos^{-1}\left(1 - \frac{2d_{sub}}{D_{log}}\right) \right. $$
$$\left. - \sin\left[2 \cos^{-1}\left(1 - \frac{2d_{sub}}{D_{log}}\right)\right] \right\} \frac{D_{log}^2}{8} \qquad (3\text{-}2)$$

- *Gravity Force (F_g)*

The gravity force is a vertical force acting in downward direction given by:

$$F_g = W_{eff} \cdot \sin \alpha$$
$$= \left(g \cdot \rho_{log} \cdot L_{log} \cdot \frac{\pi D_{log}^2}{4} - g \cdot \rho \right.$$
$$\left. \cdot L_{log} \cdot A_{sub} \right) \cdot \sin \alpha \qquad (3\text{-}3)$$

α is the angle of the channel bed in the flow direction (Figure 3.2).

- *Normal Force (F_n)*

The normal force is the force acting in the perpendicular direction to the flow:

$$F_n = W_{eff} \cdot \cos \alpha$$
$$= \left(g \cdot \rho_{log} \cdot L_{log} \cdot \frac{\pi D_{log}^2}{4} - g \cdot \rho \right.$$
$$\left. \cdot L_{log} \cdot A_{sub} \right) \cdot \cos \alpha \qquad (3\text{-}4)$$

- *Friction Force (F_f)*

This force opposes the relative motion of a body or fluid and acts in the upstream direction. It is given by equation 3.5:

$$F_f = F_n \cdot \mu_{bed} = \left(g \cdot \rho_{log} \cdot L_{log} \cdot \frac{\pi D_{log}^2}{4} - g \cdot \rho \right.$$
$$\left. \cdot L_{log} \cdot A_{sub} \right) \cdot \cos \alpha \cdot \mu_{bed} \qquad (3\text{-}5)$$

in which μ_{bed} is the coefficient of friction between log and bed. Crosato et al. (2013) found $\mu_{bed}= 0.47$ for wooden bed and $\mu_{bed}= 0.64$ for gravel bed.

- *Drag Force (F_d)*

When a piece of wood moves in a fluid with a constant velocity, the fluid opposes the motion through an additional resistance. The drag force is given by equation 3.6:

$$F_d = \frac{1}{2} \cdot \rho \cdot C_d \cdot \left(U - U_{log} \right)^2 \cdot A_{sub} \qquad (3\text{-}6)$$

in which U is the water velocity, U_{log} is the log velocity, C_d is the drag coefficient of the wood in water. Considering the log orientation and his influence on drag coefficient, if θ is the inclination of log relative to the flow direction, the drag force will be:

_____

$$F_d = F_{dn} + F_{dp}$$

<div align="right">(3-7)</div>

which are the normal and parallel components of drag force, respectively. Equation 3.7 can be rewritten as equation 3.8

$$F_d = \frac{1}{2} \rho \cdot C_d \cdot (U - U_{log})^2 \cdot \left(L_{log} \cdot h \sin\theta + A_{sub} \cdot \cos\theta\right)$$

<div align="right">(3-8)</div>

The drag force on a body is the sum of the friction drag (that depends on the log orientation) and the pressure drag called also form drag because it depends on the shape of the body (proportional to the difference between the pressure acting on the front and back of the log).

$$F_d = F_{d,friction} + F_{d,pressure}$$

<div align="right">(3-9)</div>

$F_{d,friction}$ is zero for a flat surface normal to the flow direction and maximum for a flat surface parallel to the flow direction. Under turbulent flow conditions, the roughness of the body surface can influence the friction drag while under laminar flow conditions the friction drag does not depends on the roughness of the surface.

The pressure drag is higher in presence of blunt bodies than streamlined bodies because it is proportional to the frontal area of the body.
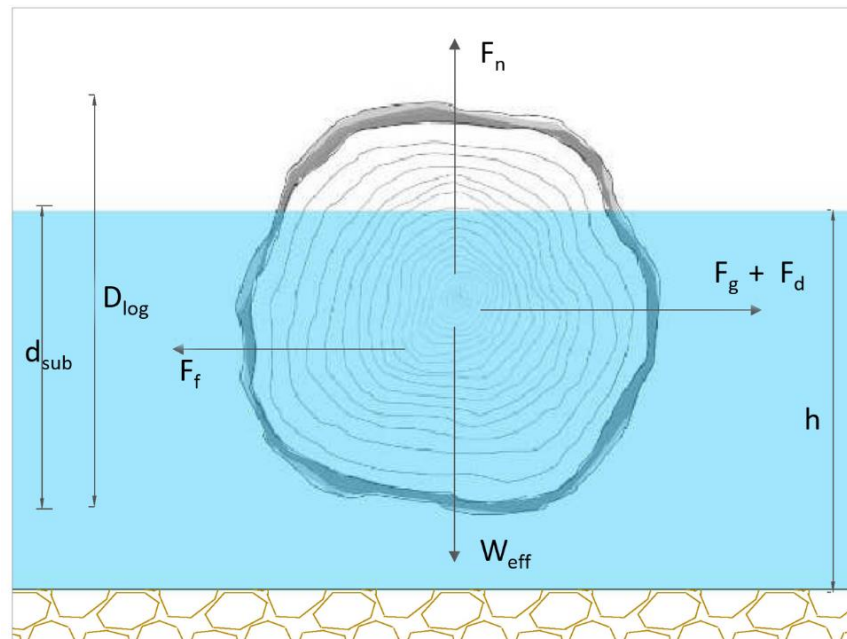
Figure 3.1 Scheme of the forces acting on a piece of wood located in water stream
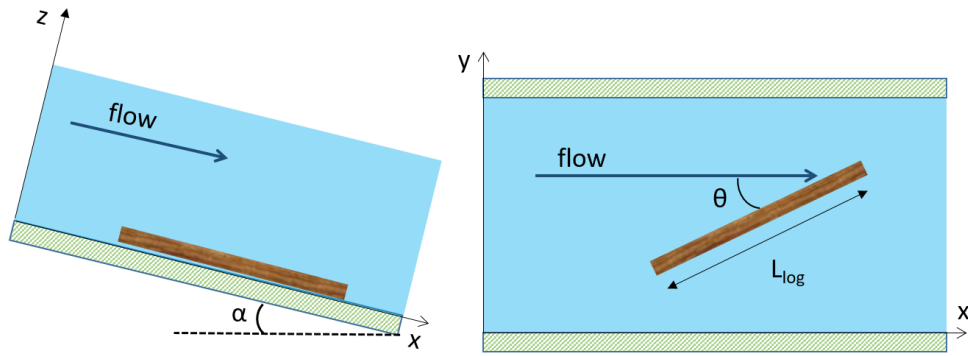
Figure 3.2 Angle of channel bed in flow direction and orientation of the log respect to the flow direction.

The incipient motion of a cylindrical log is obtained by the balance of equations (3-3),(3-5) and (3-6), i.e.,

$$F_f = F_d + F_g \qquad (3\text{-}10)$$

Substituting the corresponding forces from the foregoing equations, we get equation 3.11

$$\left(g \cdot \rho_{log} \cdot L_{log} \cdot \frac{\pi D_{log}^2}{4} - g \cdot \rho \cdot L_{log} \cdot A_{sub}\right) \cdot (\mu_{bed} \\ \cdot \cos\alpha - \sin\alpha) = \frac{U^2}{2} \cdot \rho \cdot C_d \\ \cdot \left(L_{log} \cdot h \sin\theta + A_{sub} \cdot \cos\theta\right) \qquad (3\text{-}11)$$

The velocity corresponding to $\frac{(F_g + F_d)}{F_f} = 1$ is, according to this model, the threshold velocity U_{lim} for wood incipient motion is given by equation 3.12

$$U_{lim}^2 = \\ \frac{\left((g \cdot \rho_{log} \cdot L_{log} \cdot A_{log}) - (g \cdot \rho \cdot L_{log} \cdot A_{sub})\right) \cdot (\mu_{bed} \cdot \cos\alpha - \sin\alpha)}{\left(0.5 \cdot C_d \cdot \rho \cdot (L_{log} \cdot h \cdot \sin\theta + A_{sub} \cdot \cos\theta)\right)} \qquad (3\text{-}12)$$

A single wood can move by sliding, rolling or floating. In order to determine the log transport type, Haga et al. (2002) introduced a dimensionless force Ψ parameter, which is defined as:

_____

$$\Psi = \frac{F}{R} \qquad\qquad (3\text{-}13)$$

Where F is the hydrodynamic force (F_d) and R is the resistance force (F_f-F_g). The wood log will move when the hydrodynamic force is greater than the resistance force.

The combination of Equation (3-13) and of the ratio between flow depth and log diameter (h/Dlog) qualifies the log motion type as follows (see Figure 3.3):

$$\frac{h}{D_{log}} \geq 1 \; \rightarrow floating\; condition \qquad\qquad (3\text{-}14)$$

$$\Psi \leq 1 \; and \; \frac{h}{D_{log}} < 1 \; \rightarrow resting\; condition \qquad\qquad (3\text{-}15)$$

$$\Psi > 1 \; and \; \frac{h}{D_{log}} < 1 \; \rightarrow sliding\; or\; rolling\; condition \qquad\qquad (3\text{-}16)$$
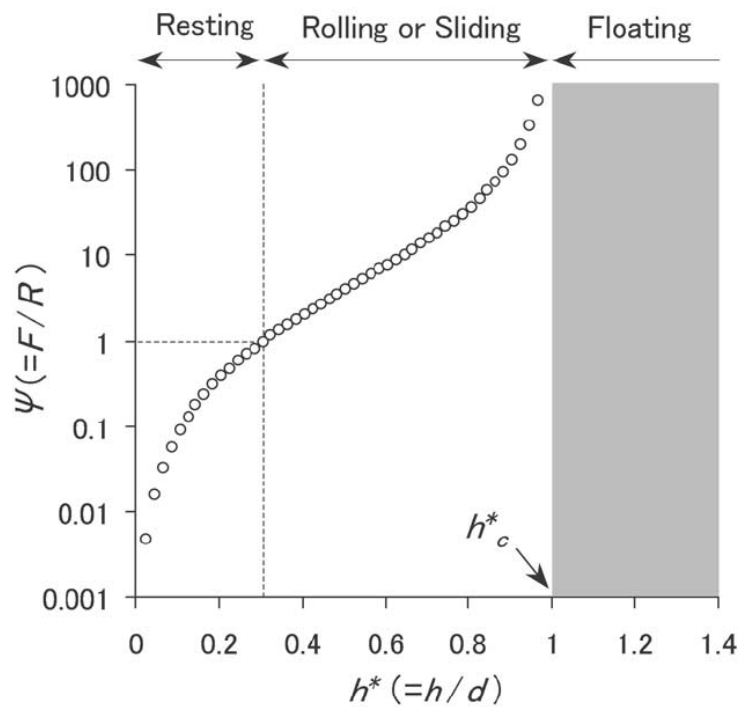
Figure 3.3 Example of the relationship between log transport regime, the dimensionless water depth h* ($d=D_{log}$) and the dimensionless force Ψ. Source: Haga et al., 2002. (Assuming that the density of log is equivalent to the water, hc* is 1).

Bocchiola et al. (2006) proposed a more detailed model that distinguishes the incipient motion for sliding from the motion for rolling. Flume experiments showed that when a piece of wood is oriented parallel to the flow direction the prevalent log motion mechanism is the sliding, while when a piece of wood is oriented perpendicular to the flow direction, rolling prevails.

The general entrainment formula (Bocchiola et al., 2006) is given by:

$$Y_w^* = \frac{\rho \cdot h}{\rho_{log} \cdot D_{log}} = \frac{1}{1 + C_d \cdot X_{S,R}^*} \qquad (3\text{-}17)$$

It accounts for the relative buoyancy, the normalization of the ratio between flow depth and log diameter for the mass density of water and log. The term $X_{S,R}^*$ is the normalization of the ratio between the drag force and the resistance to motion and it differs for sliding (X_S^*) and rolling (X_R^*) as follows:

$$X_S^* = \frac{1}{2}\frac{U^2}{gL_{log}(cos\alpha \cdot \mu_{bed} - sin\alpha)} \qquad (3\text{-}18)$$

$$X_R^* = \frac{1}{2}\frac{U^2}{gD_{log}(cos\alpha \cdot tan\delta - sin\alpha)} \qquad (3\text{-}19)$$

in which δ is the channel slope for log incipient rolling in dry conditions.

Equation (3-17) requires the knowledge of the prevailing log incipient motion mechanism.

The results obtained from flume experiments showed that is not correct to introduce the value of h in the Equation (3-17) because in real cases the profile of water around the log changes from upstream to downstream, so it is required a representative water depth should be used i.e., h_r .

A new coefficient was introduced (Bocchiola et al., 2006):

$$C_{r,S,R} = \frac{h_r}{h} = a_{S,R}(Y_w^{b_{S,R}}) \qquad (3\text{-}20)$$

in which a and b change with log orientation, they are respectively 0.84 and 0.77 for rolling and 0.91 and 0.78 for sliding motion.

Taking into account the representative water depth, the Equation (3-17) becomes:

$$Y_{r,S,R}^* = Y_w^* \cdot C_{r,S,R} \qquad (3\text{-}21)$$

3.2   Collision between logs

During flood events, more logs are transported by the flow and they may collide originating a single mass of logs (congested wood transport). When the "log carpet" bumps into the bridge pier, the clogging probability is higher than the probability of a

single floating log (uncongested wood transport), because the ratio between the cross section width occupied by wood and the pier width is higher.

If i and j are the colliding logs, the velocity mass centre of the collided logs is:

$$\left(u_{log}\right)_{i+j}^{cm} = \frac{m_i\left(u_{log}\right)^i + m_j\left(u_{log}\right)^j}{m_i + m_j}$$

(3-22)

m_i and m_j are the mass of logs i and j.

After rearranging Equation 3.22, we get:

$$\left(u'_{log}\right)^{i,j} = (1+e) \cdot \left(u_{log}\right)_{i+j}^{cm} - e \cdot \left(u_{log}\right)^{i,j}$$

(3-23)

in which $\left(u_{log}\right)^{i,j}$ is the initial log velocity, and e is the restitution coefficient.

The three transport regimes defined by Braudrick et al. (1997), are characterized by different values of the relative log input rate, that is the ratio between the volumetric log input rate and the discharge (Q_{log}/Q_{flow}).

The relative log input rate is correlated directly with wood sources: pieces of wood that enter in streams by wind throw and tree mortality will move with uncongested transport regime. Debris flow and bank erosion are the main responsible for the formation of congested wood transport in streams (Braudrick et al., 1997).

3.3 Wood budget

Another important concept which applied to study log transport is mass budget equation. The mass budget ΔS (m^3) of wood in a reach length Δx, during time Δt and caused by different recruitment processes, was proposed by Benda and Sias (2003), as follows:

$$\Delta s \ (m^3) = [I - O + Q_{log,in}/\Delta x - Q_{log,out}/\Delta x - D] \cdot \Delta t$$

(3-24)

where I (m^3/m·year) is the wood recruitment along a channel segment and it takes into account the wood mortality (I_m), bank erosion (I_{be}), windstorms and fires (I_f), the avalanches (I_s) and the exhumation of buried wood (I_e). O is the loss of wood from deposition in floods, $Q_{log,in}$ and $Q_{log,out}$ are the input and output wood transport in the reach of length Δx and D is the decay ($D= k_d \cdot S$ with k_d decay loss per unit time and S the storage volume; Harmon et al., 1986).

_____

3.4   Blockage probability

The parameters that control log transport in open waters described by the foregoing sets of equations are related to inertial and gravitational forces. The sum of the forces acting on a fluid element is called *inertial force* that is equal to the mass times the acceleration of the fluid element. The various parameters are: the ratio between inertial force and gravitational force gives the Froude number (Fr), the inertial force over viscous force the Reynolds number (Re), the derivation of pressure to inertial gives the Euler number (Eu), the surface tension to inertial force gives the Weber number (We). The state of wood transport can be investigated through the foregoing fundamental parameters (Fr, Re, Eu, We) together with the dimensionless parameters that describe the logs and the pier. Among which are the relative flow depth and spanwise and vertical flow blockage that are the ratio of horizontal bridge opening to the pier width and the ratio of pier width to the effective flow depth.

The central idea and hypothesis of the work that based on the foregoing analysis and the dimensionless parameters are presented. The following considerations, assumptions and simplifications aimed to analyze the experimental and numerical tests carried out in the current research.

The blockage probability (B) is here defined as the probability for a single log, transported by the flow in streams, to clog at the bridge pier or under the bridge deck. Clogging can cause the obstruction of the cross section and thereby reducing the flow rate through the contracted opening. Blockage probability was first introduced by Schmocker and Hager (2011) for analysing the probability of logs to clog at a bridge deck, and then by Gschnitzer et al. (2013) for the evaluation of bridge crossing obstruction caused by wood with and without a central pier (semi-circular pier shape).

In the current research study, we assume B=1 when the logs are blocked at the pier and B=0 when the logs pass the pier. Based on the foregoing section, the preliminary list of the fundamental variables considered are as follow:

The variables characterizing the hydraulics of the flow are:
- Fr (Froude number) [-]
- Re (Reynolds number) [-]
- τ_{wind} (wind shear stress) [kg $\cdot$m^{-1}$\cdot$s^{-2}]
- Q_{flow} (flow discharge) [m^3 $\cdot$s^{-1}]
- ρ (water density) [Kg$\cdot$m^{-3}]
- h (flow depth) [m]
- w (channel width) [m]

The variables characterizing the bridge pier are:
- w_p (pier width) [m]
- L_p (pier length) [m]
- c_{pier} (pier hydraulic shape coefficient, introduced here for the first time and obtained taking into account the 2D flow field upstream of the pier that changes according to the pier geometry. It represents one of the novelty of the current research) [-]
- α_{pier} (orientation of the pier respect to the flow direction) [°]
- n_{pier} (number of piers) [-]

The variables characterizing the logs are:
- L_{log} (log length) [m]
- θ (log orientation respect to the flow direction) [°]
- $Shape\ of\ log$ [-]

- Q_{log} (Volumetric log input rate) [m^3·s^{-1}]
- ρ_{log} (wood density) [Kg·m^{-3}]

The blockage probability results in:

$$B = f(Fr, Re, \tau_{wind}, Q_{flow}, \rho, h, w, w_p, L_p, c_{pier},$$
$$\alpha_{pier}, n_{pier}, L_{log}, \theta, Shape\ of\ log, Q_{log}, \rho_{log}) \tag{3-25}$$

In case of submerged logs, the Reynolds number has a great influence on the drag force while for semi-submerged logs situated near the free surface, the drag is influenced both by viscous and gravitational forces (Wallerstein et al., 2002). Considering the flow as turbulent, the Reynolds number can be omitted. For the aim of the current research, Froude number is the main fundamental flow parameter and thus the Re can be neglected.

The wind acting on the water surface of the river may generate shallow water waves and the shear stress exerted may change the water depth (Plate and Goodwin, 1965). The study does not account for the influence wind induced shear stresses.

A single pier oriented parallel to the flow direction has been reproduced in the experimental and numerical tests done in the current research, and then we can neglect n_{pier} and α_{pier}. In case of $\alpha_{pier} = 0$ (pier oriented parallel to the flow direction), L_p may have no effect on B and thus we can relax L_p as well.

The logs are assumed as wooden cylindrical dowels with no roots and no branches and we used this configuration both for experimental and numerical tests. Different log shapes were not analysed so we can remove the $Shape\ of\ log$ from Equation (3-25).

The congested wood transport was simulated through multiple randomly oriented logs while the uncongested wood transport was reproduced with a single log parallel to the flow direction but without measuring the blockage in function of the log orientation $, \theta$.

Furthermore, only the influence of the volumetric input rate is considered i.e., Q_{log}. The parameters considered are given for the formulations of P are given by function 3.26.

$$B = f(Fr, Q_{flow}, \rho, h, w, w_p, c_{pier}, L_{log} Q_{log}, \rho_{log}) \tag{3-26}$$

Among the variables listed in Equation (3-26), only Fr and c_{pier} are non-dimensional.

To get the dimensionless parameters from the remaining variables, we apply the Buckingham Theorem by selecting Q_{flow}, w_p and ρ_{log} as independent variables, we get 5(=8-3) dimensionless groups as given by function 3.27

$$0 = f(\pi_1, \pi_2, \pi_3, \pi_4, \pi_5) \tag{3-27}$$

The dimensions of the independent variables are:

_____

$$Q_{flow}^x \cdot w_p^y \cdot \rho_{log}^z = L^{3x} \cdot T^{-x} \cdot L^y \cdot M^z \cdot L^{-3z}$$
$$= L^{3x+y-3z} \cdot T^{-x} \cdot M^z \qquad (3\text{-}28)$$

The five groups are:

$$\pi_1 = Q_{flow}^x \cdot w_p^y \cdot \rho_{log}^z \cdot \rho \;\rightarrow\; \pi_1 = \frac{\rho}{\rho_{log}} \qquad (3\text{-}29)$$

$$\pi_2 = Q_{flow}^x \cdot w_p^y \cdot \rho_{log}^z \cdot h \;\rightarrow\; \pi_2 = \frac{h}{w_p} \qquad (3\text{-}30)$$

$$\pi_3 = Q_{flow}^x \cdot w_p^y \cdot \rho_{log}^z \cdot Q_{log} \;\rightarrow\; \pi_3 = \frac{Q_{log}}{Q_{flow}} \qquad (3\text{-}31)$$

$$\pi_4 = Q_{flow}^x \cdot w_p^y \cdot \rho_{log}^z \cdot L_{log} \;\rightarrow\; \pi_4 = \frac{L_{log}}{w_p} \qquad (3\text{-}32)$$

$$\pi_5 = Q_{flow}^x \cdot w_p^y \cdot \rho_{log}^z \cdot w \;\rightarrow\; \pi_4 = \frac{w}{w_p} \qquad (3\text{-}33)$$

Thus, the problem can be described by the following function of the seven non-dimensional π groups:

$$g(\pi_1, \pi_2, \pi_3, \pi_4, \pi_5, \pi_6, \pi_7) = 0$$
$$\rightarrow f\left(\frac{\rho}{\rho_{log}}, \frac{h}{w_p}, \frac{Q_{log}}{Q_{flow}}, \frac{L_{log}}{w_p}, \frac{w}{w_p}, Fr, c_{pier} \right) \qquad (3\text{-}34)$$
$$= 0$$

If we combine π_2 and π_5 to get:

$$B = f\left(\frac{\rho}{\rho_{log}}, \frac{w}{h}, \frac{Q_{log}}{Q_{flow}}, \frac{L_{log}}{w_p}, Fr, c_{pier} \right) = 0 \qquad (3\text{-}35)$$

Here, only the floating conditions for logs ($\rho_{log} < \rho$) were reproduced and thus we can neglect $\frac{\rho}{\rho_{log}}$ in the (3-35). Furthermore, the aspect ratio can be relaxed in first approximation.

Function (3.36) describes the blockage probability for a single pier with four non-dimensional groups:

$$B = f\left(\frac{Q_{log}}{Q_{flow}}, \frac{L_{log}}{w_p}, Fr, c_{pier}\right) = 0 \tag{3-36}$$

We finally define the probability of wood to accumulate at a single central pier as:

$$B = f\left(\frac{Q_{log}}{Q_{flow}}, \frac{L_{log}}{w_p}, Fr, c_{pier}\right) \tag{3-37}$$

The determination of probability defined by function 3.37 is the main basis of the present research thesis. Further details are given in Chapter 4 regarding the methodology and approach adopted to reach the main goal of this research.

It is also useful to formulate a joint probability for the function list in (3-35) that gives the overall blockage probability for the system under consideration.

The thesis analyses the probability of each variable individually both experimentally and numerically. For the case of independent variables as in the present study, the joint blockage probability is defined by the product of the marginal distributions:

$$tot\ B = B_1 \cdot B_2 \cdot B_3 \cdot B_4 \tag{3-38}$$

In which, $B_1 = f_1\left(\frac{Q_{log}}{Q_{flow}}\right)$, $B_2 = f_2\left(\frac{L_{log}}{w_p}\right)$, $B_3 = f_3(Fr)$, $B_4 = f_4(c_{pier})$ are the marginal probability functions.
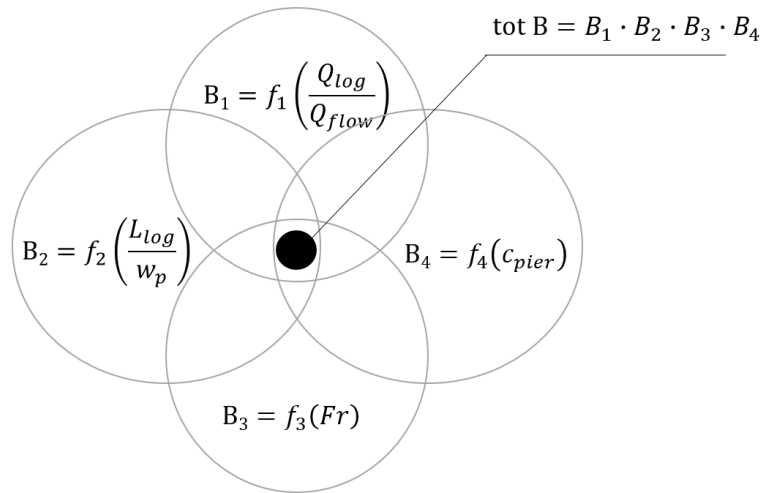
Figure 3.4 Sketch of the joint blockage probability distribution (tot B) from the marginal probability functions (B₁, B₂, B₃, B₄)

4 Methodology and approach

The study uses a combined experimental and numerical approach to investigate the main research questions outlined in the Introduction chapter of the present thesis. The focus is the formulation of the blockage probability of wood jamming as previously indicated. The numerical approach uses both 2 & 3 dimensional models to examine the relevance and possibility of modelling wood transport and jamming. Figure 1.2 shows the schematic of methods used in the thesis.

The focus of this chapter is providing the details of the experiments as well as the model setups for the 2D and 3D simulations. The technical details of the two numerical models are given in the Appendix.

4.1 General aspects

The state of the art analysis highlighted several possible research issues in wood transport and jamming at bridge crossings (Table 2.6). In particular, regarding the wood accumulation at bridge piers, the concept of blockage probability could a serve as a powerful tool for optimal design of bridge crossings and the safe management of wood transport. In the present work the blockage probability at different bridge pier shapes and the influencing factors. The goal is to find the wood accumulation probability (here called "blockage probability"), depending on the bridge geometry (such as in the case of historical cities with notable bridges characterized by non-standard pier shapes), the hydraulics and the wood transport regime.

We first introduce the concept of blockage probability as applied in this thesis prior to presenting the various methods used in the study.

4.2 The concept of blockage probability

The blockage probability (B) is the jamming probability of logs transported by the flow in streams, at a bridge pier or a bridge deck therefore causing the obstruction of the cross section and reducing the flow rate through the contracted opening. The blockage probability was first introduced by Schmocker and Hager (2011) for analysing the probability of logs to jam at the bridge decks. Latter work is by Gschnitzer et al. (2013) for the evaluation of bridge obstruction caused by wood with and without a central pier (semi-circular pier shape).

In both cases B=0 was assigned when the logs passed the bridge section and B=1 when the logs were blocked or passed over the reference bridge.

In the present thesis, we assume B=1 when the logs are blocked at the pier and B=0 when the logs pass the pier. The analysis of the main variables that influence wood jamming at the bridge pier (see section 3.4) yields:

$$B = f\left(\frac{Q_{log}}{Q_{flow}}, \frac{L_{log}}{w_p}, Fr, c_{pier}\right)$$

(4-1)

In which, $\frac{L_{log}}{w_p}$ is the ratio of the log length to the pier width, $\frac{Q_{log}}{Q_{flow}}$ is the ratio of the log discharge transported by flow to the flow discharge, Fr is the Froude number that represents the influence of flow velocity and water depth on wood accumulation; c_{pier} is a new coefficient that we name as "pier hydraulic-shape coefficient". The coefficient

is for the first time introduced into function 3.1. It was obtained considering the 2D flow field upstream of the pier that changes according to the pier geometry.

In addition to the blockage probability P (here indicated with B) introduced by Schmocker and Hager (2011), two new blockage probabilities were also defined i.e., the Effective Accumulation (EA) and the Potential Accumulation (PA). The first represents the ratio between the number of logs per classes (or for all classes) that are blocked at the pier at the end of each run and the total number of logs introduced in the flume per class (or for all classes). The second is ratio between the number of logs that touch the pier but not necessary stop, and the total number of logs introduced in the flume. It is the blockage probability that would occur if all the logs that touch the pier stopped at the pier.

Consequently, we distinguish two main cases for blockage probability definition; i) if blockage occurs or not and ii) the blockage in relation to the number of entrapped logs. *Table 4.1* summarize the various definitions and the formulas.

Table 4.1 Definition and description of the blockage probabilities determined in the flume experiments.

Code	Definition	Formula	Values	Description	Reference
B	Blockage probability	-	0,1 0 =no blockage 1=yes blockage	Probability of drift to get stuck at the bridge. When drift passes the bridge section the blocking probability is 0 while when it is blocked the probability is 1.	Schmocker and Hager (2011)
EA	Effective Accumulation	$\dfrac{\# \, blocked \, logs}{\# input \, logs}$	0÷1 0=no logs stop at the pier 1=all logs stop at the pier	The number of logs that **stop** at the pier at the end of the test. It represents the "effective" blockage probability.	New
PA	Potential Accumulation	$\dfrac{\# \, logs \, touch}{\# input \, logs}$	0÷1 0=no logs touch the pier 1=all logs touch the pier	The number of logs that **touch** the pier after each impulse of logs. It represents the "potential" blockage probability.	New

4.3   Experiments

The experiments were conducted in an open-channel flume at the hydraulic laboratory of the Department of Civil and Environmental Engineering of the University of Firenze, Italy. The main objectives of the experiments were:

- To evaluate the most critical pier shapes and flow conditions for wood accumulation at a single central pier defined in terms of the log transport regime,

_____

Q_{log}/Q_{flow} (congested or uncongested), the log length compared to the pier width L_{log}/w_p, and the hydraulic conditions set by Froude number (Fr).

- To gain insight into the general process of wood transport and jamming at bridge piers in lowland type of rivers with negligible bed slope.

4.3.1   *Setup*

The glass-walled rectangular flume used is 5 m long, 0.30 m wide and 0.16 m deep. The lateral walls are sustained by a steel structure. The flume bed had a slope of 0.001 which was covered by a layer of uniform gravel ($D_{50} = 6.81$ mm). The downstream water level was controlled by a sluice gate. Figure 4.1 shows the side and top views of the flume and the position of the pier used in the experiments.
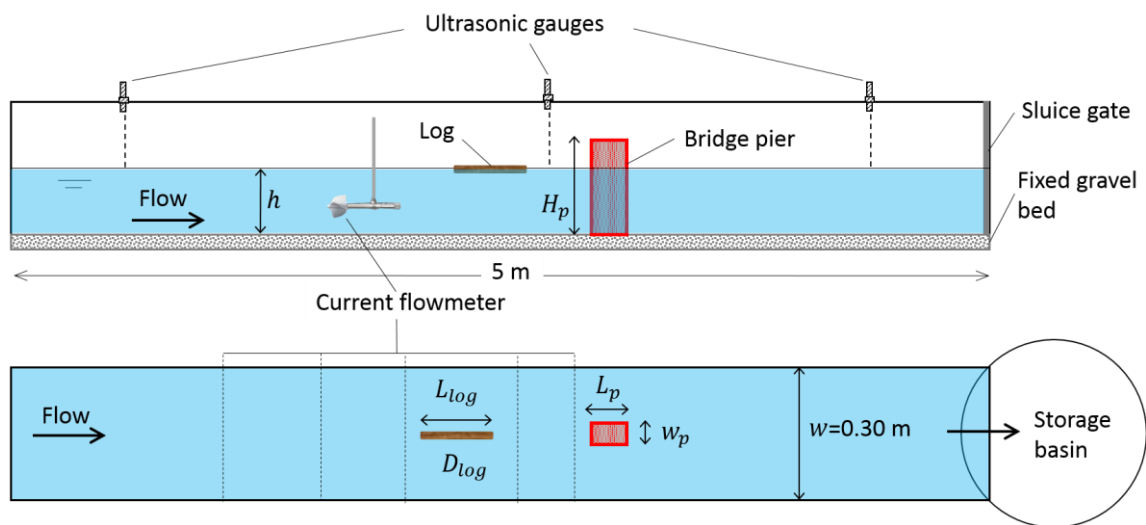
Figure 4.1 Side and planimetric view of the laboratory channel.

Five different pier shapes and three classes of logs were reproduced; two wood transport regimes and two hydraulic conditions performed in steady flow and fixed bed conditions. A total of 150 tests were realized. The details of the piers and the logs are given in the following paragraphs.

The piers were realized in 3D printing with thermo-plastic material. The pier width (W_p) and length (L_p) were defined based on the ratio between pier width and pier length (without cutwater). The ratio was kept constant i.e., $W_p/L_p=0.36$ which corresponds to the most common concrete bridges in the European cities (Figure 4.2, right).
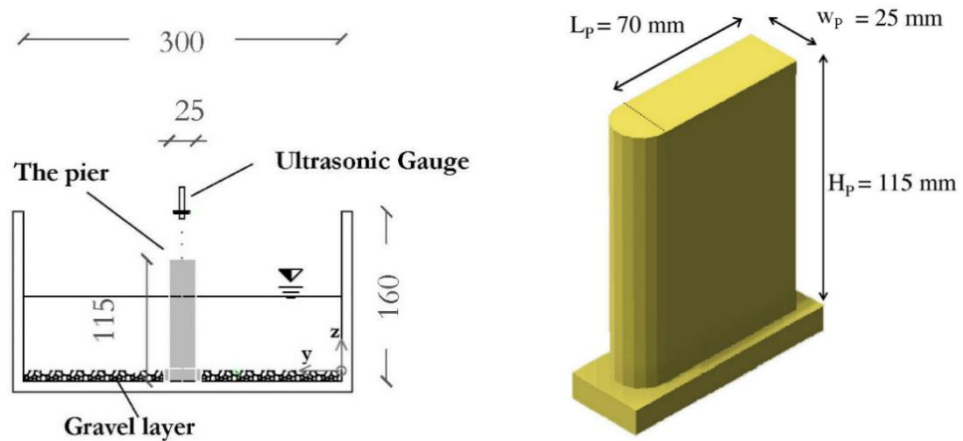
Figure 4.2 Flume cross-section with the pier located in the channel centreline (left, dimensions are in millimetres) and the notation for pier width (Wp) and length (Lp) (right).

Five cutwater shapes that characterize most of the masonry bridges of the historical European cities (such as the Ponte Vecchio in Florence, Wilson Bridge in Tours, and the Concorde Bridge in Paris) were reproduced (*Table 4.2*).

Table 4.2 Pier shape configurations reproduced in laboratory.

Code	Geometry	Figure	Example	w_p/L_p
R0	Square-nose		Tiberio Bridge (Rimini, Italy)	0.40
R1	Round-nose		Ponte Palatino (Rome, Italy)	0.38
R2	Triangular-nose (60°)		Ponte Vecchio (Florence, Italy)	0.34
R3	Ogival-nose		Wilson Bridge (Tours, France)	0.30
R4	Trapezoidal-nose		*Dattaro Bridge (Parma, Italy)*	0.33

The piers were positioned in the middle of the cross section of the channel at about 3 m from the beginning of the flume (Figure 4.1 and Figure 4.2, left).

To reproduce the wooden logs, beech wooden cylindrical dowels with no roots and no branches, were used. Here, the density of wood is an important factor. The wood density for seasoned and dry beech varies in the range 700-900 Kg/m^3. The variation of density, in function of the ability of wood to absorb and to loose water, was tested by Thevenet et al. (1998). They observed the behaviour of log pieces after wetting and drying cycles and they found that after 24 hours of water absorption the initial log mass was doubled. As consequence, the increasing mass induced the reduction of wood motion. For this reason, before each test, the dowels were put in a container filled with water for few minutes, in order to have the same log wet condition for the entire duration of each test.

The wood logs were classified into three length (L_{log}) and diameter (D_{log}) classes (*Table 4.3*): small (dowels length equal to the 20% of flume width), medium (dowels

length equal to the 30% of flume width) and large wood (dowels long as the half of flume width).

Table 4.3 Dowels sizes and classes.

Code	Classes	Length [m]	Diameter [m]	Color	Relative log length (L_{log}/W_p)
SW	Small (L_{log}= 20% flume width)	0.06	0.002	red	2.4
MW	Medium (L_{log}= 30% flume width)	0.09	0.004	yellow	3.6
LW	Large (L_{log}= 50% flume width)	0.15	0.006	green	6
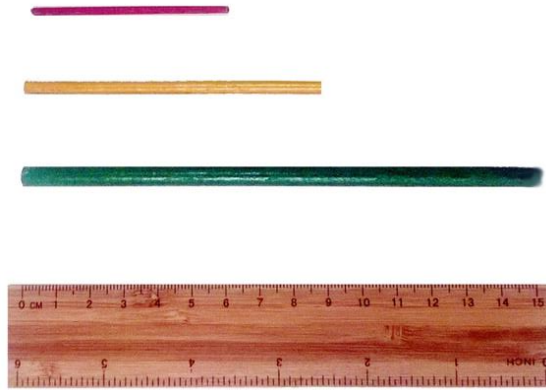
Figure 4.3 Beech wooden cylindrical dowels used in flume experiments.

Two types of wood transport were simulated: uncongested (when logs move without contact between them; each piece of wood can rotate or roll independently of the others) and congested (when the pieces of wood move together as a single mass entering in contact between them) (Braudrick et al., 1997; see Figure 2.3). In the first case, one log each five seconds was introduced in correspondence of the upstream cross-section of the flume, along the centreline and oriented parallel to the flow ($\theta = 0$ rad) for a total of 50 logs. In the last case, the log frequency was 25 logs/20 seconds (*Table 4.4*).

Table 4.4 Composition of logs and transport regimes simulated in the experimental tests.

Code	Transport Regime	Dowels classes	Dowels frequency [logs/s]	Total dowels number
U	Uncongested	SW	1/5	50
C	Congested	SW, MW, LW	25/20 (20SW, 3MW, 2LW)	125

4.3.2 *Measurements*

The recirculating water flow into the flume was regulated by a valve and measured by means of an electromagnetic flow-meter (model Asamag, flow range 0-14 l/s).

The flow velocities were measured in five points along six cross sections upstream of the piers at a distance of 8 cm from the walls (Figure 4.4) and at different depths utilizing a STREAMFLO miniature current flowmeter system designed for measuring low velocities. The measuring head of the instrument consists of a micro-propeller with five bladed rotor mounted on a hard stainless steel spindle. The head is attached to the end of a stainless steel tube connected to an electronic measuring unit via a co-axial cable. The flow velocities in the range could be measured with an accuracy of +/- 2% of true velocity and maximum immersion length of 420 mm.

The water levels were recorded by means of three ultrasonic sensors (USs) Honeywell series 943- F4V-2D-1C0-330E. All the sensors recorded the water level with a frequency of 4 Hz and a maximum error of $\pm$ 1 mm. Two sensors were fixed at the beginning and at the end of the channel, respectively, and one sensor was positioned upstream of the pier (Figure 4.1). The sensors measured the distance between the probe and the water surface continuously along the centreline of the channel. The probes were connected to a PC with a data acquisition system and then the electronic signal was converted into a distance. The data recorded were saved into a PC by means of the software LabView.
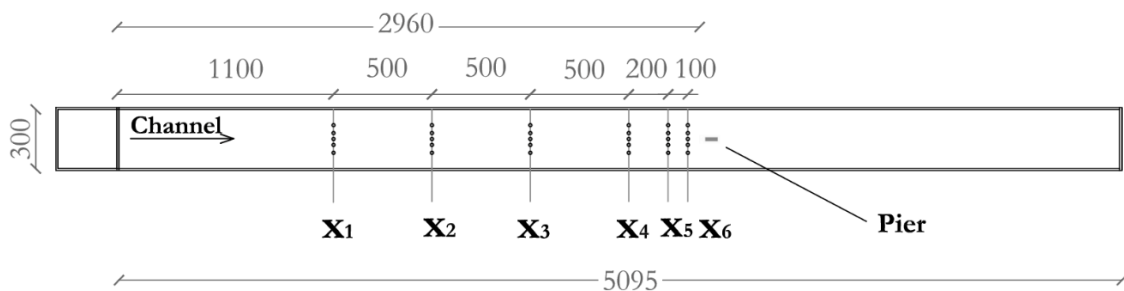
Figure 4.4 Cross sections and points for surface flow velocity measurements.

To visualize the movements of the wooden logs, two cameras were used during the tests. A Canon PowerShot camera, model SX600HS, was positioned at the beginning of the flume, for tracking the dowels movement from the input point to the section in which the pier was positioned. A second camera, a Canon PowerShot model SX230HS, was fixed in correspondence of the pier in order to record the log accumulation formation and the dowels entrapment at the pier. Through the slow motion video analysis, the velocity

of a single floating log has been calculated.   The velocity of the videos was reduced to 10%.

4.3.3   *Flow variables*

The main flow variables were discharge and water levels which are represented by Froude number. In the experiments two Froude numbers of 0.3 and 0.5 were used. These values were based on flow properties of low gradient rivers which are typically characterized by Froude numbers less than one. Wood is transported in rivers mainly during flood events that in low land rivers are often characterized by Froude number lower than one (Gippel et al., 1996). For example, the flow velocity measurements during the flood of the Arno River, in February 2014 (flood event characterized by a discharge of 1280 m^3/s), gave a mean Froude number of 0.6 at the monitoring station, in the urban reach of the river (Francalanci et al., 2016).

Another important flow variable is Reynolds number which was computed using two different regions of the flume, i.e, the walls and the flume bed. To quantify the retaining effect of the walls on the main flow the well-known "Side-Wall Correction" Method of Johnson (1942) with modification from Vanoni (1957) was used. The main assumption is that the cross section can be divided into two sub-sections, one producing shear on the bed and the other shear on the walls; the boundaries between the bed and wall sections are considered surfaces of zero shear and are not included in the wetted perimeters P_b and P_w, being the bed wetted and the wall wetted perimeter, respectively (Vanoni and Brooks, 1957). The Reynolds number for walls (R_w) and bed (R_b) are defined as:

$$Re_w = \frac{4Ur_w\rho}{\mu} \; ; \qquad Re_b = \frac{4Ur_b\rho}{\mu}$$

<div align="right">*(4-2)*</div>

In which r_w and r_b are respectively the hydraulic radius of the walls and the bed, ρ is the density of the fluid (Kg/m^3), μ the dynamic viscosity of the fluid (Kg/m·s).

The application of the foregoing procedure shows the Reynolds numbers of the bed were of the order of $4 \div 5 \cdot 10^4$, that are referred to a fully turbulent flow (for bed friction factor of about $6 \cdot 10^{-2}$ and Moody type diagram for open channels with impervious rigid boundary (Yen, 2002)).

To obtain different hydraulic conditions the discharge and the downstream sluice gate were regulated as specified in the *Table 4.5*.

<div align="center">

Table 4.5 Hydraulic conditions performed in the flume tests

</div>

Code	Discharge [l/s]	Mean surface flow velocity [m/s]	Froude number [-]	Reynolds number [-]	Sluice-gate opening [m]
Q_4	4	0.33	0.5	Re_b =4.21 ·10^4 Re_w =2.92 ·10^4	-
Q_6	6	0.25	0.3	Re_b =5.73 ·10^4 Re_w =2.04·10^4	0.02

.

4.3.4 *Test procedure and blockage probability*

For each pier shape, two Froude numbers (i.e., 0.3 and 0.5) and two wood transport regimes were tested and each test was repeated 5 times for the uncongested transport and 10 times for the congested transport. The total number of tests carried out for each pier configuration was 30. The logs were introduced in the middle of the upstream cross section of the flume and released with a random orientation, close to the water surface in order to avoid flow perturbations.

The duration of a single "uncongested" and "congested" test was respectively, 250 and 100 seconds. A string of characters was associated to every test to identify the main characteristics of the test (see the example in Figure 4.5). For congested transport each test was repeated ten times, obtaining eleven possibilities of blockage probability P=0, 1/10, 2/10,…,1 (see Chapter 3.1). In case of uncongested transport each test was repeated 5 times so six possibilities of P=0, 1/5, 2/5,…,1 derived. P=0 has been assigned when the logs passes the pier and P=1 when the logs stopped at the pier.
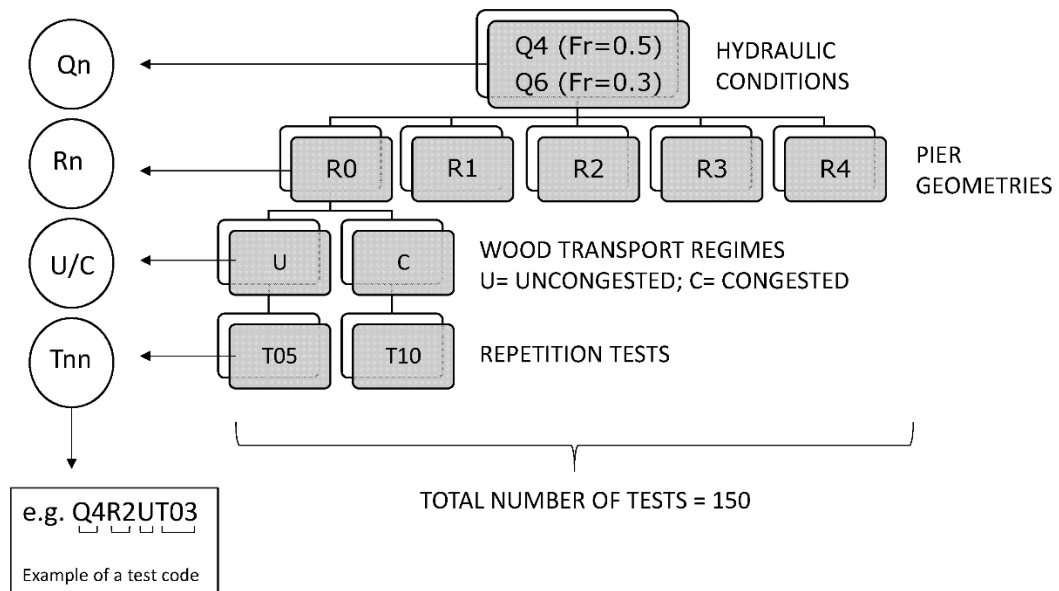
Figure 4.5 Sketch describing the labelling rational for flume tests

4.4   2-D numerical model setup

The 2-D numerical simulations were done using the tool for wood transport developed by Ruiz-Villanueva et al (2014a) and implemented into the two dimensional hydrodynamic numerical model *Iber* (Corestein et al., 2010; Bladè et al., 2012). The rationales of applying the model are:
-   To reproduce the flume experiments.
-   To determine the values of the suggested new pier coefficient depending on different pier shapes.
-   To investigate the correlation between the pier hydraulic-shape coefficient c_{pier} and the blockage probability.

The *Iber* model has three main computational modules: hydrodynamic, turbulence and sediment transport modules. It solves the 2D shallow water equations coupled with

_____

Exner sediment conservation equations and bed/suspended load transport equations. Wood transport is implemented in the model by means of Lagrangian discretization, the hydraulic variables calculated with the hydrodynamic module are used to update the position and velocity of the logs at every time step. The logs are modelled as cylinder with no roots and no branches. To solve the governing equations *Iber* applies finite volume method (FVM) with high-resolution (second order) extension of Roe's upwind scheme. The *model* interface is based on the pre-process and post-process software GID, developed by CIMNE. The various steps in applying the model are

- Define the geometry of the domain: it can be done by generating the geometry using GiD or importing it from another software (e.g., CAD or GIS);
- Specify the initial and boundary conditions
- Modelling the logs
- Simulation runs.
-

4.4.1   *Geometry and model mesh*

The first step involved to create the flume and the piers. The most important phase is the creation of the unstructured numerical mesh to approximate the geometric domain and for Finite Volume Method analysis. The model allows to assign different sizes to mesh for different objects depending on the detail level needed. Higher mesh resolution close to the pier was used (Figure 4.7) to resolve the wood-pier interaction. Furthermore, the mesh size has to be sufficiently fine in relation to the log length (Bladè et al., 2016). This is because, as described in the Appendix (A), the log velocity is calculated at the log centre and both extremities from the water velocity. If the mesh size is larger than the log length, the log centre and extremities fall into the same mesh element, thus, the same velocity is assigned to the three points and the log does not change its orientation making the approximation wrong (Bladè et al., 2016; Figure 4.6). The selected mesh sizes were 0.05 m for the flume and 0.005 m for the piers.
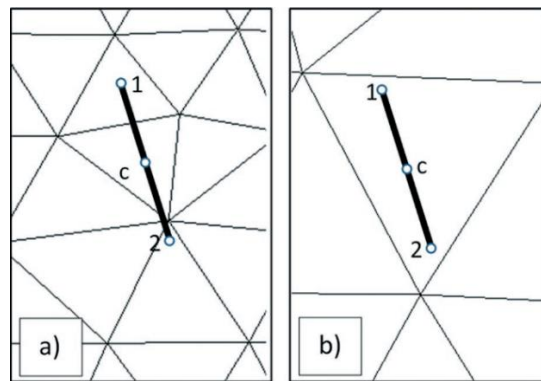
Figure 4.6 Scheme of the log that crosses different mesh elements (a) and that falls into one single element (b). (Source: Bladè et al., 2016).
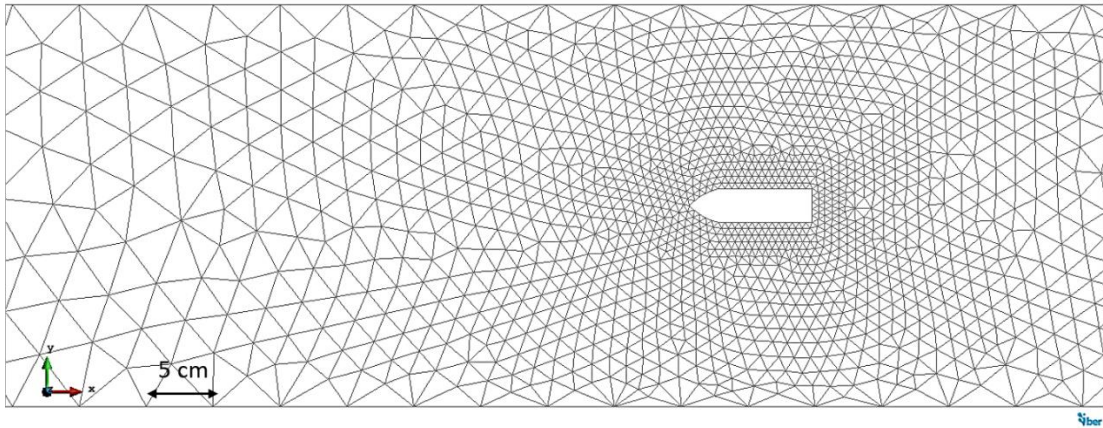
Figure 4.7 Unstructured mesh

4.4.2 *Boundary conditions*

Depending on flow regime, the *Inlet Boundary Conditions* and/or *Outlet Boundary Conditions* were assigned. We reproduced subcritical flow so the discharge and the weir opening at the downstream cross-section were assigned as conditions (*Table 4.6*). The bed roughness, defined as a Manning roughness coefficient, was calibrated and assigned to each element of the mesh and equal to 0.022 s/m$^{1/3}$.

Table 4.6 Setting of the numerical tests (with no wood).

Froude number	Inlet Boundary Condition	Outlet Boundary Condition	Bed Roughness (Manning value) [s/m$^{1/3}$]	Wall Roughness (Manning value) [s/m$^{1/3}$]
0.3	Q= 0.006 m^3/s	Flow condition: SUBCRITICAL Weir opening: 0.027 m	0.022	0.01
0.5	Q= 0.004 m^3/s	Flow condition: SUBCRITICAL Weir totally opened.	0.022	0.01

4.4.3 *Modelling the logs*

The transport of wood was implemented in the model by means of Lagrangian discretization, the hydraulic variables calculated with the hydrodynamic module are used to update the position and velocity of the logs at every time step (for details see Appendix A).

The logs are modelled as cylinder with no roots and no branches.

Numerically, the input parameters for wood are the coordinates of the log centre, the orientation of log respect to the flow, the length and diameter of log, the drag

_____

coefficient and log density (900 Kg/m^3 for wet beech wood). The screen for wood input is shown in Figure 4.8.
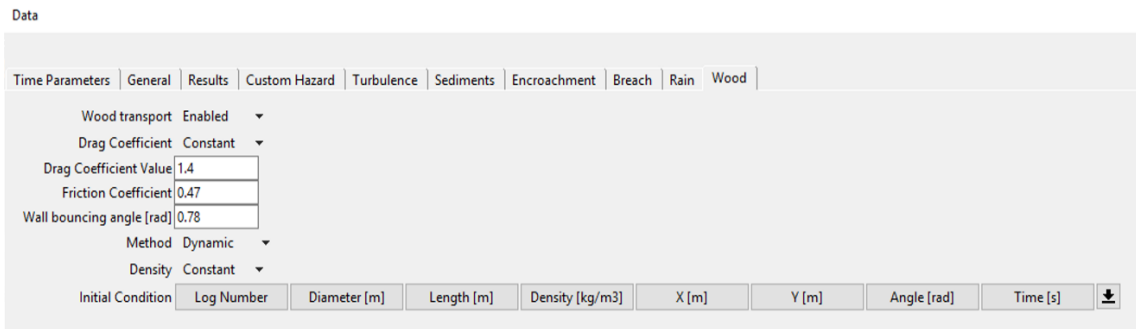
Figure 4.8 Iber screen for wood input parameters.

The two different approaches (dynamic and kinematic) and three different drag coefficient were tested in numerical modelling. The best results were obtained with the dynamic method and Cd=1.4 (according to the results from Bocchiola et al. (2010) for cylindrical and smooth dowels in flume) (see calibration in Chapter 5). The coefficient of friction between the log and the flume bed was assumed by default μ_{bed}=0.47, for dowels with no branches (Buxton, 2010). For the current tests, the friction between wood and bed does not influence the log motion because the floating condition.

Table 4.7 Log motion calibration setting.

Wood drag coefficient C_d	Friction between wood and flume bed μ_{bed}	Log density [Kg/m^3]	Numerical approach for log velocity computation
1.4	0.47	900	dynamic

4.4.4   Simulations

The same typology and number of tests on congested transport done in the flume were reproduced with the numerical model *Iber-Wood*. In the experiments, a group of 25 logs of different sizes was introduced in the flume in correspondence of the upstream cross section and in centreline. In order to reproduce the random position of logs with the numerical model, a random vector of coordinates of log centre in the range values 0.13-0.15 m in x direction and 0.10-0.20 m in y direction, and of orientation respect to the flow (0 <θ>6.28 rad) was generated in *Matlab*. The incidence angle, σ_{cr} ,between log and boundary (see Appendix A), has been set equal to 0.78 rad. The frequency of log impulses was established setting the released time of each log, so the first 25 logs were released at the same time step and then the next 25 logs released 20 seconds later.

As in flume experiments, each numerical test was repeated 10 times and 10 different log position and orientation random configurations were generated because the non-deterministic nature of the problem. The post processing record of each simulation has been analysed in slow motion as for the experimental videos in order to determine the velocity of the log centre.

4.5   3-D model: Flow-3D

Three-dimensional numerical simulations were done using the software Flow-3D (Flow Science, Inc., 2014) with the aim to study the hydrodynamic interaction between wood and bridge pier. The aim was not to calibrate the model for replicating the flume tests as it has been done with the 2D model, but to reproduce the flume hydraulic conditions in order to investigate the 3D flow field, the secondary currents, and the influence of the 3D component of the flow on wood-pier interaction. The main objectives were:

- To reproduce the log-pier interaction to assess the 3D character of the interacting.
- To analyse the path and vertical profile for the log in "uncongested" and "congested" transport modes.
- To evaluate the relation between the drag coefficient and the log orientation with respect to the flow direction for semi-submerged logs.
- To examine the flow field and the secondary currents for both hydraulic conditions reproduced in flume (Fr=0.3 and Fr=0.5).

To reach the objectives, two hydraulic simulations without wood were performed with Fr=0.3 and Fr=0.5 and the 3D turbulence intensity and velocity vectors in the cross-section upstream of the pier compared.

Wood cylindrical dowels with no roots and no branches were modelled and included in the hydraulic simulation with Fr=0.5. Five tests were run, gradually increasing the number of logs (1, 3, 6, 9, 15 logs).

The drag coefficients computed with Flow-3D were compared with the values for submerged logs from literature (Gippel et al., 1992).

The 3D modelling of wood represents the main novelty of the tests presented in this chapter: floating logs in water stream were reproduced as 3D cylindrical moving object characterized by a restitution coefficient for collision e<1 and a friction coefficient at the contact point between logs and between logs and the boundaries.

Model setup

The model setup involved the creation of 3D geometry of the flume, piers and the logs, creating the 3-D mesh, defining the initial and boundary conditions, selecting the sub-models and the numerical variables, and the choosing simulation procedure.

4.5.1   *Geometry and mesh*

The 3D model of the flume, the rectangular pier shape (R0), the gravel bed and the larger logs (L_{log} =0.15 m and D_{log} = 0.006 m) were created with AutoCAD and then each model was converted into STL file format that is readable by Flow3D. The flume bed was reproduced in 3D through a sequence of spheres having diameter equal to the characteristic diameter of the gravel bed D_{50}= 6.81 mm (Figure 4.9).

The gravel bed, depending on the relative submergence $\frac{h}{D_{50}}$, provides flow resistance in terms of form resistance and surface resistance (Bray and Davar, 1987). The former, arises because the difference of pressure between the upstream and downstream surfaces of a single gravel particle (Powell, 2014) and it is accounted in Flow-3D through the generated geometry of the flume bed with the attached half spherical elements. The

_____

latter arises because the roughness of the particle surface that influences the boundary layers normal to the solid surface.
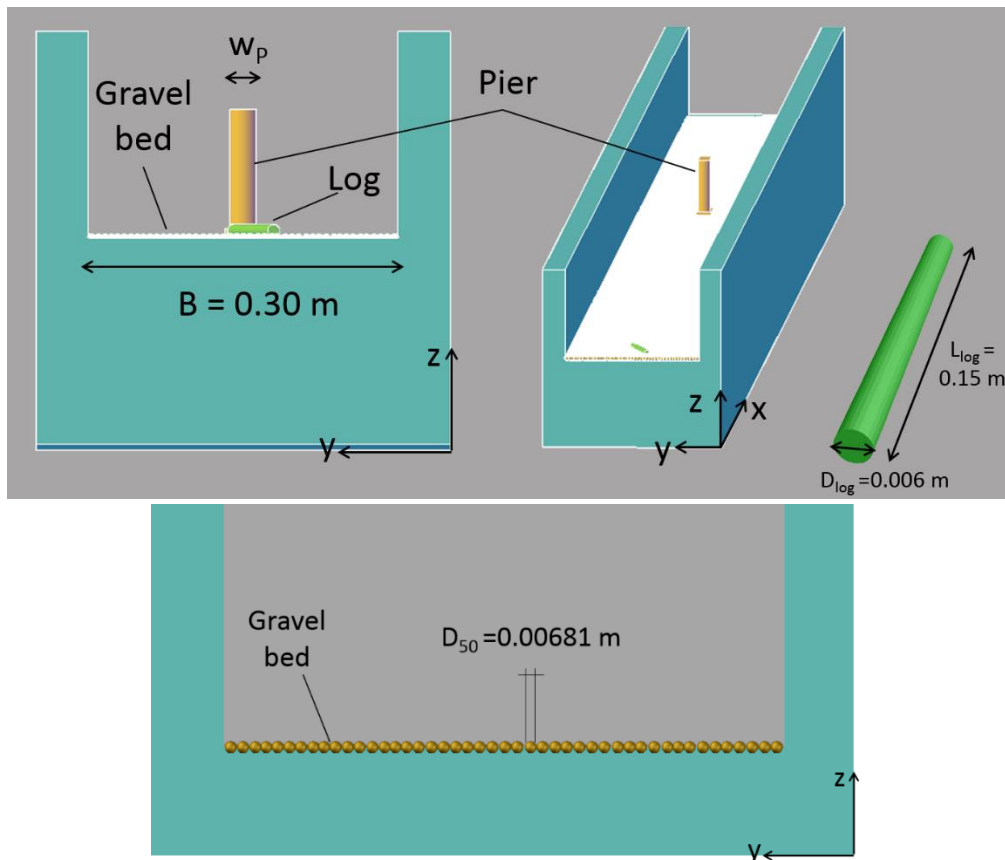
Figure 4.9 Model of flume and detail of the gravel bed.

The used grid size of the structured mesh (structured Cartesian grid) was equal to 0.002 m in all directions (x, y, z). The aim was to have a reasonably good resolution of log geometric defined by the diameter (D_{log} = 0.006 m). The number of grids in x,y,z direction were 750 x 150 x 30, respectively. The total number of meshes was 3 375 000 cells for the simulation with Fr=0.5. For the case Fr=0.3 only the logs were not included.

The mesh grid size of 0.002 m only allowed modelling the larger log (D_{log}=0.006m). Very large number of the mesh was required to model the smaller log that would exceed the available CPU capacity of the workstation. For the same reason we modelled a shorter reach of the flume (1.5 m). Modelling the entire flume length (5 m) means to work with more than 11 million of cells. We selected the flume reach taking into account the steady flow conditions upstream of the pier. The main objective of the 3D simulations was to investigate the wood-pier interaction, thus the selected length of the flume is sufficient to reproduce it.

4.5.2   *Initial boundary conditions*

The upstream boundary condition was defined as volume flow rate with its corresponding water level and the downstream boundary condition was defined with the water level. The modeled reach of the flume was 1.5 m long (from x=2 m to x=3.5 m) out of a total of 5 m and that included only one ultrasonic sensor for water level

measurements (S3 at x=2.7 m from the upstream cross section; see Figure 4.1). The various boundary conditions are listed in *Table 4.8*.

Table 4.8 Hydraulic characteristics of the 3D simulation and calibration of the model.

Discharge [m^3/s]	0.004	0.006
Froude number	0.5	0.3
Upstream boundary condition	$h_{x=2m}$ = 0.0474 m Q = 0.004 m^3/s	$h_{x=2m}$ = 0.0808 m Q = 0.006 m^3/s
Downstream boundary condition	$h_{x=3.5m}$ = 0.0418 m	$h_{x=3.5m}$ = 0.0783 m
Measured water level at sensor S1 (x=2.7m)	$hobs_{x=2.7\,m}$ = 0.045 m	$hobs_{x=2.7\,m}$ = 0.077 m
Calculated water level at x=2.7 m	$hpred_{x=2.7\,m}$ = 0.0455 m	$hpred_{x=2.7\,m}$ = 0.0761 m
Water level difference at x=2.7 m $\lvert y_{obs} - y_{pred} \rvert$	0.0005 m	0.0009 m

4.5.3 *Modelling the logs*

The logs were modeled as GMO (General Moving Object). The GMO model has two numerical methods to treat the interaction between fluid and moving objects: an explicit and an implicit method. If no coupled motion exists, the two methods are identical. For coupled motion (see Appendix B), the explicit method, in general, works only for heavy GMO problem, i.e., all moving objects under coupled motion have larger mass densities than that of fluid and their added mass is relatively small. The implicit method, however, works for both heavy and light GMO problems. A light GMO problem means at least one of the moving objects under coupled motion has smaller mass densities than that of fluid or their added mass is large (Flow Science, Inc. 2014). For the current tests, the implicit method was used. For the GMO's motion constraints, 6 Degrees of Freedom were set. The collision model was activated: we assigned 0.2 to the coefficient of restitution and 0.95 to the friction at the point of contact during collision. The log mass density was set to 900 Kg/m^3. The log characteristics and parameters used in Flow-3D are summarized in *Table 4.9*.

To correctly reproduce the release of the logs at the upstream of the modeled flume reach, a control upward force equal to the log weight W_{log} (Equation (4-3) was applied to each log at the initial time step of the simulation and then the load was removed (setting it to zero) to release the log into the upstream water surface as schematized in Figure 4.10. The logs were released parallel to the flow direction in order to analyze how the log orientation changes approaching the pier and increasing the number of logs. Furthermore, the method used to release the logs does not allow the logs to be overlapped when they are released and thus to reproduce the logs input as in flume experiments. The method allows the input of logs in the form of carpet of multiple logs, thus one layer of parallel logs was reproduced (Figure 4.11).

_____

$$W_{log} = g \cdot \rho_{log} \cdot L_{log} \cdot \frac{\pi D_{log}^2}{4}$$

Table 4.9 Log parameters adopted in 3D numerical simulation with Flow-3D.

Log length [m]	0.15
Log diameter [m]	0.006
Log density [Kg/m³]	900
Restitution coefficient	0.2
Friction coefficient in collision	0.95
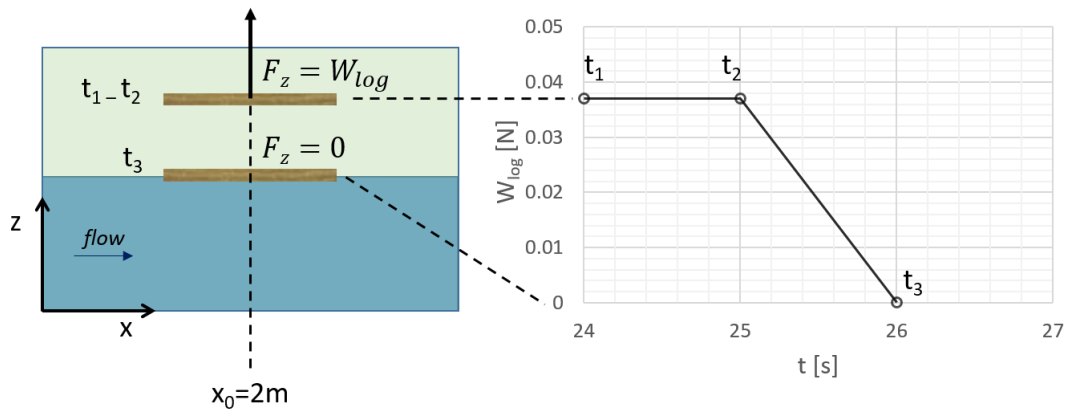
Figure 4.10 Scheme of the control upward force applied to the log to reproduce the log release according to the experimental tests.

4.5.4   *Simulation procedures*

Five tests on wood transport and their interaction with the central rectangular pier (R0) were done with Fr=0.5 and one log size (large log), gradually increasing the number of logs from 1 to 15 (see Figure 4.11). Only one log size was reproduced because, as specified in Section 4.5.1, the 3D tests were finalized to better understand the influence of the 3D component of the flow on wood-pier interaction and not to reproduce the flume experiments as in 2D numerical modelling.
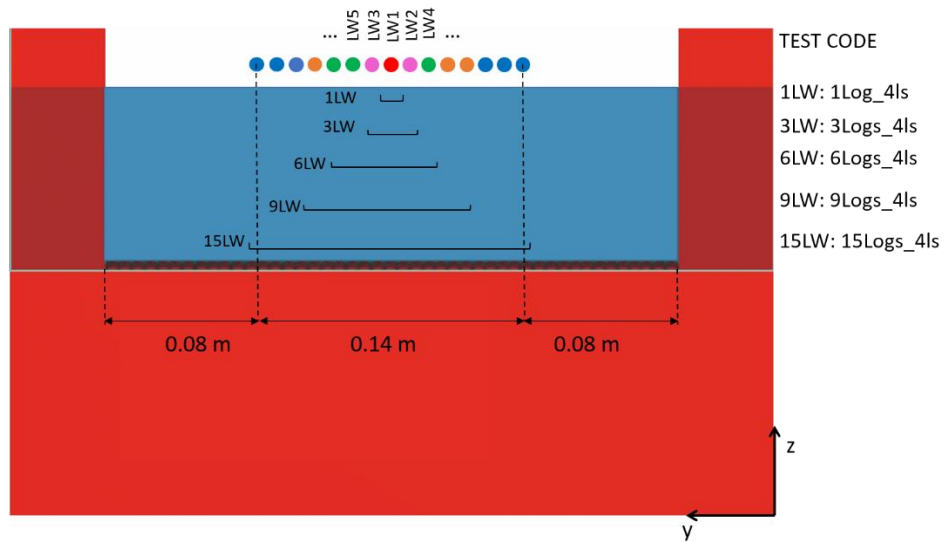
Figure 4.11 Scheme the 3D numerical tests and number of logs.

Each new log simulation was created as a *Restart file of the previous simulation* The duration of the simulation was 25 seconds so the restarting simulation started from $t_s = 24$ s. One log took 5 seconds, from the releasing time to cover the flume reach 1.5 m long, so the log moved with the velocity $U_{log} = 0.3$ m/s, that is in agreement with the velocity of the log centre measured from the video recording (observed $U_{log} = 0.33$ m/s).

5   Results

The chapter presents the experimental and numerical results for both 2-D and 3-D models. The main focus of the experiments was the determination of blockage characteristics based on Equation (3-37) and (4-1).

5.1   Experiments

The experimental results were used to compute different probabilities as explained in the following paragraphs. The probabilities are computed separately for the variables listed in Equation (4-1) (Q_{log}/Q_{flow}, L_{log}/w_p…).

5.1.1   *Blockage probability B vs. ratio of log discharge Q_{log} to the flow discharge Q_{flow}*

Figure 5.1 illustrates that P is higher in congested than in uncongested wood transport. In the first case the flatter pier shapes, as the square (R0) and the trapezoidal (R4), were the most critical for wood accumulation for both Froude numbers. The highest blockage probability was observed for the flat pier shape and Fr=0.5: in nine cases out of ten the logs stopped at the pier at the end of the tests. The pier shape less prone to "capture" logs was the Ogival one, for which blocking probability equal to zero for both wood transport regimes and all hydraulic conditions.

For uncongested transport the higher blocking probability was observed at lower flow velocity condition (i.e., Fr=0.3) and with the trapezoidal pier shape (R4). For the same hydraulic conditions, no logs stopped at the other four pier shapes. For Fr=0.5 the logs stop only at the flatter pier shapes: 4 times out of 10 at the square pier shape (R0) and two times out of ten at the rounded (R1) and trapezoidal (R4) piers. Wood discharge clearly affects the blockage probability, in congested transport the logs are in contact between them and there is not enough space for a single log to rotate and thus the collision with the obstacle may result in blockage. When a single log moves approaching the pier, it may collide and after collision it may undergo a greater rotation, because the absence of close logs, and flow away. When the logs stop at the pier, they tend to accumulate assuming the shape of the pier (see Figure 5.2).
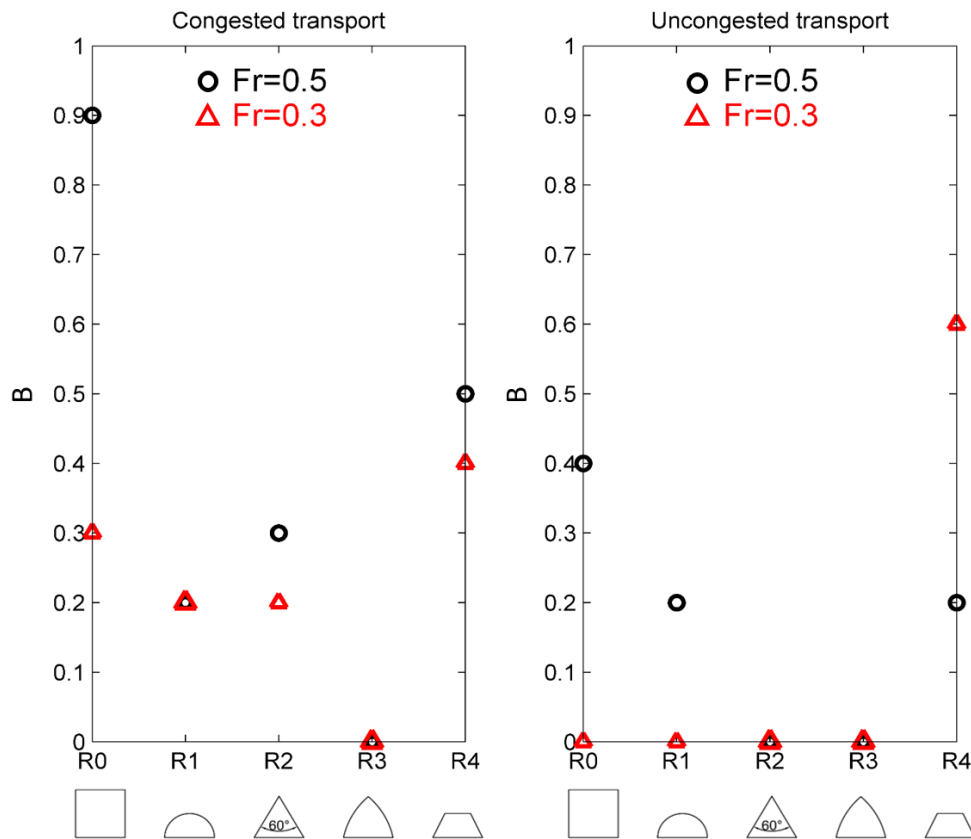
Figure 5.1 Blockage probability for congested and uncongested wood transport, different pier shape configurations and Froude numbers.

Figure 5.2 Wood accumulation at the triangular pier shape in flume experiments (a), and in the real case (b) of the Ponte Vecchio in Florence after the flood of November 2016.

5.1.2 *Blockage probability B vs. ratio of log length L_{log} to the pier width w_p*

The blockage probability (B) plotted versus the relative log size (L_{log}/w_p) (Figure 5.3), shows that, even if large logs (L_{log}/w_p=6) are less frequent (8% of the total logs versus the 80% of the small logs), the probability to block at the pier is relatively high (e.g. the flat pier shape and Fr=0.5) and frequent (e.g. for Fr=0.3 large logs blocked in correspondence of four pier shapes on five).
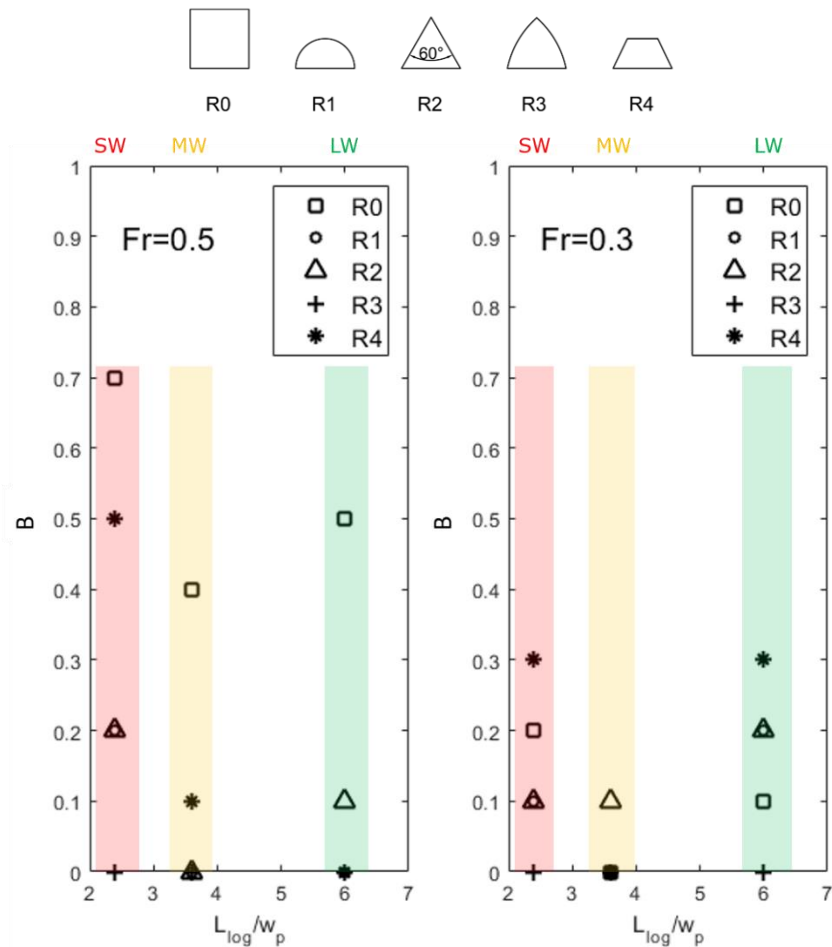
Figure 5.3 Blocking probability versus L_{log}/w_p for Fr=0.5 and Fr=0.3.

For higher flow velocity, i.e., Fr=0.5 all log sizes stopped at the flat pier shape (R0) while at the rounded pier shape (R1) only the small logs blocked and the large logs got stuck at the flat (R0) and triangular (R2) pier. No logs stopped at the Ogival pier (R3) for both hydraulic conditions.

In case of lower flow velocity (Fr=0.3) the highest probability for small and large logs was observed for the trapezoidal pier shape (R4), as shown in Figure 5.3. All logs size stopped only at the triangular pier (R2) while the large and small logs stopped at all pier shapes except for the Ogival (R3). For logs with the same length, e.g. the small logs, the blockage probability is higher when the flow velocity is higher (Fr=0.5). This is not valid for medium and large logs for which, in most cases, the blockage probability is higher at lower flow velocity (Fr=0.3) than at higher flow velocity (Fr=0.5).

5.1.3 *Logs accumulation size*

The volume of logs accumulations at the pier at the end of each test has been calculated from the number of blocked logs for each class size. The results are illustrated in Figure 5.4. The volume of wood accumulation increases with the increasing wood discharge, and thus for congested transport regime, except for few cases, i.e. the Ogival (R3) and semi-circular (R1) pier shapes. For both Froude number and congested

transport regime, the lower volumes of wood accumulation occurred at the semi-circular (R1) and Ogival (R3) pier shape. For uncongested transport regime, a low number of logs accumulates at the flat pier shape and for Fr=0.5.
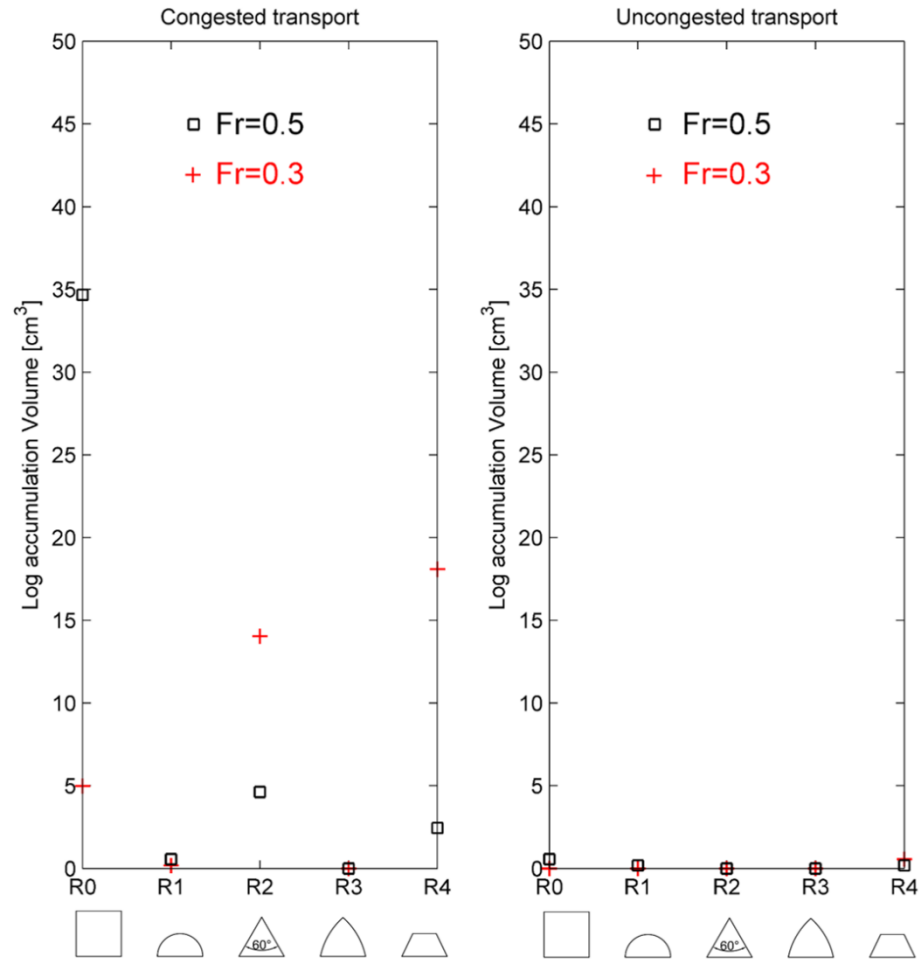
Figure 5.4 Log accumulation volume [cm³] at bridge piers for congested and uncongested wood transport, different pier shape configurations and Froude numbers.

Figure 5.5 shows the ratio between the logs accumulation volume and the total volume of logs introduced in the flume during each simulation. More than half of the floating logs volume accumulated at the flat pier shape (R0) for Fr=0.5. In congested transport regime 3 times out of 10, more than 20% of transported logs volume accumulated at the bridge pier, while for uncongested transport in all cases less than 10% of the total logs volume accumulated at the pier.
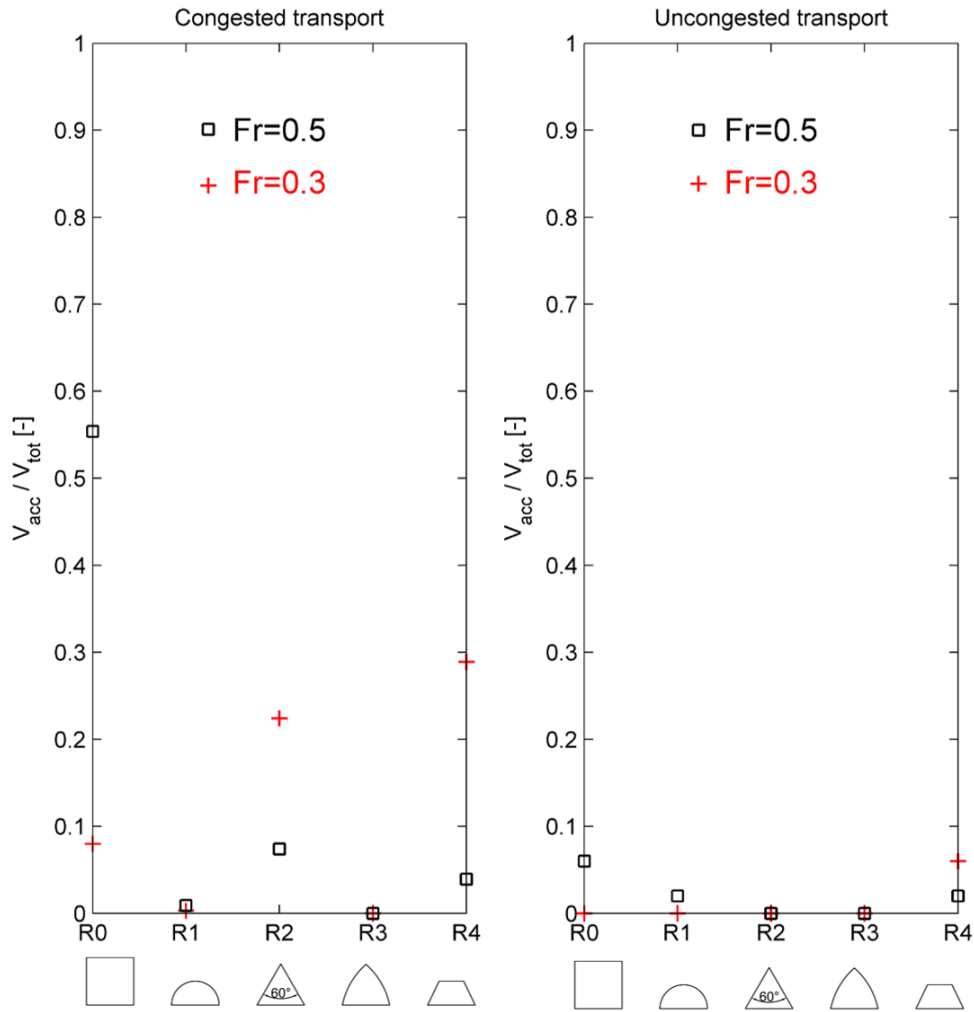
Figure 5.5 Log accumulation volume (V_{acc}) relative to the total volume of the released logs (V_{tot}) for congested and uncongested wood transport, different pier shape configurations and Froude numbers.

5.1.4 *Effective (EA) and Potential (PA) Accumulation*

The blockage probability B given by Equation (4-1) represents the probability of logs to block or not at the pier at the end of each test, without taking into account the number of logs. In order to analyse the influence of the flow field on log motion and, as consequence, on the accumulation at the bridge piers, we investigated also the probability of logs to touch or not the pier (PA) and the probability of logs to block or not at the pier (EA), taking into account the number of logs.

As described in detail in the section 3.1, the main difference between the minimum and maximum blockage probability is that, in the first case only the blocked logs at the pier were counted after each test (EA = Effective Accumulation). In the second case, only the logs that touched the pier after each impulse (but not necessarily stopped) were considered (PA= Potential Accumulation).
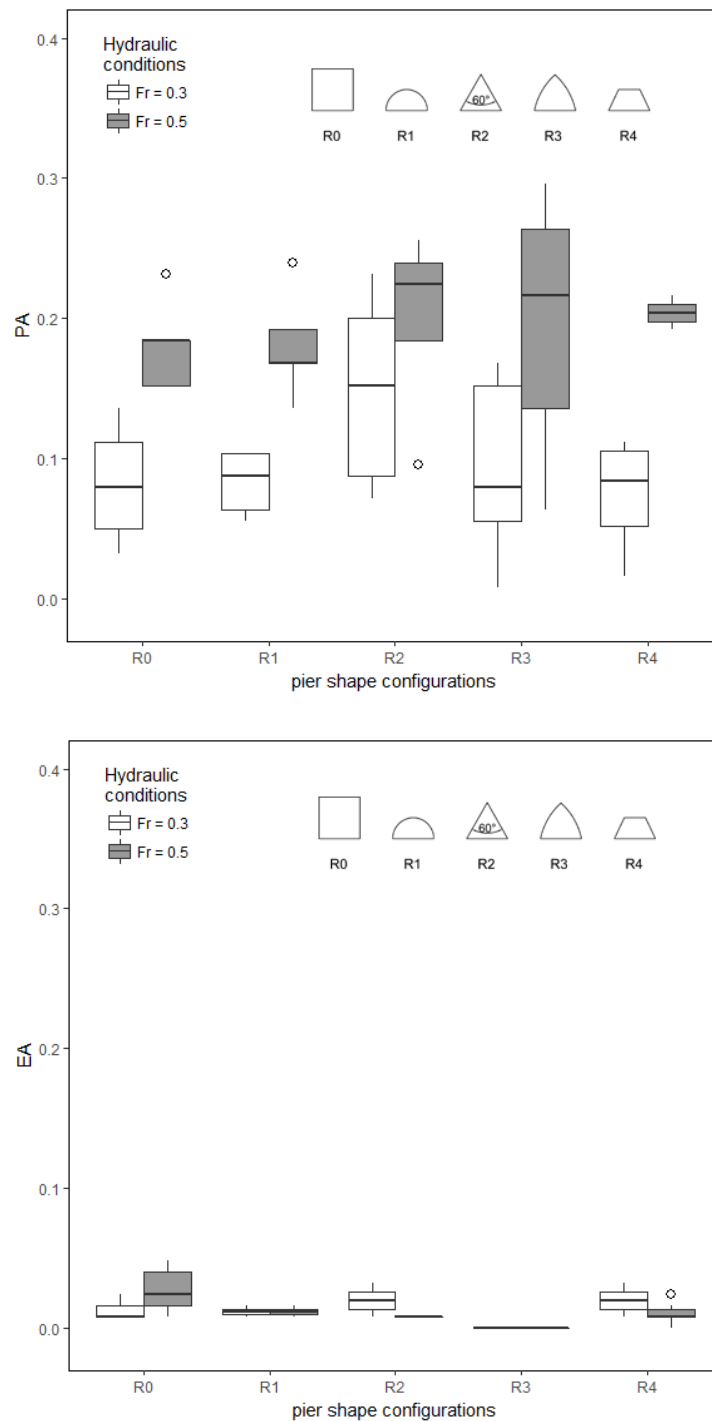
Figure 5.6 Potential (upper panel) and Effective (lower panel) Accumulation for different pier shape configurations and Froude numbers in congested transport regime.

Figure 5.6 shows that the most critical conditions for "effective" wood accumulation are Fr=0.5 and flat pier shape (R0) while the least critical are Fr=0.3 and Ogival pier shape (R3), both for minimum and maximum blockage probability.

However, high values of "Potential Accumulation" (PA) do not necessary correspond to high values of "Effective Accumulation" (EA). For Fr=0.5 and Fr=0.3 the highest mean value of PA was obtained in presence of the triangular pier shape (R2) while the mean highest value of EA for Fr=0.5 and flat pier shape (R0). This means that

_____

probably the pier shape plays an important role in logs entrapment, so even if a large number of logs touch the pier, the pier shape and the flow field around the pier favour or not the sliding of logs downstream to the pier (as in the case of Ogival pier shape, R3).

5.1.5   *Blockage probability B vs. Froude number Fr*

Figures Figure 5.1 and Figure 5.3 show that in most cases analysed, the blockage probability is higher at Fr=0.5 than at Fr=0.3.

In order to investigate how the flow velocity and thus the Froude number affect the log motion and consequently the blockage probability, the flow velocity distribution measured in the cross-sections along the flume has been compared with the logs trajectory observed in flume.

The measured flow velocity distribution (red and black dots in Figure 5.7) shows that for Fr=0.3 (black dots) the velocity distribution at a cross section is rather flat, the entire fluid flows at the same velocity value. For Fr=0.5 (red dots) the velocity distribution is more like a parabolic distribution in shape with the maximum velocity at the centre. This means the floating logs following the flow are more prone to be more spread out in the first case (grey area in Figure 5.7) and to move along the centreline in the second case (red area in Figure 5.7) likely due to the formation of secondary currents more pronounced in one case than the other. In the latter case, the logs move mainly in the centreline having a greater probability to touch the central pier (see red segments in Figure 5.7).
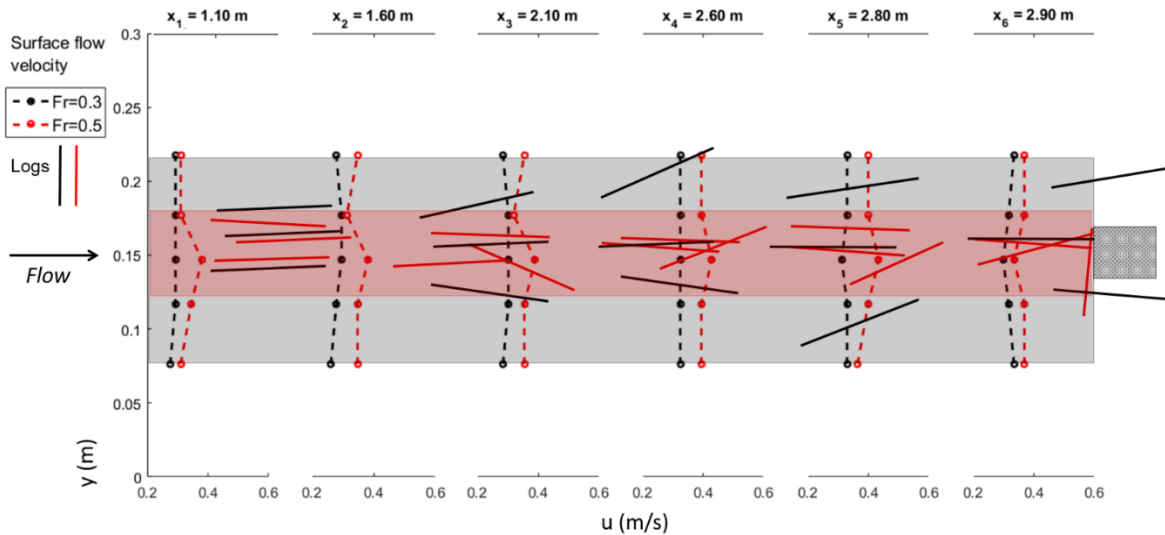
Figure 5.7 Scheme of the log movement observed in flume experiment in case of Fr=0.5 and Fr=0.3.

Figure 5.8 shows the sketch of the main experimental results.
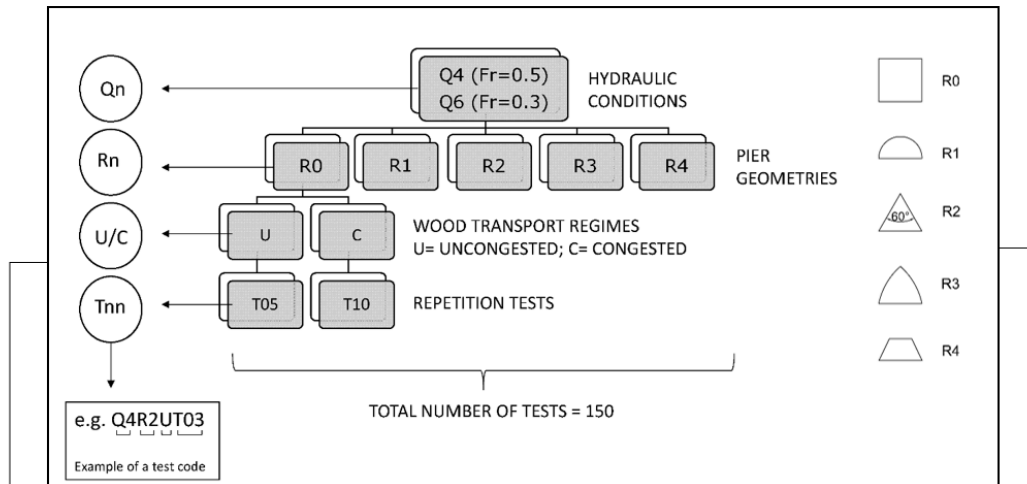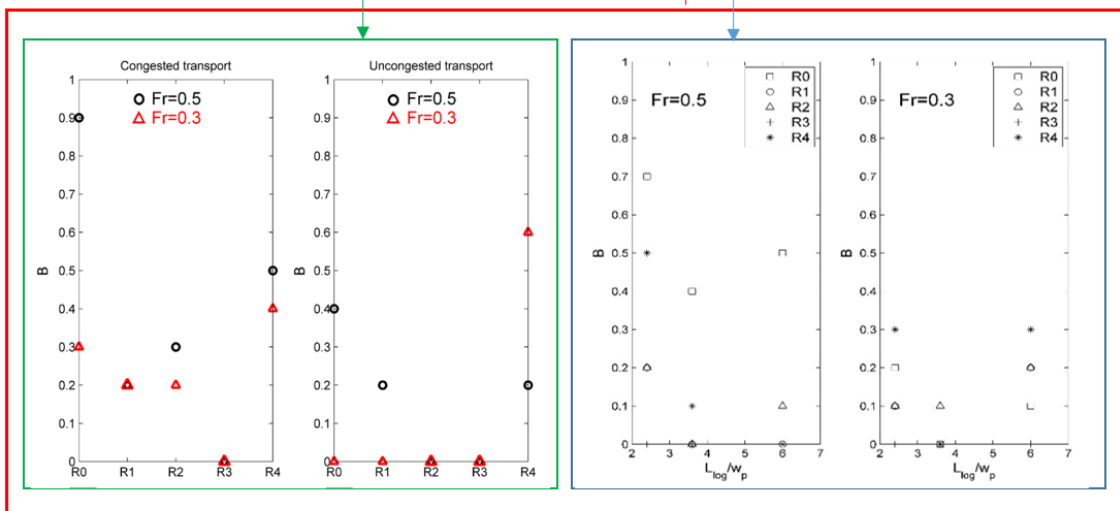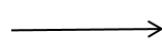
Figure 5.8 Graphical summary of the experimental results.

_____

5.2   2D- numerical model

First step in the application of the 2-D model was calibration of flow and log transport. The following paragraphs presents the respective details.

Figure 5.9 shows an example of the *Iber-Wood* model output: in white is represented the pier (in this case is the Ogival pier) and the black lines are the logs.
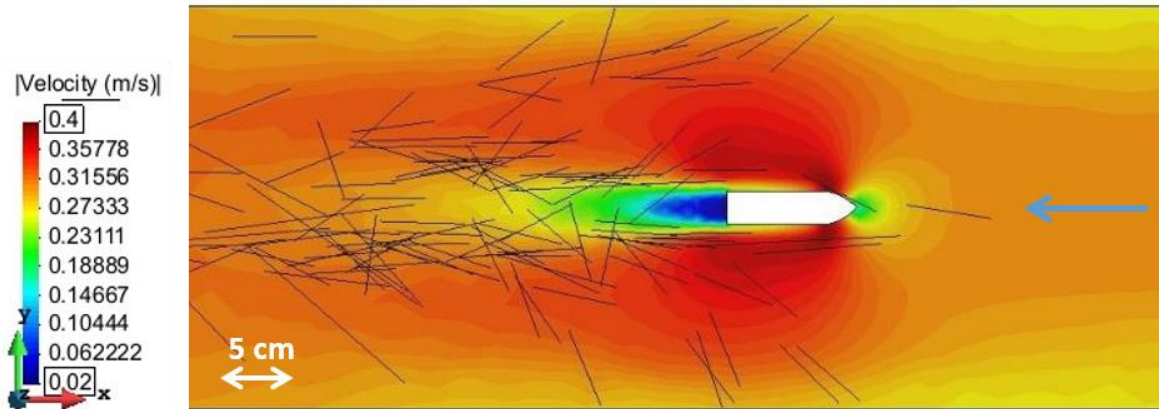
Figure 5.9 Example of the log movement in the flume predicted by the 2D numerical model Iber.

5.2.1   *Hydraulic- Model calibration*

We compared the water depth measured in the flume at the gauging stations indicated with S1, S2, S3 in Figure 4.1 and the depth averaged flow velocity measured along the cross sections X_1, X_2, X_3, X_4, X_5, X_6 as indicated in Figure 4.4, with the numerical values. The results are represented in Figure 5.10 (a,b).

The comparison between the measured and calculated water depths (Figure 5.10, a) shows that all data points fall close to the line with gradient of unity (the dashed line). The water depth has a correlation coefficient of 0.87 (R^2=0.75) for Fr=0.3 and 0.97 (R^2=0.95) for Fr=0.5.

The measured over numerical depth averaged flow velocities indicate that all points fall inside the ±25% range of variation (dotted lines) relative to perfect agreement (dashed line). The correlation coefficient is of 0.75 (R^2=0.57) for Fr=0.5 and 0.24 (R^2= 0.06) for Fr=0.3, the MAE and RMSE are very low ($\cong 10^{-2}$) in both hydraulic conditions.

The details on deviations are given in the discussion section.

In Figure 5.11 the depth-averaged flow velocities calculated with the power law velocity distribution method from the vertical velocities data points, are compared with the numerical values for both Froude numbers and at different cross sections. The velocity is measured at distance of 8 cm from the walls in order to avoid the wall-effect on the flow velocity field.

While the depth averaged flow velocity computed numerically is uniformly distributed along each cross-section for both Froude numbers, the measured velocity distribution changes with the Froude number. In case of Fr=0.5 (lower panel in Figure 5.11) the flow velocity is higher in the centreline from x=1.10 m to x= 2.60 and it decreases when the flow approaches the pier (x=2.80-2.90). For Fr=0.3 the flow moves with the same velocity along the cross section, the shape of velocity distribution is flat.

(a)

(b)
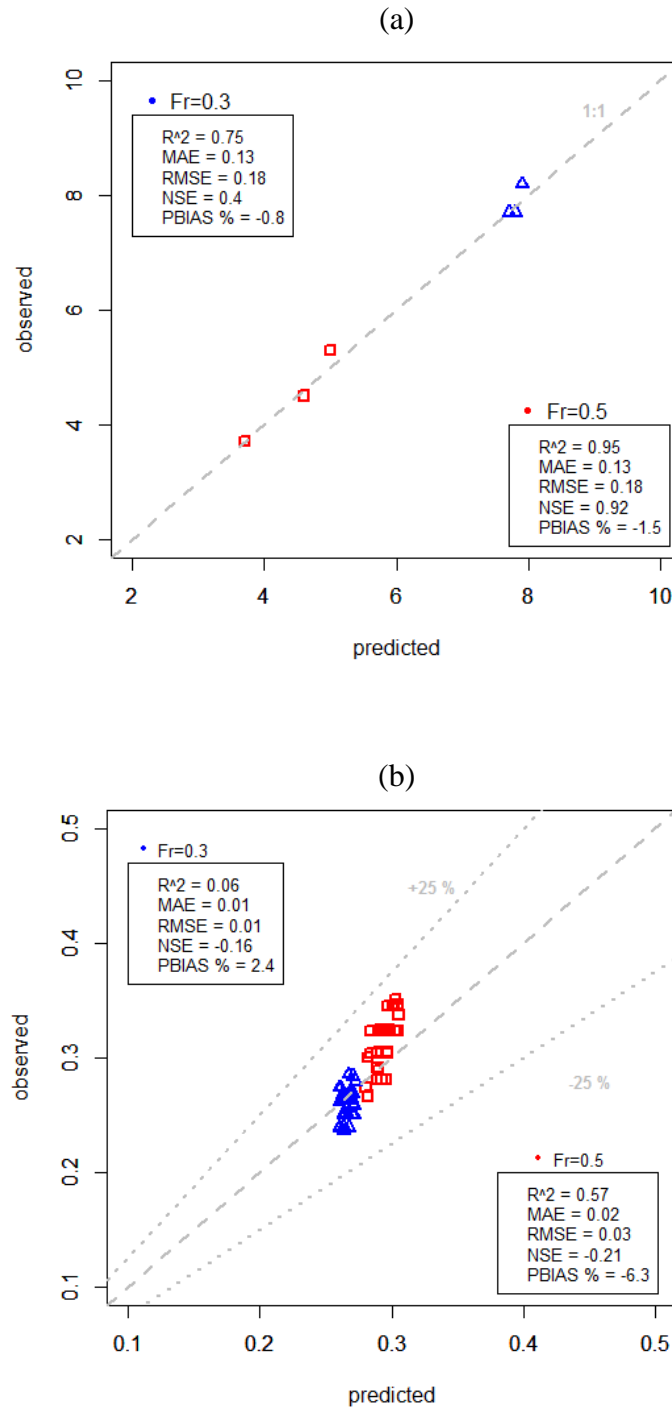
Figure 5.10 Comparison between the predicted and observed values of flow depth, expressed in cm (a) and depth averaged flow velocity, expressed in m/s (b)
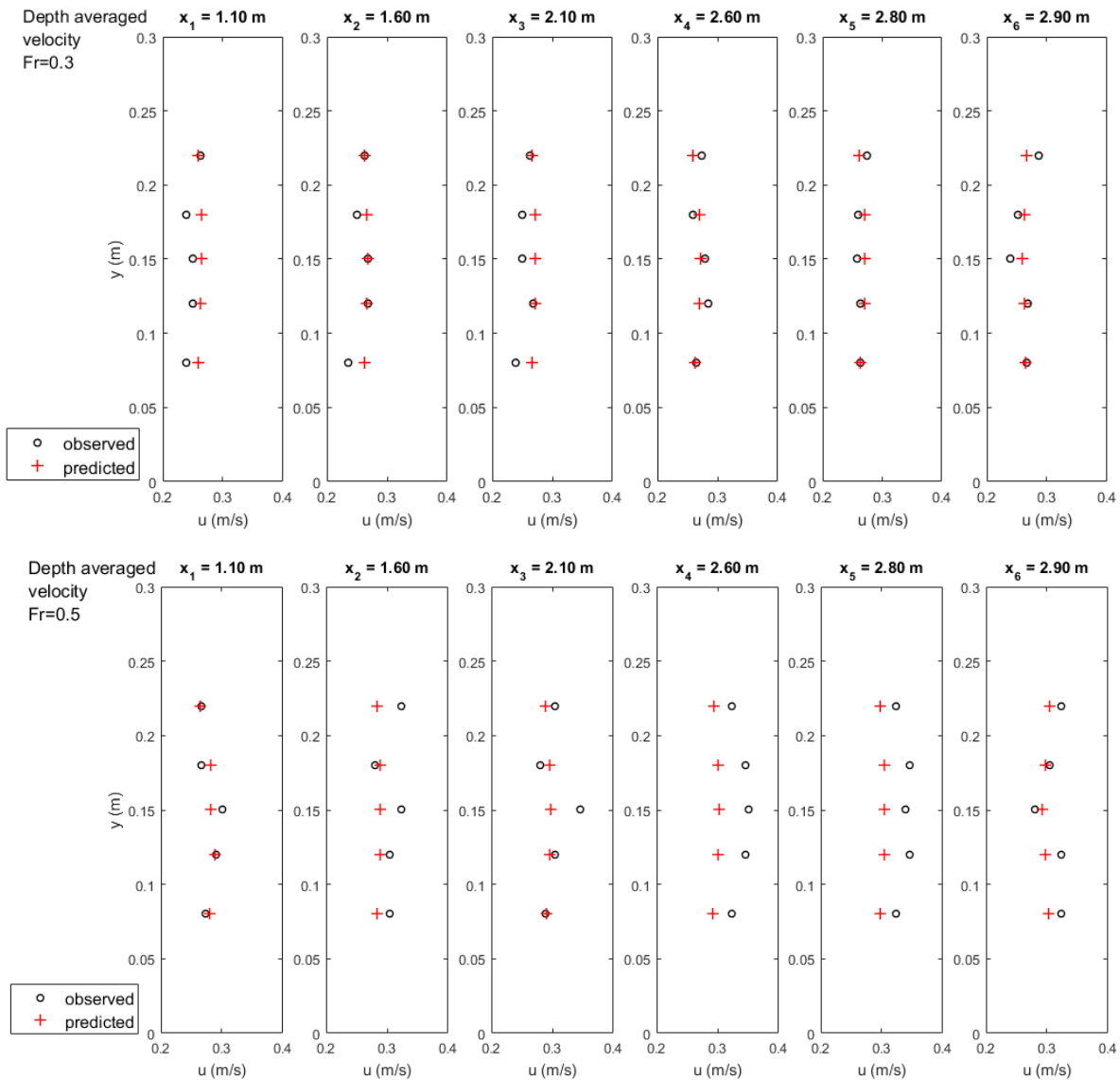
Figure 5.11 Measured depth averaged flow velocities and calculated with numerical model along six cross sections for Fr=0.3 (upper panel) and Fr=0.5 (lower panel).

5.2.2 *Log motion calibration*

The aim of calibration of log motion was to find the optimal values of drag coefficient for determining the advection velocity of the log centre point by the model. Here two different approaches were chosen i.e. kinematic or dynamic approach. In the kinematic approach, the log velocity is calculated based on the transport regime. Log density, log diameter and water depth are used to calculate the transport regime: e.g. in floating condition the log velocity is equal to flow velocity. In the dynamic approach, the log velocity is calculated at each time step starting from the equations for log movement.

Figure 5.12 compares the results for these approaches for Fr=0.5.

The computed log centre velocities by the numerical model were compared through the slow motion analysis of videos recorded during each experiments and the post-processed video from numerical tests.

As mentioned in Chapter 4.4.3 and as shown in Figure 5.13, the best results were obtained with the dynamic method and drag coefficient (Cd) 1.4.
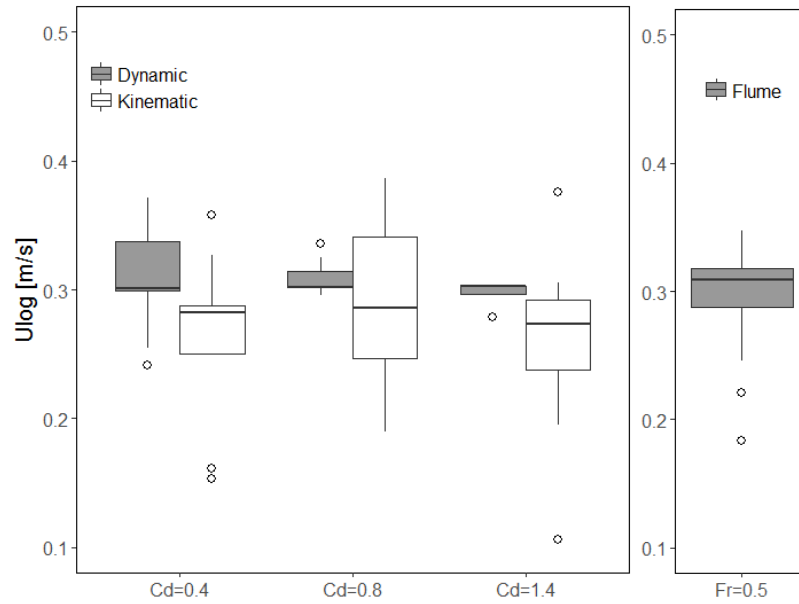
Figure 5.12 Comparison between the experimental (right) and numerical values (left) of log centre advection velocity at Fr=0.5 using two different numerical approaches.
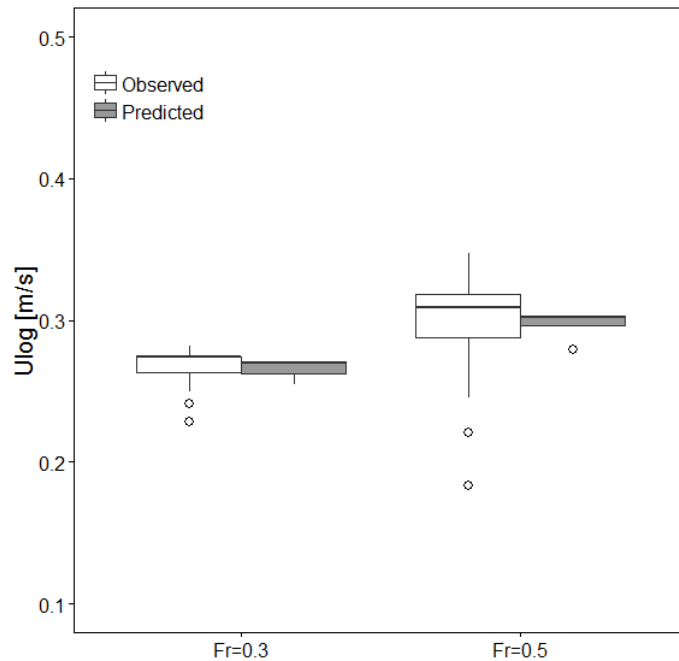
Figure 5.13 Boxplot of the velocity of log centre in flume and numerical tests for both Froude numbers obtained with the dynamic method for computing the log centre velocity and C_d=1.4.

_____

5.2.3 *Potential Accumulation (PA)*

The comparison of the Potential Accumulation (PA) obtained through numerical *Iber* simulations and experiments for different pier geometrical configurations showed different results for Fr=0.3 and Fr=0.5. In the former case (Figure 5.14) all points fall outside the ±20% range of variation. The residuals (difference between the observed PA and predicted PA) are negative; this means that the *Iber* numerical model overestimates the PotentialAccumulation.

In the latter case of Fr=0.5 (Figure 5.15) the numerical model fits well the experimental data, all points fall within the ±20% range of variation (dotted lines) relative to perfect agreement (dashed line), in particular between the line 1:1 and the line +20% of variation. The residuals are positive but anyway close to zero, thus the numerical model slightly underestimates the experimental PotentialAccumulation .

The Nash-Sutcliff efficiency coefficient (NSE) indicates how well the plot of observed versus simulated data fits the line of perfect agreement: values close to the unit indicate a good fitting. For Fr=0.5 NSE is -1.77 while for Fr=0.3 is -14.26 (see also *Table 5.1*). The Root Mean Square Error (RMSE) shows is the model performance for Fr=0.5 (RMSE=0.02) respect to Fr=0.3 (RMSE=0.11). The main model evaluation statistics, for both hydraulic conditions, are listed in *Table 5.1*.

The boxplots of the numerical and experimental PA plotted for both Froude numbers (Figure 5.16) highlight the overestimation of the model in comparison with the flume experiments for Fr=0.3.

In numerical tests, no logs blocked at the pier at the end of the numerical tests, for this reason only the PA has been used for comparison with *Iber* model results. This aspect will be discuss in the Discussion section.

Table 5.1 Model evaluation statistics values obtained from the comparison between experimental and numerical tests.

Symbol	*Range value*	*Fr=0.3*	*Fr=0.5*
R^2 (coefficient of determination)	$(0 \div 1)$ 1= optimal value	0.31	0.42
MAE (mean absolute error)	0=perfect fit	0.1	0.01
RMSE (root MEA)	0=perfect fit	0.11	0.02
RSR (RMSE-observations standard deviation ratio)	$(0 \div +\text{inf})$ 0=perfect fit	3.49	1.49
NSE (Nash-Sutcliffe efficiency)	$(-\text{inf} \div +1)$ 1=optimal value	-14.26	-1.77
PBIAS (%) (percentage bias)	0=perfect fit + overestimation bias - underestimation bias	107.1	-7.5
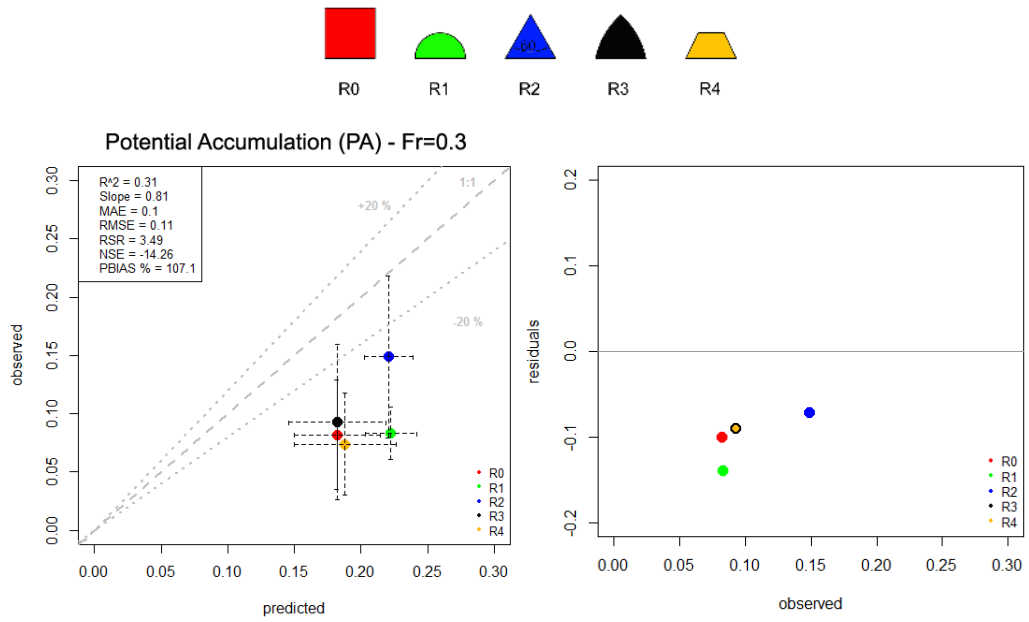
Figure 5.14 Comparison between the Potential Accumulation (PA) of wood at different pier shapes in flume and in numerical tests (left) for Fr=0.3 and residuals of the data (right).
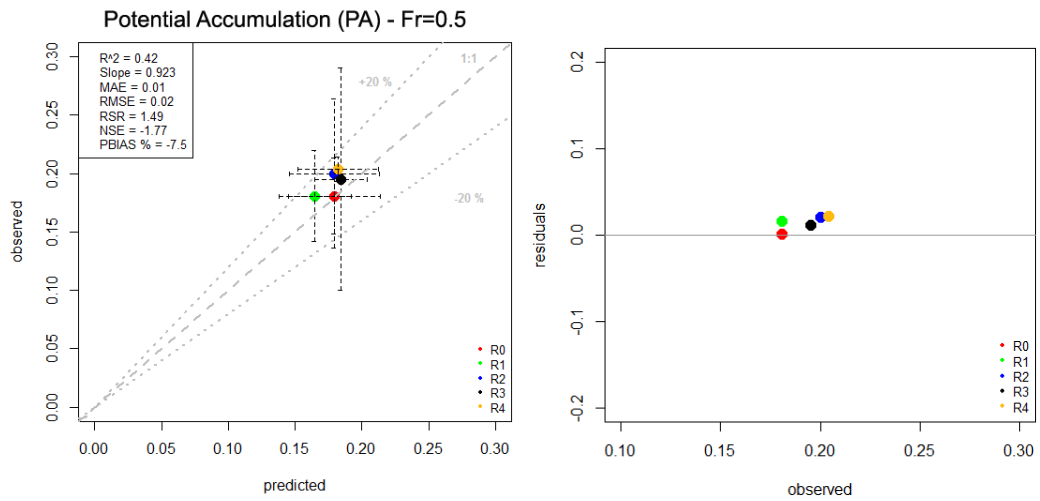
Figure 5.15 Comparison between the Potential Accumulation (PA)of wood at different pier shapes in flume and in numerical tests (left) for Fr=0.5 and residuals of the data (right).

_____

(a)

(b)
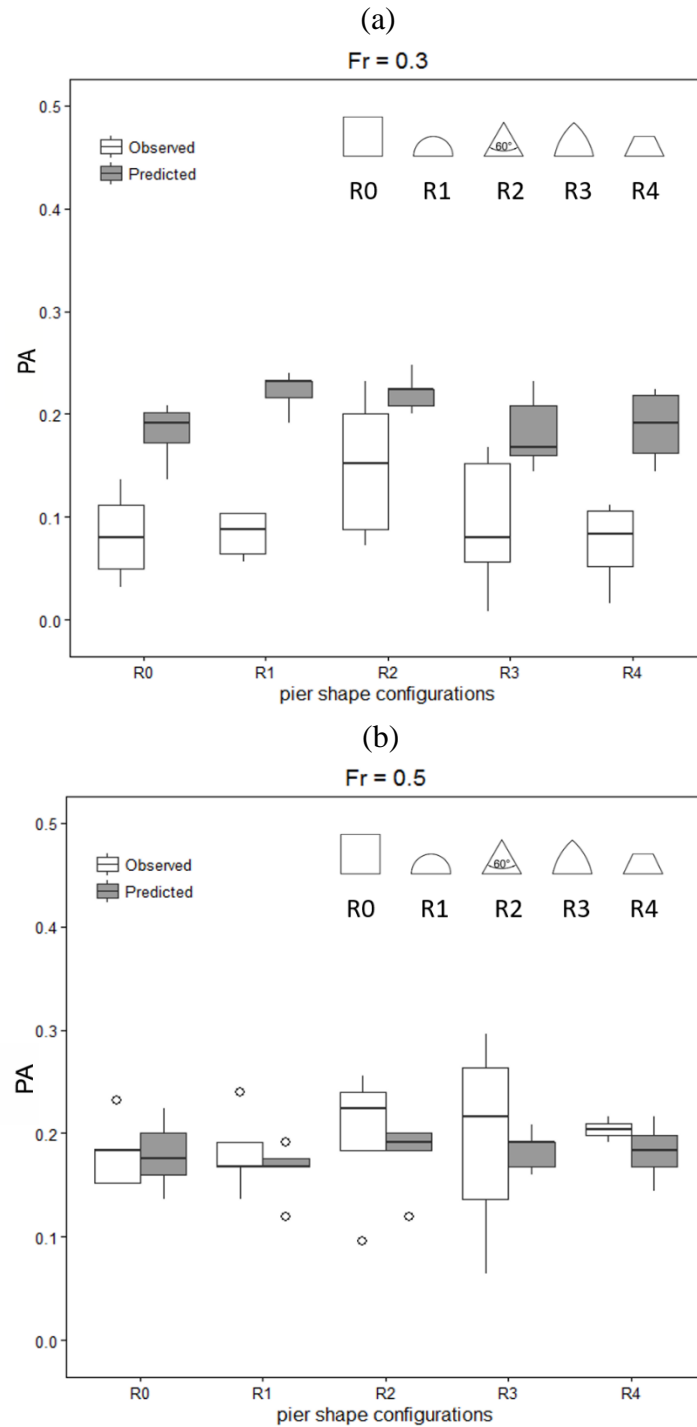
Figure 5.16 Boxplot of PA (Potential Accumulation) in flume experiments
(observed) and numerical tests (predicted) for Fr=0.3 (a) and Fr=0.5 (b).

If we compare the measured and simulated depth averaged velocities (Figure 5.17)
we observe how the shape of the velocity distribution along the cross sections is flatter
in numerical model for both hydraulic conditions (lower panel) than in the experiments
(upper panel). In numerical simulations, the fluid moves with the same velocity along
the cross sections.

The higher discrepancy was observed for Fr=0.3, as already showed in the hydraulic calibration (Figure 5.10b).

In the numerical model logs tend to move along the centreline either for Fr=0.3 and Fr=0.5. In flume experiments logs mainly move along the centreline for higher flow velocity (Fr=0.5), for which we obtained the best results in physical and numerical comparison. The reason of the different log motion may be attributed to the secondary flows; this aspect will be discussed in detail in the discussion section.
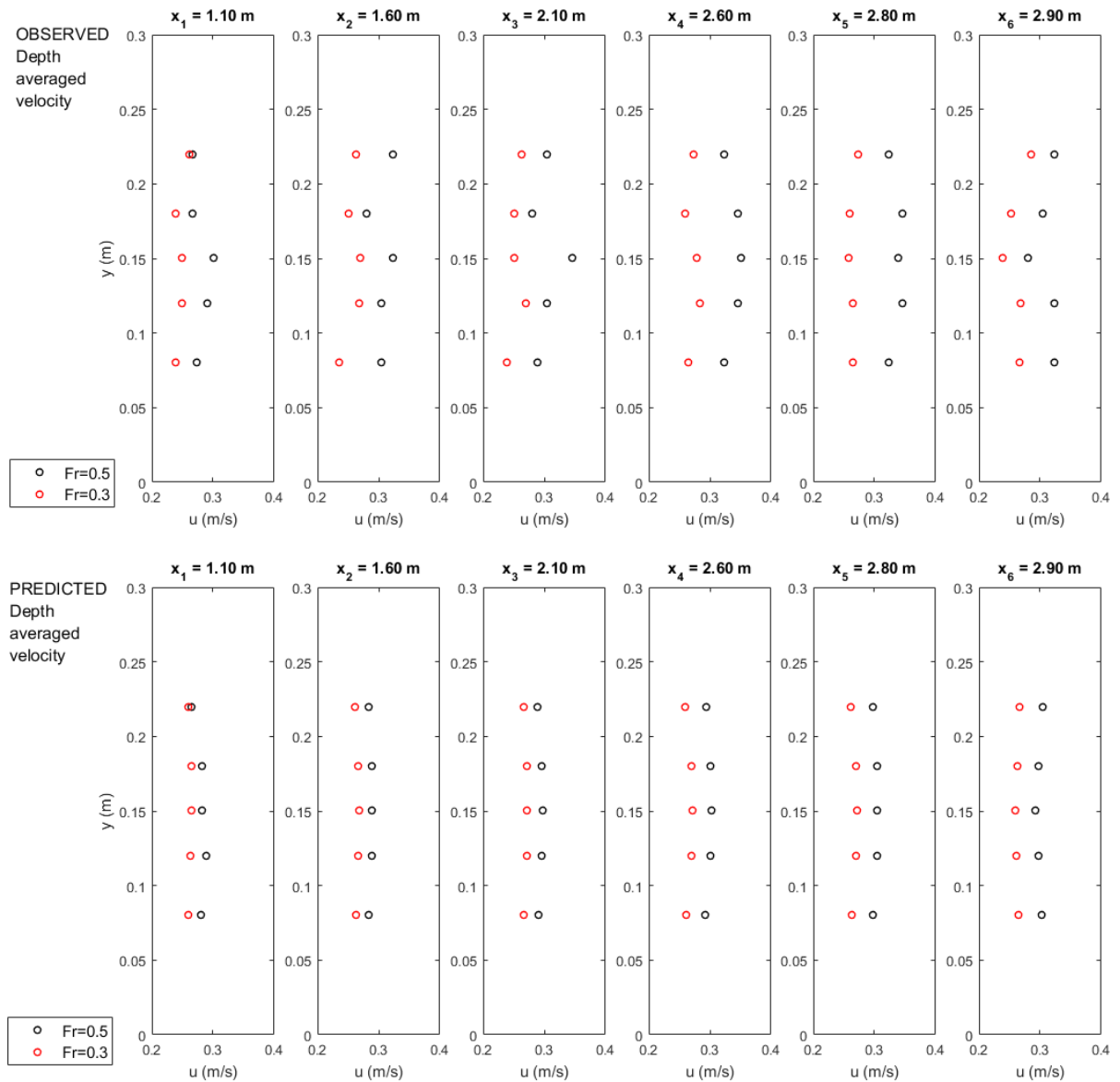
Figure 5.17 Comparison between observed (upper panel) and predicted (lower panel) depth averaged velocities for different Froude number.

5.2.4 *Blockage probability B vs. pier hydraulic-shape coefficient C_{pier}*

In Chapter 3 the definition of blockage probability and the main influencing factors for wood accumulation at the bridge piers were introduced with the relation (3-37):

_____

$$B = f\left(\frac{L_{log}}{w_p}; \frac{Q_{log}}{Q_{flow}}; Fr; c_{pier}\right)$$

The experiments yielded the relation between the blockage probability B and the first three non-dimensional groups in the relation (3-37).

A pier hydraulic-shape coefficient that takes into account of the flow field generated upstream of the pier for different pier geometric configurations is here introduced for the first time: c_{pier}.

Because of the presence of the obstacle the flow velocity upstream of the pier decreases and a "low flow velocity area" (A_{LFV}) is formed.

Here A_{LFV} is defined as the area, expressed in m^2, upstream to the pier delimitated by the isovels $i = 0$ and $i = 0.6 \cdot U_\infty$ (the area where the flow velocity is about the 60% lower than the undisturbed mean surface flow velocity U_∞, in the upstream reach of the flume, U_∞). The upper limit of the low flow velocity area ($i = 0.6 \cdot U_\infty$) delineates the homogenous area, upstream of the pier, where the flow velocity assumes the minor values and that is computed numerically (Figure 5.18).
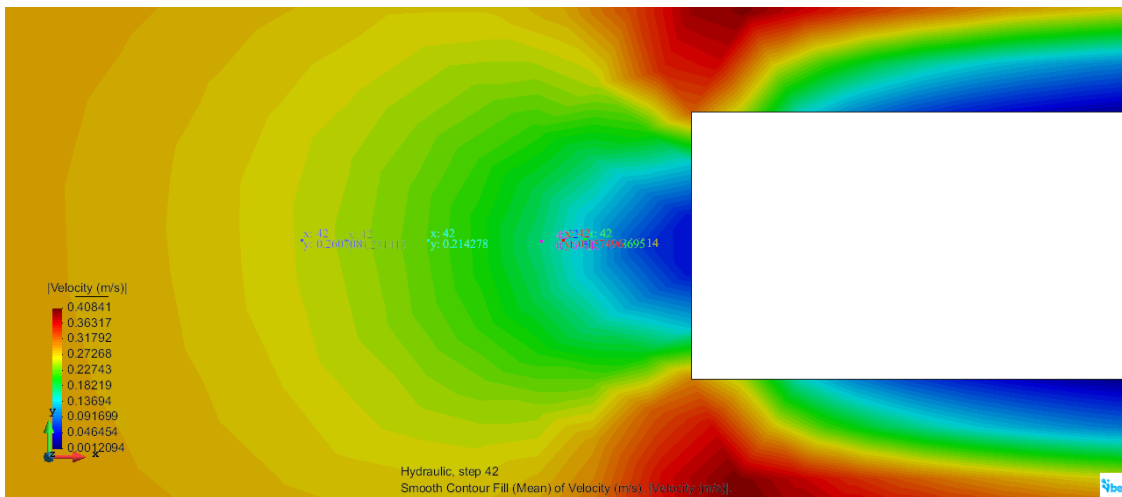
Figure 5.18 Smooth Contour fill plot of flow velocity for Fr=0.5 and rectangular pier shape (R0).

A_{LFV} was estimated for each pier shape configuration from the contour plots of the 2D numerical simulations with *Iber* for Fr=0.5, that gave the best predicted-observed results in terms of flow velocity and Potential Accumulation (PA). Figure 5.19 represents the isovels in two representative cases of flat pier shape and rounded pier shape

The pier hydraulic shape coefficient was calculated as:

$$C_{pier} = \frac{A_{LFV}}{L_{EFF}} \cdot \frac{1}{w_p} \qquad\qquad\qquad (5\text{-}1)$$

in which w_p is the pier width equal for all piers, and L_{EFF} is the width of the pier bounded by the arc of the isovel $i = 0.6 \cdot U_\infty$.
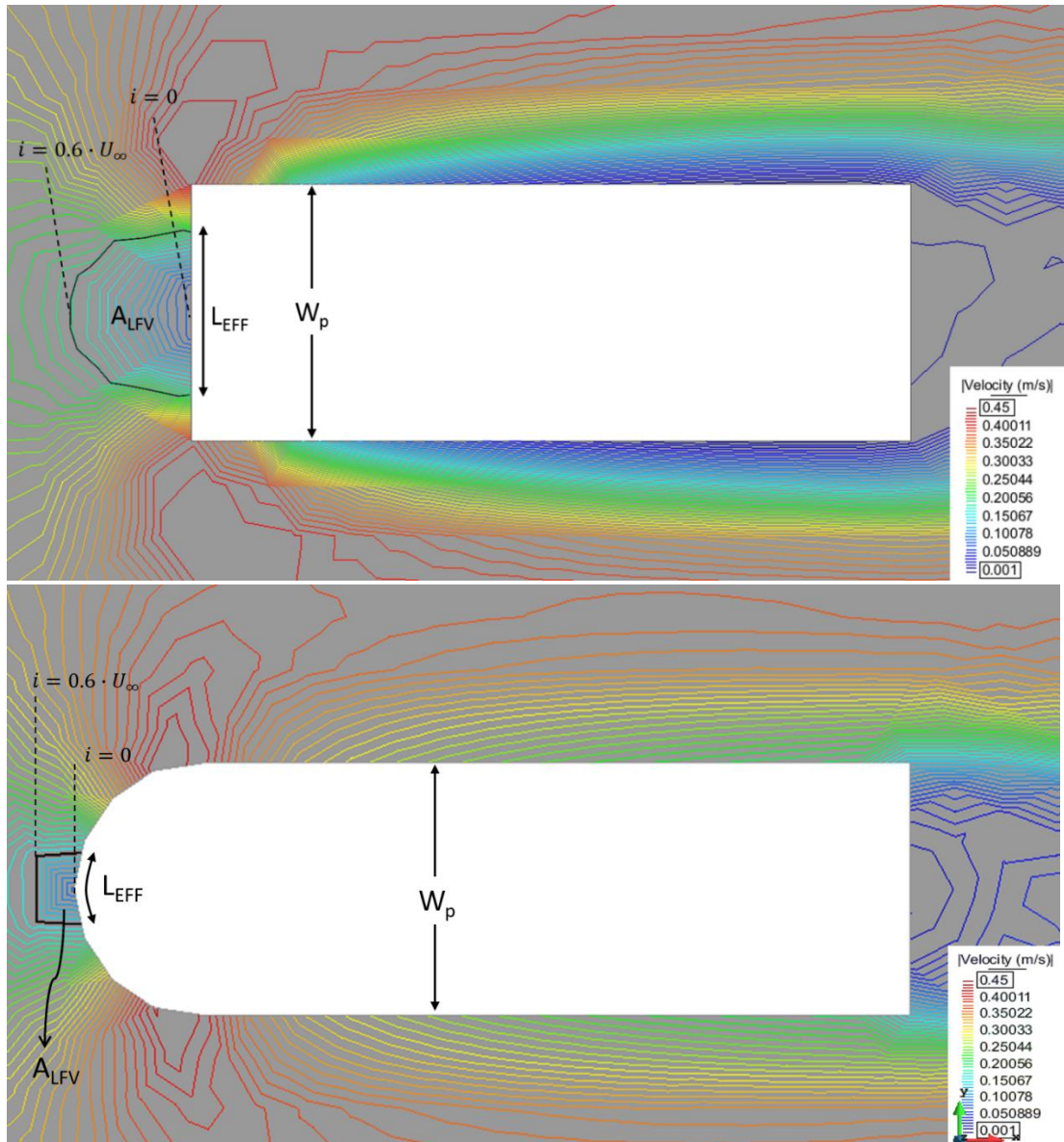
Figure 5.19 Isovels plot for Fr=0.5 and rectangular pier shape (R0) and semi-circular pier shape (R1). The dashed lines indicate the Isovels i=0 and i=0.6·U∞ that delimit the low flow velocity area (A_LFV).

The pier hydraulic shape coefficient for each pier shape is listed in *Table 5.2*. In two cases C_{pier}=0, for triangular and Ogival pier shapes, both characterized by a more pointed pier shape. The highest value was obtained in correspondence of the rectangular pier, so the flatter is the pier cutwater higher is the low flow velocity. High values of A_LFV correspond to high values of pier hydraulic shape coefficient.

The correlation between B and C_{pier} is shown in Figure 5.20. The probability of logs to stop at the pier increases for higher C_{pier}, in the presence of more flat pier shapes (R0, R4).

The correlation between blockage probability and pier hydraulic shape coefficient for each class of log size is presented in Figure 5.21-Figure 5.23.

Table 5.2 Values of pier hydraulic shape coefficient for different pier geometries and Fr=0.5.

Code	Geometry	Figure	C_{pier}
R0	Square-nose		0.324
R1	Round-nose		0.075
R2	Triangular-nose (60°)		0.000
R3	Ogival-nose		0.000
R4	Trapezoidal-nose		0.095
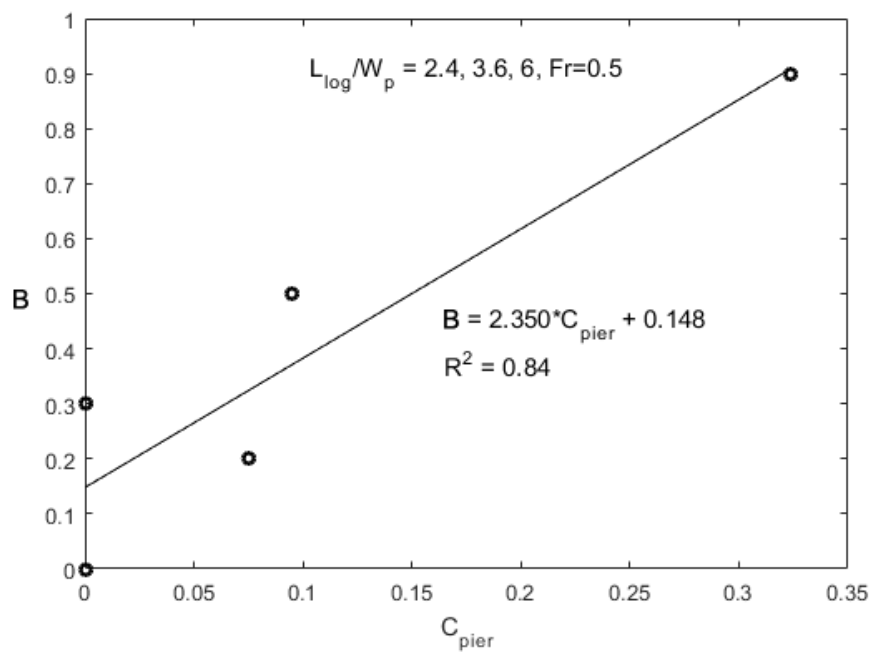
Figure 5.20 Blockage probability B versus pier hydraulic shape coefficient c_{pier} for Fr=0.5 and all log size classes.
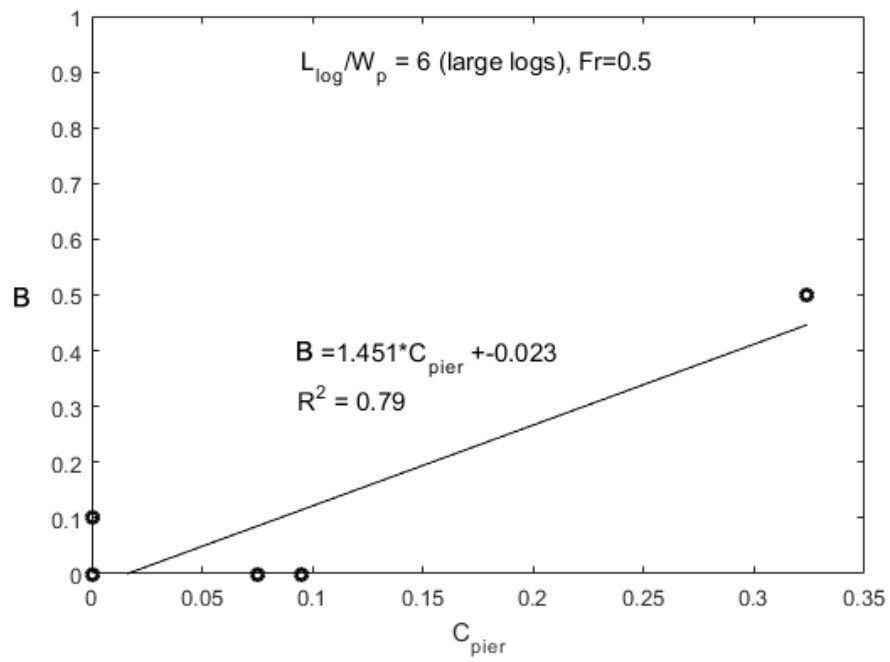
Figure 5.21 Blockage probability B versus pier hydraulic shape coefficient c_{pier} for Fr=0.5 and large logs.
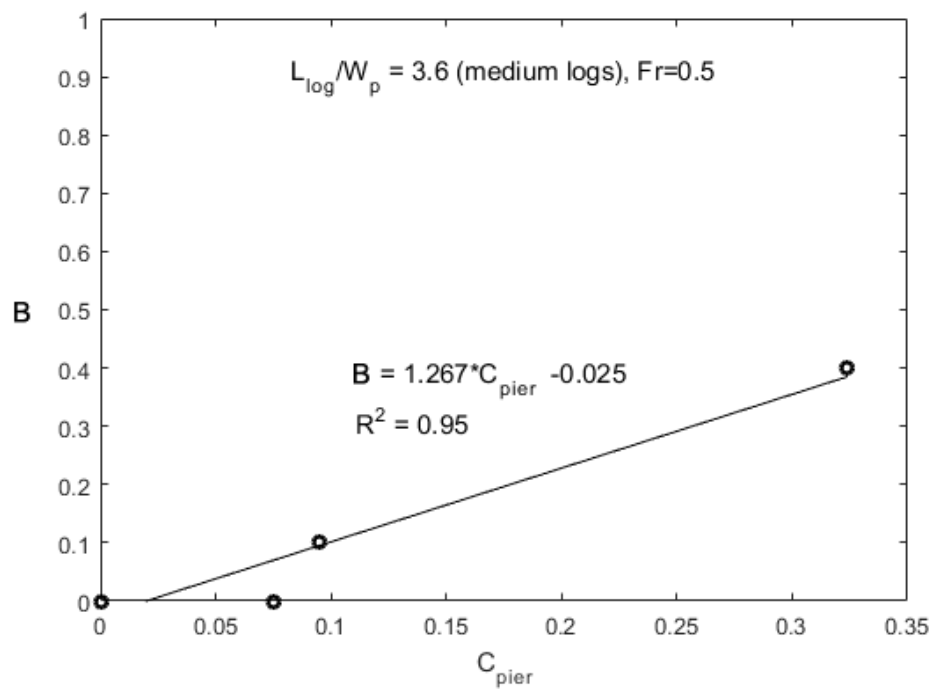
Figure 5.22 Blockage probability B versus pier hydraulic shape coefficient c_{pier} for Fr=0.5 and medium logs.

_____
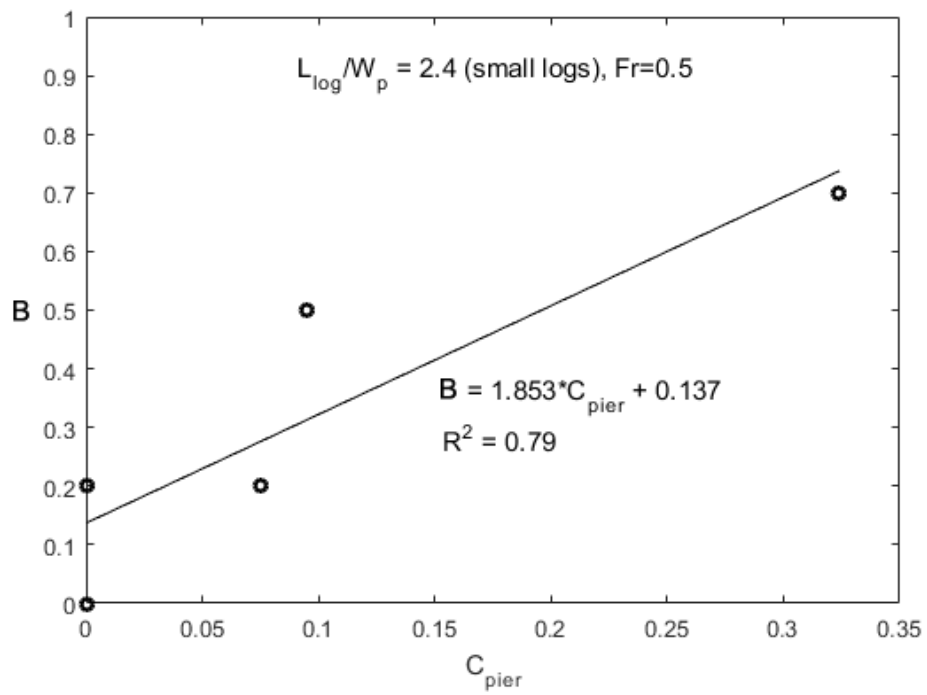
*Figure 5.23 Blockage probability B versus pier hydraulic shape coefficient c_{pier}
for Fr=0.5 and small logs*
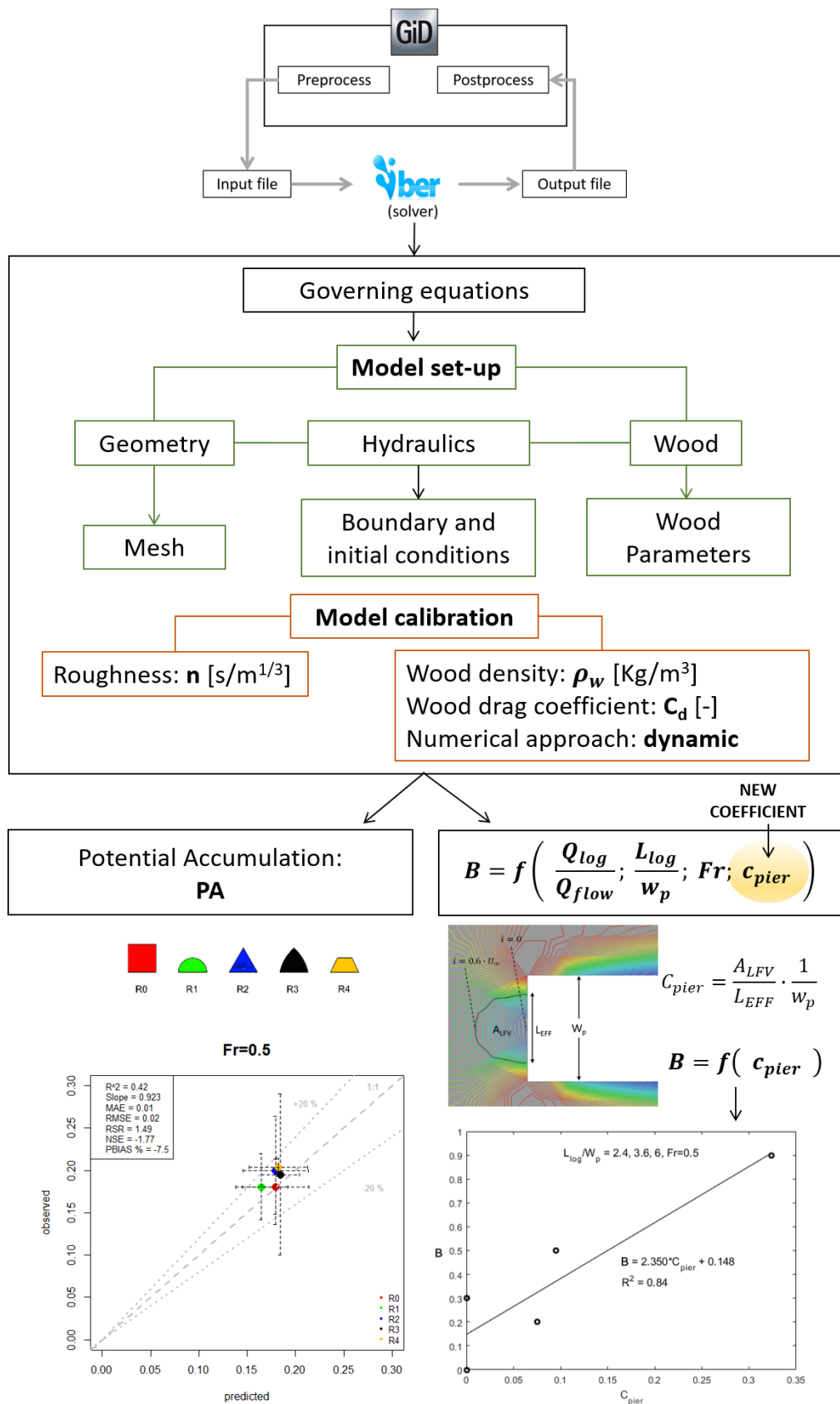
Figure 5.24 Graphical summary of the 2D numerical simulations with Iber.

_____

5.3   Joint Blockage Probability

Based on Equation (3-38), the joint blockage probability for the independent variables identified has been calculated by the product of the individual blockage functions in case of congested transport regime. The Figure 5.25 shows the total blockage probability plotted versus the pier shape coefficient, the ratio between the log length and pier width and for different Froude numbers.

The vertical blue contoured plans define each class of log size, while the red and blue points are respectively, the total blockage probability at Fr=0.5 and at Fr=0.3. The star indicates the cases in which the total blockage probability is higher than 0.5, while the triangle identifies the values of *totB* comprised between 0.10 and 0.50. The values of joint probability are listed in *Table 5.3*. The higher values of the total blockage probability were obtained for Fr=0.5 and flat pier shapes. The combination of congested wood transport regime, Fr=0.5, square pier shape (R0) and small logs gives the highest total blockage probability (*totB*=0.63). The logs size is not influential on blockage as the Froude number and the pier shape. In case of higher Froude number (Fr=0.5), the blockage probability is high only in presence of the less pointed pier shapes.
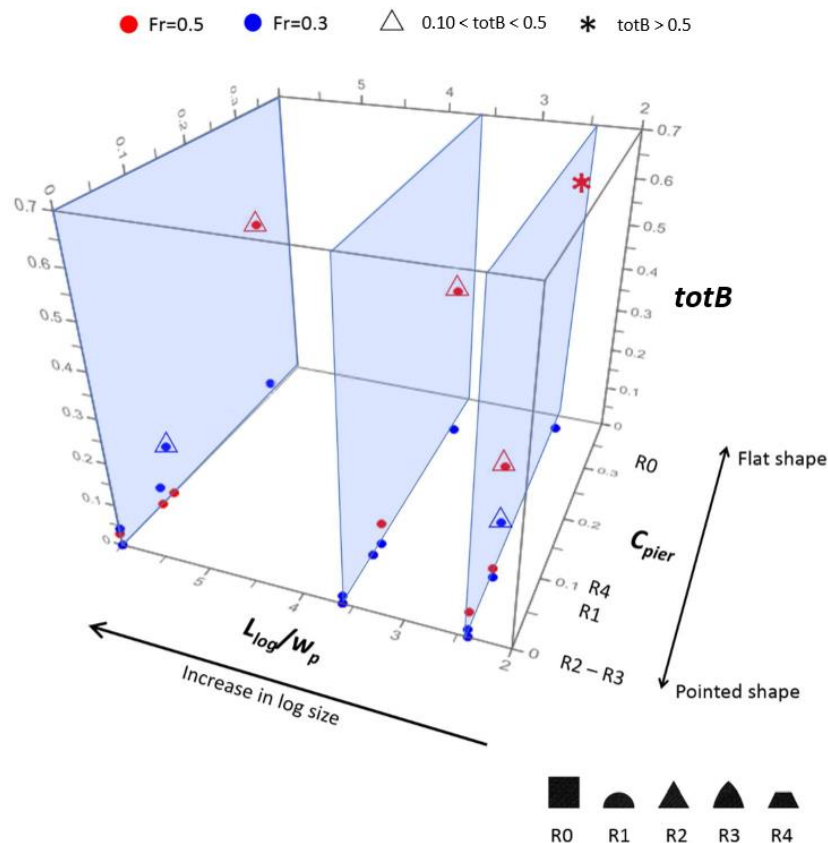
Figure 5.25 Joint Blockage probability (totB) for the most influential independent variables for blockage at the bridge pier, in congested wood transport regime.

Table 5.3 Values of the joint blockage probability in case of congested transport regime and for different pier shapes, log size and Froude numbers.

pier shape	Fr	C_{pier}	$\dfrac{L_{log}}{w_p}$	$totB$
R0	0.5	0.324	2.4	**0.63**
R1	0.5	0.075	2.4	0.04
R2	0.5	0	2.4	0.06
R3	0.5	0	2.4	0
R4	0.5	0.095	2.4	**0.25**
R0	0.5	0.324	3.6	**0.36**
R1	0.5	0.075	3.6	0
R2	0.5	0	3.6	0
R3	0.5	0	3.6	0
R4	0.5	0.095	3.6	0.05
R0	0.5	0.324	6	**0.45**
R1	0.5	0.075	6	0
R2	0.5	0	6	0.03
R3	0.5	0	6	0
R4	0.5	0.095	6	0
R0	0.3	0.324	2.4	0.06
R1	0.3	0.075	2.4	0.02
R2	0.3	0	2.4	0.02
R3	0.3	0	2.4	0
R4	0.3	0.095	2.4	**0.12**
R0	0.3	0.324	3.6	0
R1	0.3	0.075	3.6	0
R2	0.3	0	3.6	0.02
R3	0.3	0	3.6	0
R4	0.3	0.095	3.6	0
R0	0.3	0.324	6	0.03
R1	0.3	0.075	6	0.04
R2	0.3	0	6	0.04
R3	0.3	0	6	0
R4	0.3	0.095	6	**0.12**

5.4   3D- numerical model

The first step in using the 3-D model (*Flow-3D*) was calibration, which involved the comparison of simulated streamwise velocity profiles and the measured profiles which are presented in Figure 5.26. Here, the black lines and red dots correspond to the cross sections located upstream of the pier. The correlation between observed (measured) and predicted (simulated) values of local flow velocity with the ±25% range of variation (dotted lines) relative to perfect agreement (dashed line), is presented in Figure 5.27.
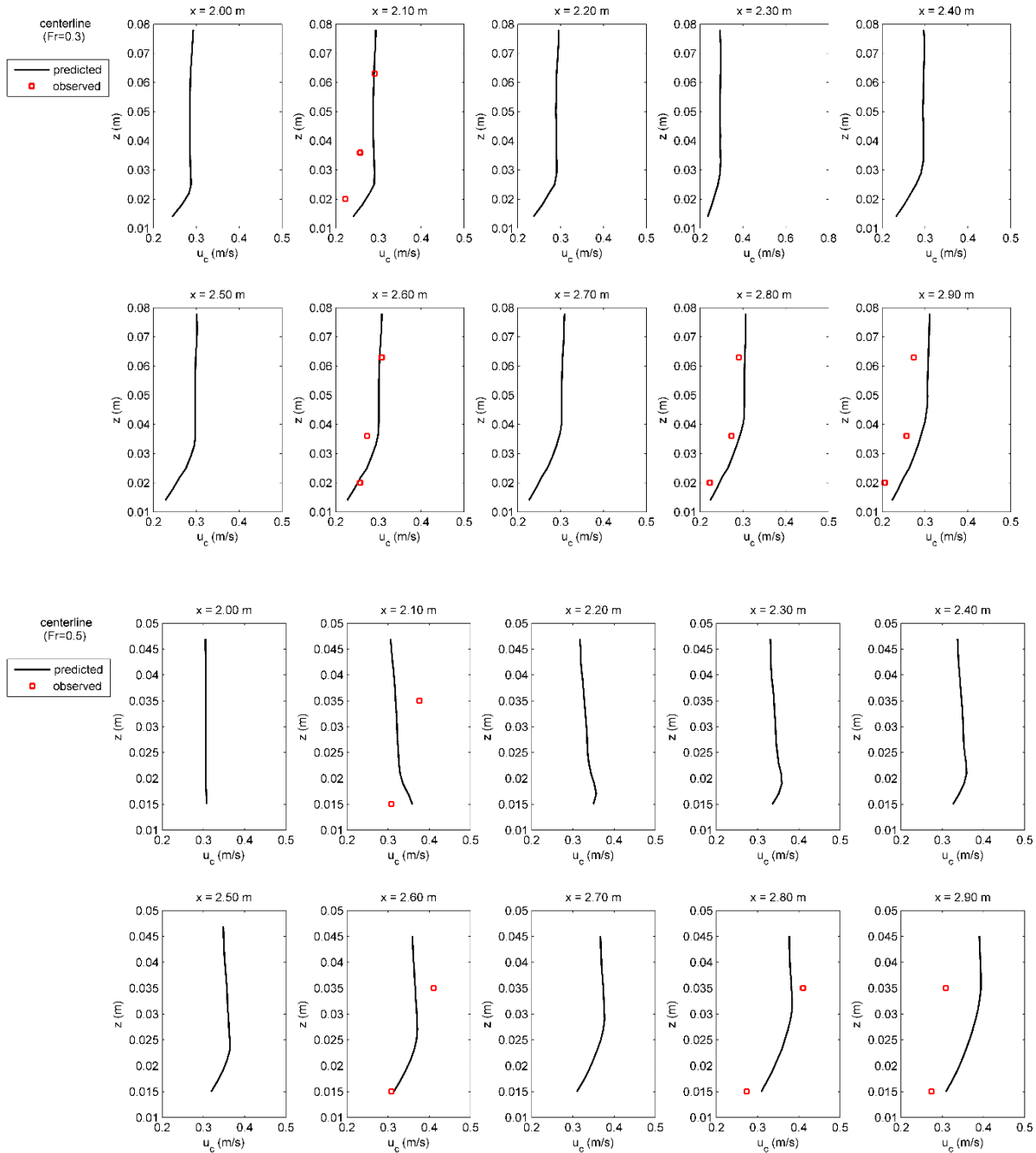
Figure 5.26 Predicted (black line) and observed (red dots) flow velocity in the cross sections upstream of the pier for Fr=0.3 (upper panel) and Fr=0.5 (lower panel).
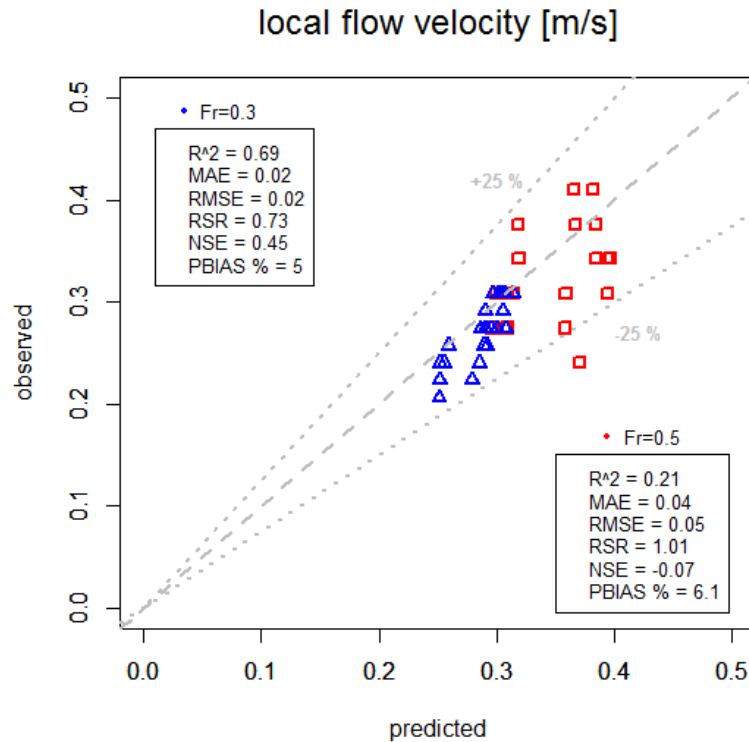
Figure 5.27 Local flow velocity values measured (observed) and simulated (predicted).

Figure 5.28 shows the advection paths for a single log under "uncongested" transport condition (red line) and the same log in "congested" transport when, the number of logs in each test is gradually increasing, as schematized in Figure 4.11. For example, in Figure 5.28 the code "LW1/6" indicates the log path for log LW1 that was positioned in the middle of the cross section (see Figure 4.11) in the simulation done with six logs.

For the "uncongested" transport condition the log moved along the centreline of the flume and it touched and stopped at the pier below the water surface (the log was submerged), for few seconds (see Figure 5.29, A) and then moved along the upstream vertical side of the pier in analogy with some of the experiments.

Under "congested" transport conditions, the same log passed close to the pier without stopping because of the collision with other logs. This does not mean that no logs stopped in "congested transport". For example, in the simulation with six logs the log number 2 (LW2) stopped at the pier and then moved along the vertical face of the pier (seeFigure 5.29, B and Figure 5.30).

_____
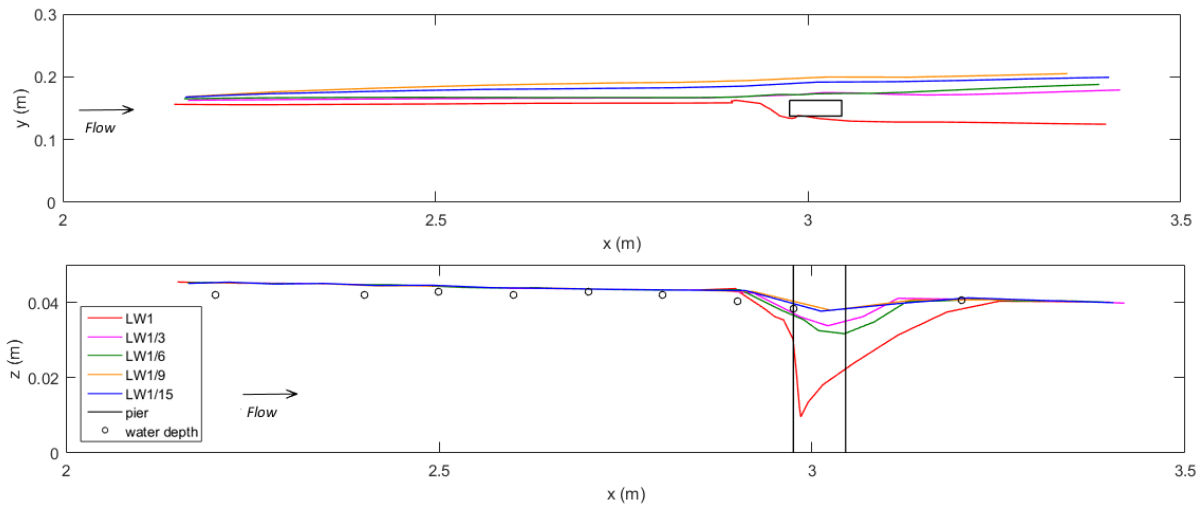
Figure 5.28 Top (upper panel) and side (lower panel) view of the trajectory of one single log (LW1) and of the same log in presence of more logs (3, 6, 9, 15).
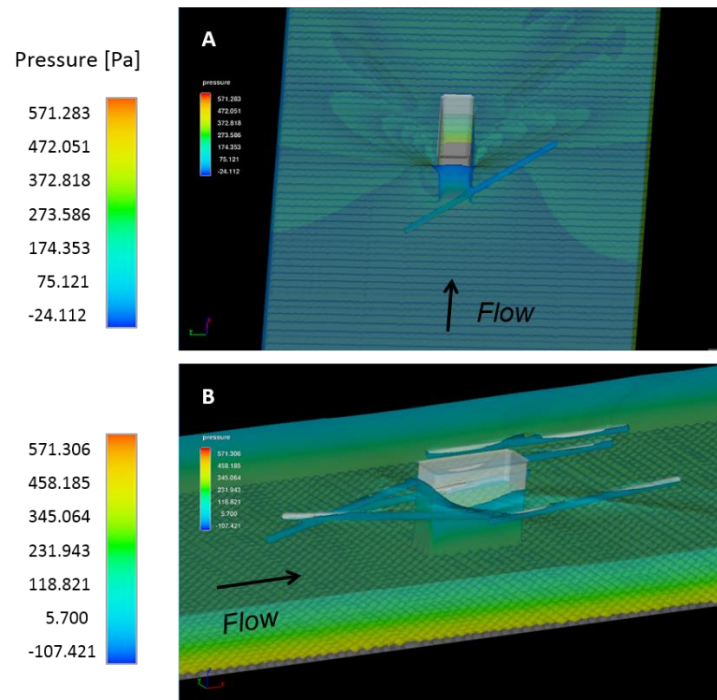
Figure 5.29 Wood-pier interaction reproduced with Flow-3D, in the case of single log and submerged conditions (A), and more logs in semi-submerged conditions (B).
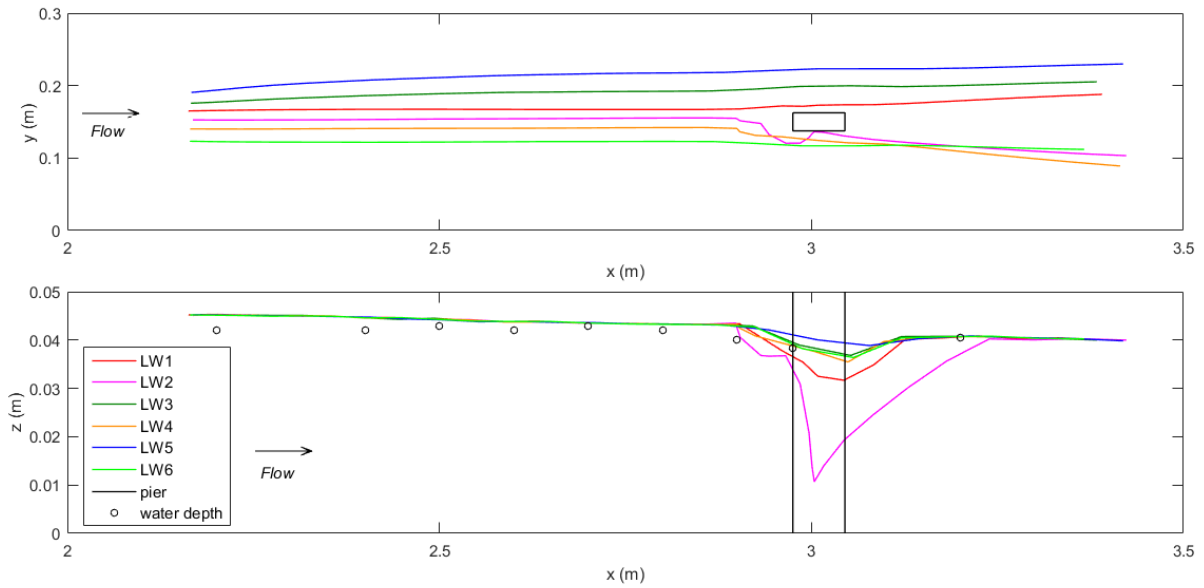
Figure 5.30 Top (upper panel) and side (lower panel) view of the trajectory of logs in "congested" transport simulation with 6 logs.
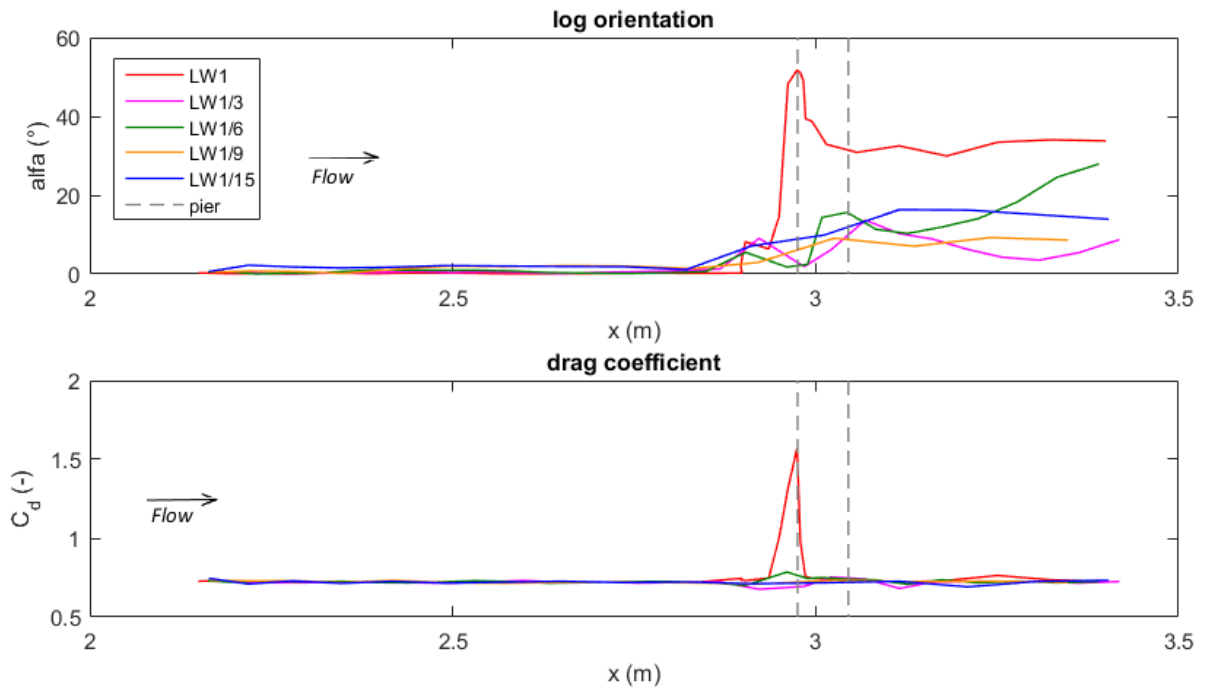
Figure 5.31 Log centre orientation (upper panel) and correspondent drag coefficient (lower panel) plotted for one single log (LW1) and for the same log in presence of more logs (3, 6, 9, 15 logs).
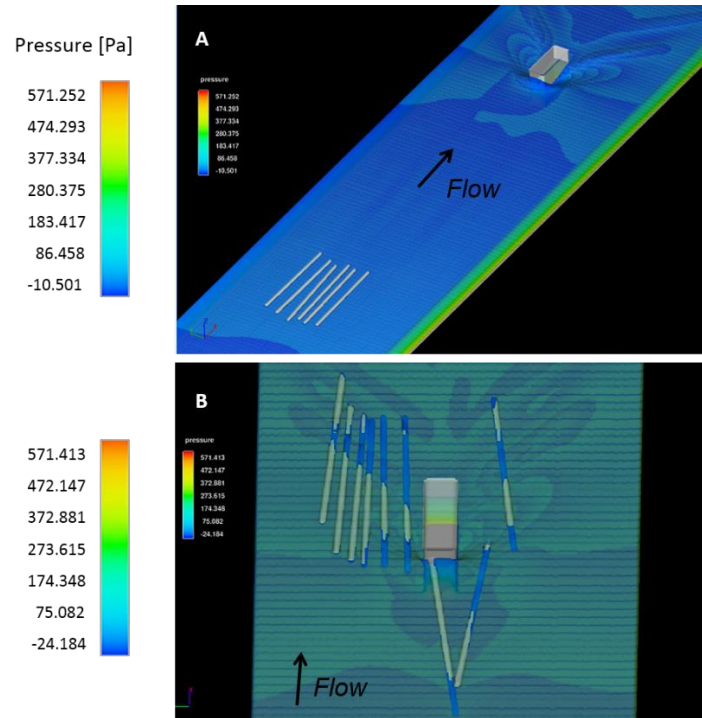
Figure 5.32 Orientation of logs, with respect to the flow direction, before encountering the pier (A) and at the moment of the collision with the pier (B).

For comparison purpose, the drag coefficient was determined from Equation (3-6) (with $U_{log} = U$). *Flow-3D* calculates the two components of the drag force: the friction force (that depends on the log orientation) and the pressure force (proportional to the difference between the pressure acting on the front and back of the log). The drag force results from:

$$F_d = F_{d,friction} + F_{d,pressure}$$

(5-2)

The angle of the log respect to the flow direction at each time step is calculated from the angular velocity of the log around the vertical axis.

The drag coefficients from Gippel et al. (1992) were calculated measuring the drag force exerted by flow on a completely submerged log with no roots and no branches and different orientations with respect to the flow direction. Subcritical flow conditions (Fr=0.3-0.6) and Reynolds 'numbers (Re=10^4-10^5) were reproduced in experiments.

The relation between the orientation of the log with respect to the flow and the drag coefficient in uncongested and congested transport is represented in Figure 5.31. In congested transport conditions, the logs, because the collisions, do not achieve great rotation with respect to the flow direction (see e.g. Figure 5.32) and the value of the drag coefficient is lower than one. Otherwise, in uncongested transport the log has more space to rotate. The angle of the log with respect to the flow is higher than in congested transport and also the drag coefficient increases up to the value of 1.5. The normalized values of C_d derived from flume experiments by Gippel et al. (1992) were compared with the values obtained from the numerical simulation with *Flow-3D* in uncongested transport.

_____

The result, shown in Figure 5.33 A, indicate that the values from numerical simulation are lower than the values obtained by Gippel et al. (1992) in the range 0-10°. For α= 14° the values are very similar, while in the range 48-52° the numerical values are slightly higher. No information exists in the range 15-45°.

In numerical simulation with *Flow-3D*, the log floats on the water surface and in semi-submerged condition until it bumps into the pier then it rotates (Figure 5.33, C) and slides below the water surface and along the upstream vertical face of the pier (Figure 5.33, B).

In Figure 5.33, the green and red areas represent the log path in semi-submerged condition and in complete submerged conditions, respectively. The yellow area is the transition region upstream of the pier.

Few authors analysed the hydrodynamic coefficients for cylindrical logs differently oriented respect to the flow direction (Gippel et al., 1992, 1996; Shields et al. 2012).
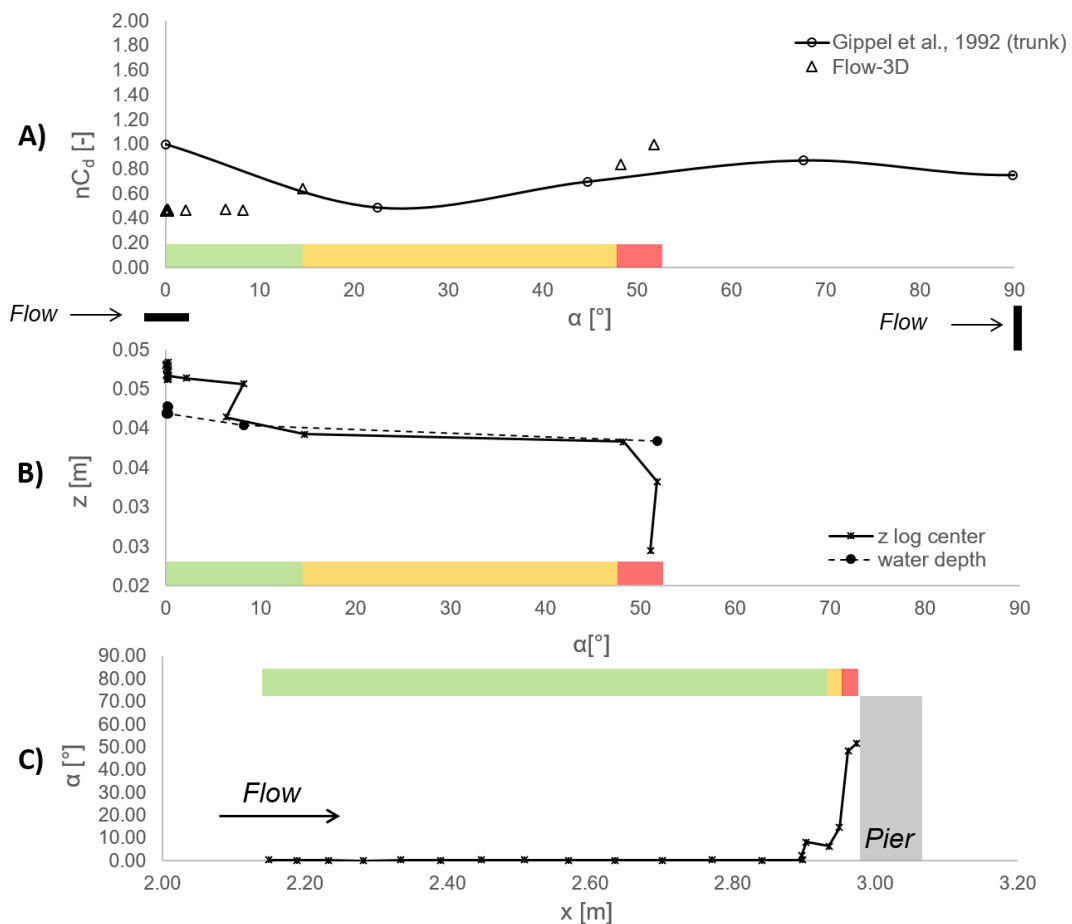
Figure 5.33 A) Normalized drag coefficient from simulation with Flow-3D compared with data from Gippel et al. (1992); B) elevation of the log centre versus the orientation respect to the flow direction; C) log orientation along the x coordinate of the flume.

_____
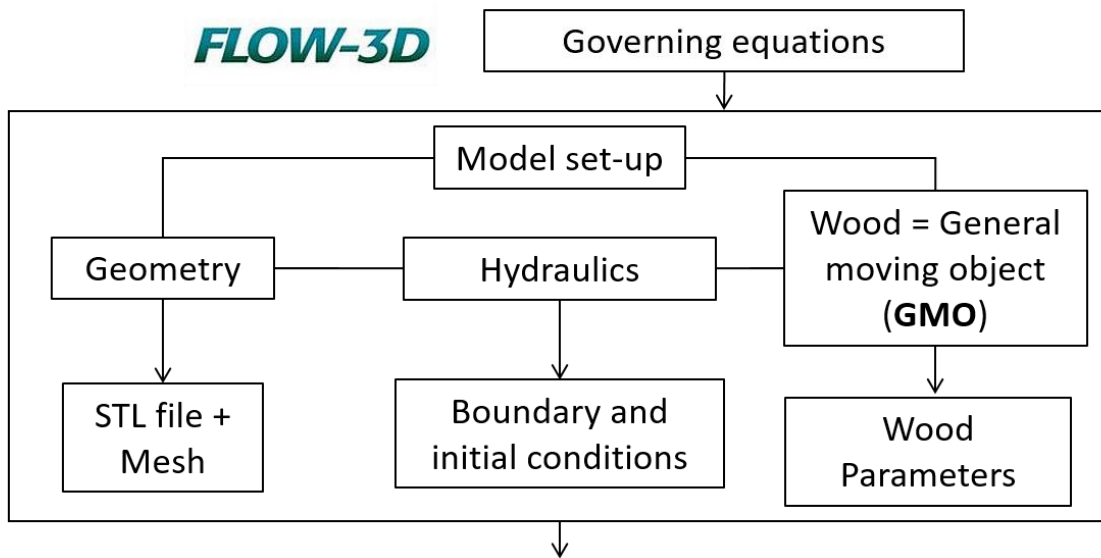
1. 3D character of the flow: log stopping in submerged condition
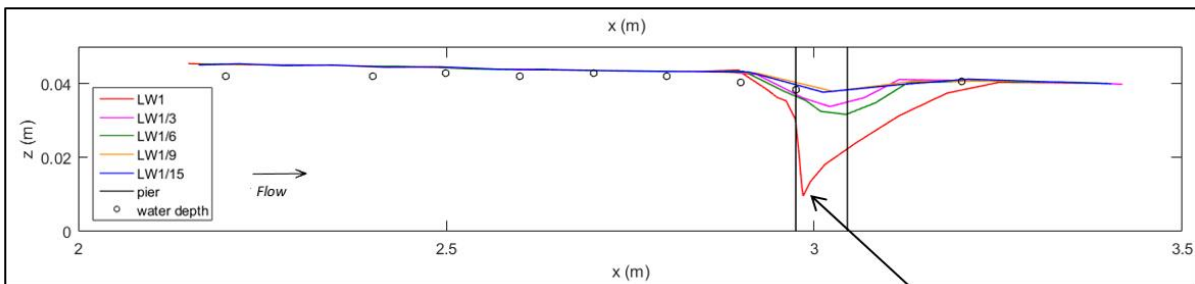
2. Variation of Cd with log orientation for semi-submerged logs (comparison with Gippel at al., 1992)
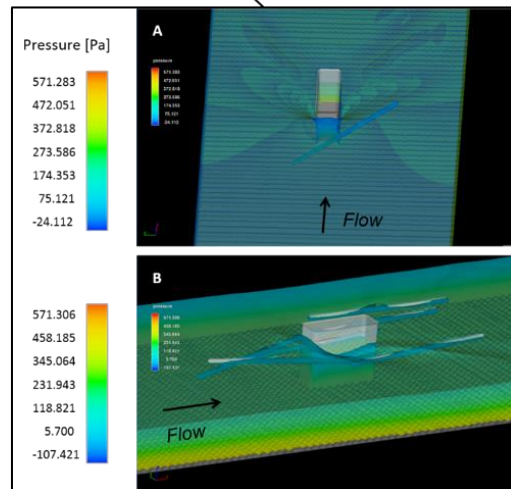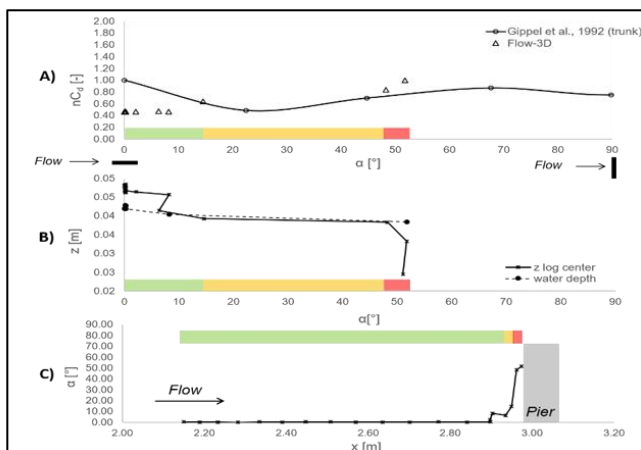
Figure 5.34 Graphical summary of the 3D numerical simulations with Flow-3D.

6   Discussion

6.1   Thesis assumptions

The main thesis hypothesis was the possible formulation of a valid probability function of wood accumulation at bridge piers. The thesis was successful in achieving the task. However, a number of assumption were made both in the experiments and in the numerical simulation (see Chapter 4). Here, we first discuss the implications of these assumptions.

The limitations of the 2D numerical model emerged from the comparison between experimental and numerical simulations; for this reason, further tests were done with the 3D numerical model in which accounted for the non-elastic collisions and the skin friction drag of the logs (see Section 6.3).

The main simplification in the experimental and numerical tests is the cylindrical shape of the log with no roots and no branches. This geometry may be not realistic but it represents an acceptable approximation of defoliated and non-rooted pieces of wood during fluvial transport (Allen and Smith, 2012; Xu and Liu, 2016; Ruiz-Villanueva et al., 2014a; Braudrick et al. 1997; Bocchiola et al. 2008; Buxton 2010; Mazzorana et al. 2011).

Concerning the flow conditions, as mentioned in Chapter 4, wood is transported in rivers mainly during flood events that in low land rivers are often characterized by Froude numbers lower than one as used in the present thesis.

We reproduced only a single pier because the aim of the current research was only to investigate the influence of the pier shape on the blockage. For the same reason we positioned the pier in the middle of the cross-section in a straight rectangular channel to avoid the influence of the channel curvature on the log motion and then on the single-pier accumulation.

Of course, there are many possibilities that might be investigated that arise from the combination of flow conditions, channel geometry, number and position of piers, and that necessitate future research.

6.2   Hydraulic interpretation of log movement at bridge piers

The experiments showed different modes of log movement depending on the flow hydraulics and pier shape (see Figure 6.1).

Potential flow theory can provide a preliminary interpretation to explain the experimental observation of the log movements in the flume. The 2-D streamlines around any object in the flowing water can be analytically derived by assuming the flow is irrotational. Under this assumption the stream function upstream of the pier is obtained in two different representative cases: the rounded pier and the square pier. The rounded pier is modeled as a Rankine Half-Body and it is obtained combining the configurations of the source and uniform flow.
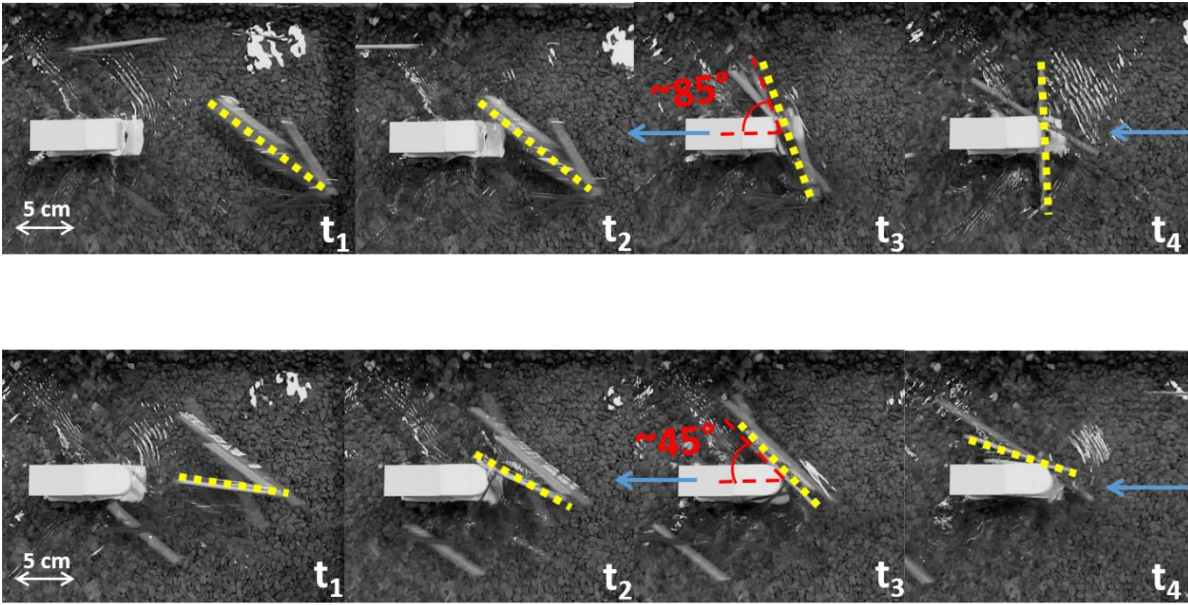
Figure 6.1 Experimental observation on orientation and travelled path logs approaching the flat pier (upper panel) and the rounded pier (lower panel) at 4 different time intervals (Flow direction from right to left).

The stream function in cylindrical coordinate is given by Equation 6-1 (Kundu and Cohen, 2008):

$$\psi = U_\infty r \sin \theta + \frac{m}{2\pi} \theta$$

(6-1)

in which U_∞ is the undisturbed free stream velocity, m is the strength of the source at the origin expressed in m²/s and calculated as:

$$m = 2\pi U_\infty a$$

(6-2)

in which $a = h_{max}/\pi$ is the position of the stagnation point from the origin and $h_{max} = w_p/2$ The equation of the streamline passing through the stagnation point is obtained by setting $\psi = m/2$.

The flow around a rectangular pier shape is reproduced using the Schwarz-Christoffel transformations applied to the half plane.

The streamlines in Figure 6.2 at Fr=0.5, show that the angle of the log with respect to the flow direction is about 85° for the flat pier shape and about 45° for the rounded pier. In the former case, the log undergoes a greater rotation with respect to the main flow direction, and then it flows downstream; in the latter case, the rotation angle is lower and the log easily follows the flow. The consequence is that the blockage probability is higher for the flat pier shape. However, this depends on the orientation angle of the log with respect to the flow, the position of the log centre when it bumps into the pier (if the log centre follows the stagnation streamline or the streamlines close to it), the log length, the local changes in depth and velocity fields.

Most of the experimental observations confirm the simplified theoretical analysis of the streamlines, as illustrated in Figure 6.1, that shows the time-lapse sequence of congested transport of logs at the flat pier shape (upper panel) and at the rounded pier (lower panel). The yellow dashed line indicates one single log to analyse its travelled path and orientation close to the pier frontal side. At the time step t_3 the log touches the pier following the curvature of the streamlines as represented in Figure 6.2. At the flat pier shape (upper panel) the log centre moves along the stagnation point and it get blocked at the pier; at the rounded pier (lower panel), even if the log centre moves close to the stagnation point, the lower curvature causes the log sliding. This confirms also the higher blockage probability for Fr=0.5 (see Figure 5.1 on left) at the flat pier shape (P=0.9) than at the rounded pier (P=0.2).
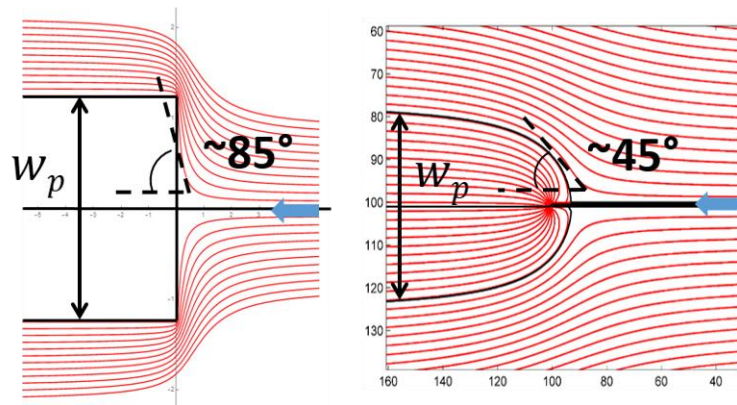
Figure 6.2 Streamlines at a flat pier shape (left) and semi-circular pier shape (right). Flow from right to left.

6.3   Comparison between experimental and numerical results and limitations

The experiments showed that congested wood transport, higher Froude number (Fr=0.5) and flat pier shape (R0) are the most critical conditions for wood accumulation at a single central pier (P=0.9). In case of Ogival shape (R3) zero blockage probability was found for both cases of Froude numbers, wood transport regimes and log length. The flatter is the pier shape, the higher is the blockage probability (*P*): the potential flow analysis of two different cases (rectangular and rounded pier) indicated that the lower curvature of the streamlines at the rounded pier favours the log sliding.

For blockage probability, the different flow velocity distributions play an important role: at Fr=0.5 the velocity distribution is more parabolic in shape than at Fr=0.3 and thus the logs move mainly in the centreline having a greater probability to touch the central pier. But, the comparison between the "potential" and "effective" blockage probability suggests that even if a large number of logs touch the pier, not all are effectively stopped at the pier since rounded shape piers will allow the sliding of logs.

The 2D numerical model *Iber-Wood* reproduces the log motion, log velocity and trajectory very well, as showed by Ruiz-Villanueva et al (2014a), and confirmed by the current research. Thus, it represents a valuable tool. On the other hand, it revealed weaknesses in simulating the collisions and the blockage of the logs.

The other shortcoming is that the numerical model implements only elastic collisions (e=1) that is not realistic if we consider wetted logs floating in water that bump

into each other or into a concrete bridge pier (in reality) or the thermoplastic pier (in experiments). In numerical tests, no logs were blocked at the pier by the end of the simulation. When a log touches the pier, the model recalculates the position of the log depending on the incidence angle, so the log can slide or bounce back. Furthermore, the 2D model does not simulate the superposition of floating logs. For this reason, we compared only the "potential blockage probability", that is the probability of logs touch the pier without stopping.

The comparison between experimental and numerical data showed that for Fr=0.5, all data fall into the region between line 1:1 and the line +25% of variation. While for Fr=0.3 the numerical model overestimates the potential blockage probability. The explanation for the discrepancy may be attributed to the 3D character of the flow neglected in the two-dimensional model. In the straight rectangular flume, in addition to the Reynolds number, the different roughness between the bed and the walls is a minor factor influencing the secondary flow generation. The vortexes of secondary currents may be stronger towards the centreline in one case (Fr=0.5) than the other (Fr=0.3). This means that experimentally the logs are more prone to move along the centreline and touch the pier at Fr=0.5, while numerically there is no evidence of the different log motions. The effects of secondary currents on log motion will be discussed in Section 6.4.

In addition to the collision, others two issues need to be improved in the 2D *Iber-Wood* numerical model that are the "skin friction drag coefficient" and the variation of drag coefficient with log orientation.

In case of interaction between logs and pier, the skin friction is an additional drag force that may favour the log blockage at the pier. In *Iber-Wood* model, the logs are modelled as smooth cylinders without considering a skin friction coefficient. The drag force exerted by tree trunks is higher than smooth dowels because of the higher skin friction coefficient (Merten et al., 2010). However, the latter does not imply that can neglect the presence of a surface friction for smooth cylindrical beech dowels. The Figure 6.3 shows an experimental case done with a semi-circular pier shape, in which the dowels stopped at the pier. Probably the log stops at the pier because the friction between the log and the pier surface or because the equilibrium between the hydrodynamic forces acting on the logs, but measurements or data of the acting forces, are not available to assert this.
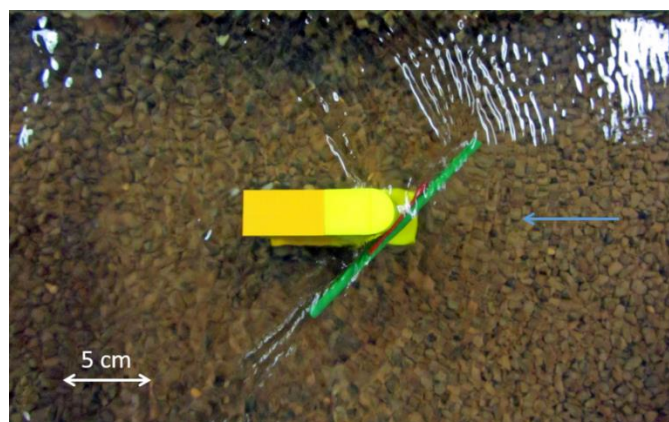
*Figure 6.3 Example of "Effective Blockage Probability" (MinBP) in flume
experiments: the log stopped at the pier at the end of the tests.*

Equation (3-8) shows that the drag force F_d varies with log orientation because the effective log area exposed to the acting force of the flow increases when a log is perpendicular to the flow direction. Consequencely, the drag coefficient changes with the log orientation angle with respect to the main flow direction, therefore assuming constant drag coefficient, results drag force acting on a log which is not correct. The variable drag coefficient may influence the blockage probability by changing the log velocity (from Equations (3-12) and (A-3)) and it is more significant in the dynamic approach (the method used here) for which the forces acting on a log are calculated at each time step.

The variation of drag coefficient with log orientation has been largely investigated by Gippel et al. (1992, 1996) with experimental tests on submerged logs of different sizes and shapes. The numerical model considers a constant drag coefficient, but advances are ongoing to define a "variable" drag coefficient according to log orientation respect to the flow.

Next, we discuss the 3D model (Flow-3D) with the focus of the 2D model limitations.

The two important aspects in the 3D simulations were: i) the logs stop at the pier because the friction at the point of contact during collision between the log and the pier; ii) the log touches the pier in some cases and then moves along the vertical side of the pier depending on the vertical hydrodynamic forces acting on the log and against the pier (see Figure 5.29A).

The orientation of the log under uncongested and congested transport conditions and the correspondent drag coefficients were analysed that are presented in Figure 5.31. The results confirm the increase of drag coefficient with the orientation angle of the log with respect to the flow direction. The latter is agreement with findings of some authors (e.g. Gippel et al., 1992). The simulation results show that the presence of more near floating logs oriented parallel with the flow reduces the log rotation in the plan x-y because of their interactions and collisions.

In semi-submergence condition, the effective log area that are exposed to the acting force system is lower than the area of a log completely immersed in water stream, which gives lower drag coefficient in the first case. This is probably the explanation for the lower values of the hydrodynamic coefficient computed with Flow-3D when the log is semi-submerged (Figure 5.33, A - green area) and the slightly higher values for totally submerged logs (Figure 5.33, A – red area).

The main limitation of the 3D numerical model is the computational complexity in reproducing the input of multiple overlapped moving objects (logs) in water and the required CPU capacity. The logs were released in the upstream cross section of the flume in the form of carpet of multiple logs, thus one layer of parallel logs was reproduced (Figure 4.10). If the logs are introduced as done in the experiments, and thus as a group of overlapped logs or just distributed in two overlapped layers, the simulation would stop after a single time step and the logs would be pushed towards the walls, as illustrated in Figure 6.4. This limitation makes difficult the reproduction of the logs input in rivers from external sources as e.g. the bank erosion or landslides, in which overlapped logs enter in rivers and then move as a carpet of multiple logs. In this case, the aim of the 3D numerical tests was not to reproduce the experimental tests but to examine the physical process of wood-pier interaction and the 3D flow field, so the most important aspect was to reproduce the congested transport and not the log input in the flume.

_____
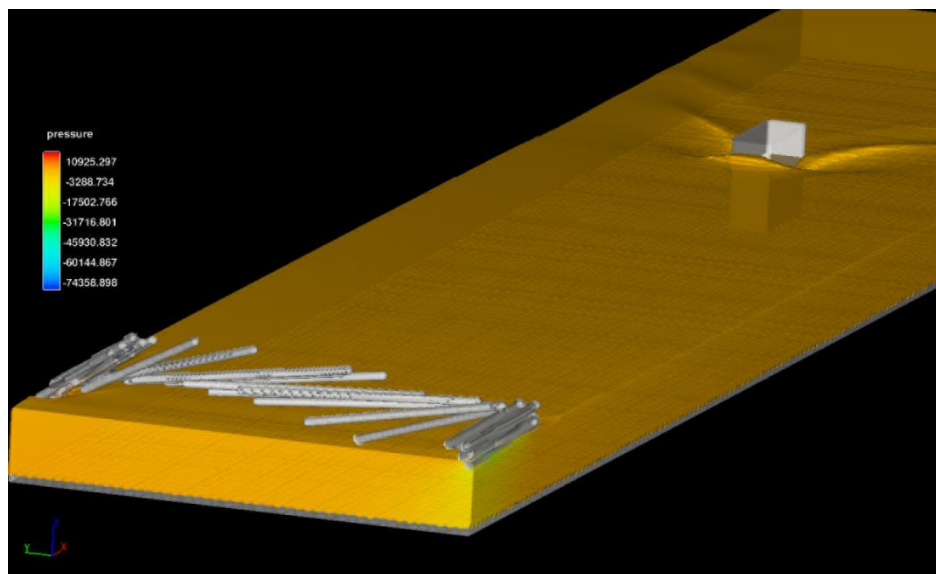
Figure 6.4 Congested wood transport simulated with Flow-3D positioning the logs in two overlapped layers.

The experimental and numerical simulations presented in Chapter 5 and here discussed, allowed to investigate individually the prevailing influencing factors for wood accumulation at bridge piers. The next step has been the definition of the joint blockage probability distribution determined by the product of the marginal distributions (Equation (3-38) that represents one of the main contributions of the current thesis.

The joint blockage probability provides a useful approach to prevent wood accumulation at bridge piers defining the blockage probability for a given set of flow, log and pier geometry. The results (Figure 5.25 and Table 5.3) show that the combination of congested wood transport regime, Fr=0.5, square pier shape (R0) and small logs gives the highest joint blockage probability (JP=0.63) and that pier shape and Froude number are important influential factors for blockage.

6.4   The effects of secondary flows

As mentioned, the formation of secondary flows in a straight channel is controlled by the Reynolds number, and the difference in roughnesses between the bed and the walls in a straight channel that are known as Prandtl's second kind of secondary flows (the first kind of secondary currents are associated to the channel curvature and to the transverse pressure gradient). These secondary currents extend over the water column and affect the depth flow field and the free-surface flow pattern (Albayrak and Lemmin, 2011).

The strength of the secondary vortices defined by circulation is influenced by the aspect ratio B/h between the channel width and the flow depth as demonstrated experimentally and numerically (Nezu and Nakagawa 1993; Auel et al. 2014; Albayrak and Lemmin 2011). The critical value of the aspect ratio is $B/h = 5$ (Nezu and Nakagawa 1993). Lower values of this ratio are characteristic of narrow channels while hihger values characterize wide channels.

Albayrak and Lemmin (2011) found that the longitudinal mean velocity in the lateral direction appears to be organized between faster and lower moving zones. The

faster zones correspond to the downwelling regions while the lower zones to the upwelling regions. In wide channels ($B/h > 5$), the latter develop in the centre of the channel and the secondary currents move towards the centreline near the surface and towards the walls near the bed (see Figure 6.5). This may be the reason why the floating logs at Fr=0.5 and $B/h = 7.5$ are mainly directed to the centre of the flume.
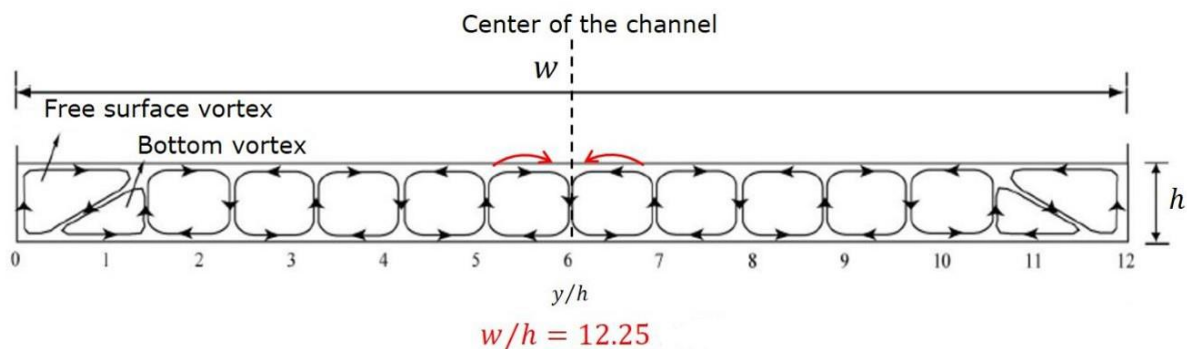
Figure 6.5 Idealized sketch of secondary currents across the channel for the aspect ratio w/h =12.25 (from Albayrac and Lemmin, 2011).

The 2D model does not reproduce secondary motions and then the dependence of log motion on Froude number does not yield.

6.5 Comparison with previous works

How the pier shape affects the blockage probability is the novelty of the present thesis. Some of the studies described in the "Literature review" (Chapter 2) analysed the blockage probability at bridge decks or the influence of a central pier on blockage (Schmocker and Hager, 2011; Gschnitzer et al., 2013; Rusyda, 2015). They all agree that congested transport and the presence of the pier are critical conditions for blockage. Schmocker and Hager (2011) encourage adopting a smoother bridge deck design to favour log passing. Results confirmed by the current research: we found that congested wood transport and a not-streamlined pier favour wood jam formation at the bridge pier.

The present research provides also interesting observations and results on the influence of the flow field on the log motion and wood-pier interaction. The experimental observation on the orientation and track logs approaching the pier confirm the experimental results of Adachi and Daido (1957). They did not analyse the effect of the pier shape on the wood-pier interaction but just the cases for wood to pass after touching the pier. They defined the percentage of logs to be washed away after touching the pier depending on the way in which the log approaches the pier. The Figure 6.6 (left) represent four main cases: (a) when the log passes without touching the pier; (b) the log touches the pier and slides down; (c) the log bumps into the pier and bounces backward and then it flows away; and (d) the log bumps into the pier and the pressure of the running water on the left and right of the log is balanced, so the log stops at the pier. Although Figure 6.6 illustrates the case of logs introduced perpendicular to the flow, the authors (Adachi and Daido, 1957) affirm to obtain quite similar results for logs introduced parallel to the flow direction. The highest percentage of logs blocked at the pier was obtained with Fr=0.4 and in the case (d).
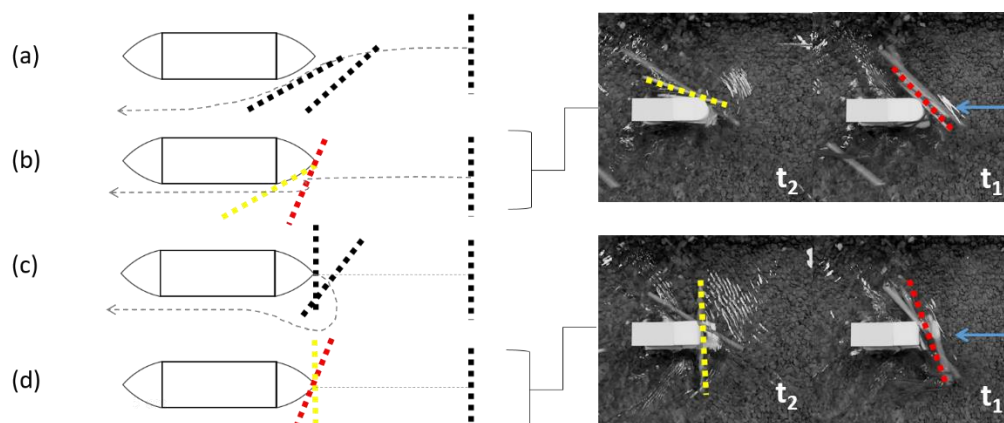
Figure 6.6 Cases of state for timbers to be washed away, on the left (Adapted from Adachi and Daido, 1957) compared with the experimental observation presented in the current research, on the right.

In the current research, the cases (c) and (d) were observed more often at Fr=0.5, when the logs moved mainly in the centreline and then the blockage probability was greater, while the cases (a) and (b) were more frequent at Fr=0.3, when the logs moved both in the centreline and towards the walls. Figure 6.6 (on right) shows the comparison between the experimental observations by Adachi and Daido (1957) and the present experimental observations for cases (b) and (d) revealing similar results.

The application of the 2D model *Iber* to the real case study of the Dlugopole bridge in the Czarny Dunajec River in Poland, is recently presented by Ruiz-Villanueva et al. (2016a). They reached the same conclusions: the wood accumulation formation cannot be reproduced with a 2D model because it is a 3D process. Even if the *Wood-Iber* tool reproduces the interactions between two floating logs, it does not simulate the superposition of logs. Thus, the application of a 2D model only permits to determine the "potential blockage probability", i.e. the logs that touch the pier but not the logs that stop at the pier.

Flow 3D allowed for the first time to investigate the 3D character of the process of single-pier accumulation. The only existing 3D model of a piece of wood is due to Xu and Liu (2016) that was used to simulate the streamflow around a complex shaped log but not its movement in water. 3D data to compare with the results presented in this research do not exist.

The drag coefficient of a single log calculated from the drag force computed with the 3D numerical model was compared with the experimental value by Gippel et al. (1992), obtained measuring the drag force on a submerged log. The comparison showed a good agreement of drag coefficients for submerged logs while for floating semi-submerged logs the drag coefficient is lower than the values from Gippel (Figure 5.33, A).

6.6   Insights into the physics of the problem

The transport of floating logs in rivers may be assumed as a 2D process if we consider the transport of a single log or a "carpet" of multiple logs that move without interacting each other. The process becomes more complicated when the logs interact with an obstacle as the bridge pier. The single-pier accumulation formation is a totally

3D process: the accumulation grows vertically, not only in horizontal plane and it starts with few logs that stop at the pier and then the upcoming logs deposit above and below the existing logs.

This research demonstrated the difficulties in reproducing the wood-pier interaction with a 2D numerical model while the application with the 3D model reproduces the movement of the log along the vertical face of the pier.

Further, the results showed also interesting observations on log motion with varying the Froude number. What emerges is that the transport of logs in straight rectangular flume may be a quasi-3D process, because the vortices that originate the secondary currents from a different roughness between the bed and the walls pushes the flow towards the walls or the centreline according to the ratio between the flume width and the water depth. In natural streams, the more irregular geometry and morphology of the river (e.g. the meandering rivers) affect the log motion and thus the deposition (e.g., the secondary currents are associated to the channel curvature and to the transverse pressure gradient). This is also the reason why the application of the 2D model to real cases study (as specified in Chapter 2 and in Section 6.5) gives good results in terms of volume of wood deposited on the river banks. However, the same application did not give the "effective" number of deposited logs at the bridge pier but only the "potential" blockage probability, i.e. the number of logs that touch the pier (see Ruiz-Villanueva et al., 2016a).

In the wood-pier interaction, the skin friction at the contact point between the log surface and the pier surface plays an important role. Some of the 3D numerical tests showed the approaching logs touching the pier and stopping at the pier for few seconds before floating away. This behaviour has been observed in the experimental tests but not in 2D simulations where the logs are simulated as smooth cylinders. However, a more complete approach requires many factors to be considered, as the acting forces on the log, the resultant moment of the forces, the position of the log centre when it bumps into the pier and the friction between the log and the pier.

7 Conclusions

In the present work, the process of interaction between wood and bridge piers has been investigated combining experimental and numerical approaches. The former, aimed to find the wood accumulation probability as a function of the pier geometry, hydraulic conditions and wood transport regime. The latter, to assess the capability of 2D and 3D numerical models in reproducing the wood-pier interaction. The main points investigated are:

- the examination of the main controlling parameters for a single-pier accumulation through the identification of the non-dimensional groups that define the probability function (P);
- the definition of the joint blockage probability (JP) at bridge pier valid for the prevailing variables used in the study;
- the effect of the pier shape on the flow field upstream of the pier and thus on the log motion and its blockage at the pier;
- the influence of the secondary currents on log motion and thus on log blockage probability at the pier;
- the ability of 2D and 3D numerical models to reproduce the wood-pier interaction process and to capture the log travel path and thus the blockage probability at the pier.

This topic is of importance to river scientists and public authorities, because the inherent dangerous caused by bridge clogging by wood in urbanized areas (inundation of populated areas) and for river structures (collapse and pier scour). The other aspect is its significance as a functional component of fluvial ecosystems. Regarding the foregoing aspects, the current research contributes to progress the knowledge in wood-pier interaction.

The results suggest that the pier shape has a great influence on blockage probability because it affects the flow field region upstream of the pier. The flow field changes according to the hydraulic conditions defined by the Froude number. The ratio between the channel width and flow depth affects the formation of secondary currents along the channel centreline that determines the horizontal log travel path. With the interaction of the log with the obstacle the process become 3D. The log moves also along the vertical face of the pier because the vertical hydrodynamic forces acting on the log and against the obstacle. Thus, the accumulation grows also vertically as well as horizontally. The numerical simulations carried out with both 2D and 3D models, proved this aspect.

The numerical modelling may provide useful support to researchers and authorities for analysing different possible wood blockage scenarios and for planning prevention management strategies such as the installation of wood retention structures.

The current research highlights the strengths and weaknesses of the existing 2D models (e.g. *Wood-Iber*) and presents the application of a new 3D model (*Flow-3D*) of wood-pier interaction.

Despite the capabilities of the 2D model in reproducing the log transport and a quasi-3D process obtained reproducing the interaction between two logs floating at different water depths, the main shortcoming are the lack of secondary flows, the log-pier interactions, the superposition of logs, the non-elastic collisions between logs and the skin friction of logs. The 3D simulations confirmed the influence of secondary currents on log motion and reproduced the non-elastic collisions between non-smoothed logs floating along the vertical upstream face of the pier.

The ratio between wood discharge and flow discharge is an additional important influencing blockage. The increasing number of floating logs approaching the pier promotes log interactions and superposition that are critical conditions in presence of an obstacle.

The main contribution is the definition of a joint blockage probability at a bridge pier for the prevailing influencing factors. Given the pier geometry, the hydraulic conditions and the wood discharge it is possible to determine the value of wood blockage probability of logs at a single pier. This approach is useful specially to prevent wood accumulation at non-standard pier shapes typical of historical cities.

8   Future work

The current research provides insight into a number of key factors that define the blockage probability of wood accumulation at bridge piers but there are still many remaining challenges to address. Concerning the experiments, we investigated subcritical flow conditions (Fr<1) because the aim of the research was to analyze the wood accumulation at piers in lowland rivers. Froude numbers between 0.5 and 1, need to be investigated as well for analyzing the same process in high slope torrents. Furthermore, only the single pier accumulation was reproduced in flume, the suggestion for future research is to investigate the pier-to-pier wood accumulation, as well.

Numerical models provide a powerful tool, especially as they can be used to analyze possible flood hazard scenarios related to the presence of wood in rivers. *Iber-Wood* proved to be a good tool for wood transport and wood deposition simulation in rivers. At the time of this research, some aspects concerning the wood-structure interactions can be considered for further developments, such as the implementation of non-elastic collisions and the skin wood friction.

More 3D simulations with different pier shapes (triangular, semi-circular, Ogival and trapezoidal) and Froude numbers are needed.

The results from the current research may provide a support to design bridge or countermeasures aimed at minimizing wood-related hazards. In this regard, field data on wood transport (especially during high-magnitude flood events) and accumulation at bridges, are needed. The lack or insufficient field data constitute one of the main problems for researchers.

The monitoring activity and the implementation of multiple processes and factors in numerical models such as sediment transport, the complex nature of log shapes (incl. roots and branches), the number of piers, as well as different river morphologies. The combination of numerical modelling, together with experiments is a powerful approach for prevention strategies. It also may furnish more details with respect to the mechanisms of bridge clogging or cross-section obstruction by wood.

_____

References

Abbe, T. B. and D. R. Montgomery (1996), Large woody debris jams, channel hydraulics and habitat formation in large rivers, Regul. *Rivers, Res. Mgmt.*, 12, 201–221.

Abbe, T. B., and Montgomery, D. R. (2003). Patterns and processes of wood debris accumulation in the Queets river basin, Washington. Geomorphology, 51(1-3), 81–107.

Adachi, S. and Daido, A. (1957). Experimental study on washed timbers, Annuals Disas. Prev. Res. Inst. Kyoto Univ., No. 1, pp41–49.

Albayrak, I.,and Lemmin, U. (2011)."Secondary currents and corresponding surface velocity patterns in a turbulent open-channel flow over a rough bed." J. Hydraul. Eng., 10.1061/(ASCE)HY.1943-7900 .0000438, 1318–1334.

Allen, J. B. & Smith, D. L. (2012). Characterizing the impact of geometric simplification on large woody debris using CFD. Int. J. Hydr. Eng. 1, 1–14.

Auel, C., Albayrak, I., and Boes, R. (2014). "Turbulence Characteristics in Supercritical Open Channel Flows: Effects of Froude Number and Aspect Ratio." *J. Hydraul. Eng.*, 10.1061/(ASCE)HY.1943-7900.0000841, 04014004.

Badoux, A., M. Böckli, D. Rickenmann, C. Rickli, V. Ruiz-Villanueva, S. Zurbrügg, and M. Stoffel (2015), Large wood transported during the exceptional flood event of 24 July 2014 in the Emme catchment (Switzerland). Proceedings of the Wood in World Rivers Conference, Padova, Italy, July 2015.

Benda, L. E., and J. C. Sias (2003), A quantitative framework for evaluating the mass balance of in-stream organic debris, For. Ecol. Manage., 172(1), 1–16, doi: 10.1016/S0378-1127(01)00576-X.

Benke, A.C. and B.J. Wallace (2003), Influence of wood on invertebrate communities in streams and rivers. In: Gregory, S.V., Boyer, K.L., Gurnell, A.M. (Eds.), *The Ecology and Management of Wood in World Rivers*. American Fisheries Society, Symposium 37, Bethesda, MD, pp. 149–177.

Bertoldi, W., M. Welber, L. Mao, S. Zanella, and F. Comiti (2014), A flume experiment on wood storage and remobilization in braided river systems, *Earth Surface Processes and Landforms*, 39(6), 804–813. doi,10.1002/esp.3537.

Bilby, R.E., and Ward, J.W., (1989). Changes in characteristics and function of woody debris with increasing size of streams in western Washington: Transactions of the American Fisheries Society, v. 118, no. 4, p. 368–378.

Bilby, R.E., (2003). Decomposition and nutrient dynamics of wood in streams and rivers. Gregory, Stan V., Boyer, Kathryn L., Gurnell, Angela M. The Ecology And Management Of Wood In World Rivers: 135-147

Bladé, E., Sánchez-Juny, M., Ruiz-Villanueva, V. (2016). Strategies in the 2D numerical modelling of wood transport in rivers. Proceeding of the Eight International Conference on Fluvial Hydraulics. St. Louis, Mo, USA 12-15 July 2016.

Bladé, E., Cea, L., Corestein, G., Escolano, E., Puertas, J., Vázquez Cendón, M. E., Dolz, J. & Coll, A. (2012). Iber – Herramienta de simulación numérica del flujo en ríos. Rev. Int. Metod. Numer. 30 (1), 1–10.

Bocchiola, D., M. C. Rulli, and R. Rosso (2006), Flume experiments on wood entrainment in rivers, *Advances in Water Resources,* 29(8), 1182–1195.

Bocchiola, D., M. C. Rulli, and R. Rosso (2008), A Flume Experiment on the Formation of Wood Jams in Rivers, *Water Resources Research,* 44 (2). doi,10.1029/2006WR005846.

Bradley, J.B., Richards, D.L., Bahner, C.D. (2005). Debris control structures: Evaluation and countermeasures. Report No. FHWA-IF-04-016, Hydraulic Engineering Circular No. 9, 3rd ed. Federal Highway Administration, Washington, DC.

Bray, D.I., Davar, K.S., (1987). Resistance to flow in gravel-bed rivers. Can. J. Civ. Eng. 14, 77–86.

Braudrick, C. A., G. E. Grant, Y. Ishikawa, and H. Ikeda (1997), Dynamics of wood transport in streams , a flume experiment, *Earth Surface Processes and Landforms,* 22, 669–83.

Braudrick, C. A., and G. E. Grant (2000), When do logs move in rivers?, *Water Resources Research*, 36(2), 571–583. doi,10.1029/1999WR900290.

Braudrick, C. A., and G. E. Grant (2001), Transport and deposition of large woody debris in streams, a flume experiment, *Geomorphology*, 41(4), 263–283. doi,10.1016/S0169-555X(01)00058-7.

Buxton, T. H. (2010), Modeling entrainment of waterlogged large wood in stream channels, Water Resour. Res., 46, W10537, doi:10.1029/2009WR008041.

Chin, A., Daniels, M.D., Urban, M.A., Piégay, H., Gregory, K.J., Bigler, W., Butt, A.Z., Grable, J.L., Gregory, S. V., Lafrenz, M., Laurencio, L.R., Wohl, E., (2008). Perceptions of wood in rivers and challenges for stream restoration in the United States. Environ. Manage. 41, 893–903. doi:10.1007/s00267-008-9075-9.

Chin, A., Laurencio, L.R., Daniels, M.D., Wohl, E., Urban, M.A., Boyer, K.L., Butt, A., Piegay, H., Gregory, K.J., (2012). The significance of perceptions and feedbacks for effectively managing wood in rivers. doi:10.1002/rra.

Comiti F., A. Andreoli, M.A. Lenzi, and L. Mao (2006), Spatial density and characteristics of woody debris in five mountain rivers of the Dolomites (Italian Alps), *Geomorphology*, 78, 44-63.

Comiti F, A Andreoli, L Mao, MA Lenzi. (2008). Wood storage in three mountain streams of the Southern Andes and its hydro-morphological effects. Earth Surface Processes and Landforms 33: 244-262.

Comiti, F. (2012), How natural are Alpine mountain rivers? Evidence from the Italian Alps. Earth Surf. Process. Landforms, 37: 693–707. doi:10.1002/esp.2267

Comiti, F., V. D. Agostino, M. Moser, M. A. Lenzi, F. Bettella, A. D. Agnese, and B. Mazzorana (2012), Preventing wood-related hazards in mountain basins , from wood load estimation to designing retention structures, Interpraevent 12th Congress Proceedings, Grenoble, France.

Comiti, F., Lucía, A., & Rickenmann, D. (2016). Large wood recruitment and transport during large floods: A review. Geomorphology, 269, 23–39. http://doi.org/10.1016/j.geomorph.2016.06.016.

Corestein, G., Bladé, E., Cea, L., Lara, Á. & Escolano, E. (2010) Iber, a river dynamics simulation tool. In: Proceedings of GiD conference: GiD 2010, CIMNE

Crosato, A., & Rajbhandari, N. (2011). Experimental study on entrainment of large wood in lowland rivers, Euromech Colloquium 523. Ecohydraulics: linkages between hydraulics, morphodynamics and ecological processes in rivers. Clermont-Ferrand, France, 15-17 juni 2011.

Crosato, A., Rajbhandari, N., Comiti, F., Cherradi, X., & Uijttewaal, W. (2013). Flume experiments on entrainment of large wood in low-land rivers. Journal of Hydraulic Research, 51(5), 581–588. http://doi.org/10.1080/00221686.2013.796573

Curran, J. C. (2010), Mobility of large woody debris (LWD) jams in a low gradient channel, *Geomorphology*, 116(3-4), 320–329. doi,10.1016/j.geomorph.2009.11.027.

Curran, J.H., E.E. Wohl (2003), Large woody debris and flow resistance in step-pool channels, Cascade Range, Washington, *Geomorphology*, 51 (1–3), 141. Diehl, T. H. (1997). Potential Drift Accumulation at Bridges. U.S. Geological Survey, Water Resources Division.

De Cicco, P.N., Paris, E., Solari, L., (2016). Wood accumulation at bridges: laboratory experiments on the effects of pier shape. Proceeding of the Eight International Conference on Fluvial Hydraulics. St. Louis, Mo, USA 12-15 July 2016.

Diehl, T.H. (1997). Potential drift accumulation at bridges. Publication No. FHWA–RD–97–028. Federal Highway Administration, Washington, DC.

Dolloff, C. A., & Warren, M. L. (2003). Fish Relationships with Large Wood in Small Streams. American Fisheries Society Symposium, 37, 179–193.

Dongol, M. S. (1989). "Effect of Debris Rafting on Local Scour at Bridge Piers," Report No. 473, School of Engineering, University of Auckland, Auckland, New Zealand.

_____

Francalanci S., Paris E., Solari L., Federici G.V. (2016). Monitoraggio e idraulica del tratto urbano del fiume Arno a Firenze, Atti del XXXV Convegno di Idraulica e Costruzioni Idrauliche, Bologna, 14-16 Settembre 2016.

Francalanci, S., E. Paris, and L. Solari (2013), A combined field sampling-modeling approach for computing sediment transport during flash floods in a gravel-bed stream, Water Resour. Res., 49, 6642–6655, doi:10.1002/wrcr.20544.

Fremier, Alexander K., Jung Il Seo, and Futoshi Nakamura. (2010). "Watershed Controls on the Export of Large Wood from Stream Corridors." *Geomorphology* 117(1-2): 33–43. http://linkinghub.elsevier.com/retrieve/pii/S0169555X09004681 (May 13, 2014).

Gippel, C.J., O'Neill, I.C., and Finlayson, B.L., (1992). The hydraulic basis of snag management: Melbourne, University of Melbourne, Center for Environmental Applied Hydrology, 116 p.

Gippel, C. J., O'Neill, I. C., Finlayson, B. L., and Schnatz, I.(1996). "Hydraulic guidelines for the re-introduction and management of large woody debris in lowland rivers." Regulated Rivers: Research Management, **12**, 223–236.

Gregory, Stan V.; Boyer, Kathryn L.; Gurnell, Angela M., (2003) eds. The Ecology and Management of Wood in World Rivers. Symposium 37. American Fisheries Society.

Gschnitzer, T., Gems, B., Aufleger, M., Mazzorana, B.,Comiti, F. Physical Scale Model Test on Bridge Clogging. (2013) Proceedings of the 35th IAHR World Congress. Beijing: Tsinghua University Press, 2013, ISBN 978-7-89414-588-8, elektronisch.

Gurnell, A (2013). Wood in Fluvial Systems. Treatise on Geomorphology, Chapter 236 - 9.11 9(1994), 163–188. doi:10.1016/B978-0-12-374739-6.00236-0.

Gurnell, A. (2012). Fluvial Geomorphology: Wood and river landscapes. *Nature Geoscience*, *5*(2), 93–94. doi:10.1038/ngeo1382

Gurnell, A. M., Piegay, H., Swanson, F. J., & Gregory, S. V. (2002). Large wood and fluvial processes. Freshwater Biology, (47), 601–619.

Haga, H., Kumagai, T., Otsuki, K., & Ogawa, S. (2002). Transport and retention of coarse woody debris in mountain streams: An in situ field experiment of log transport and a field survey of coarse woody debris distribution. Water Resources Research, 38(8), 1–1–1–16. http://doi.org/10.1029/2001WR001123

Harmon, M.E., J.F. Franklin, and F.J. Swanson (1986), Ecology of coarse woody debris in temperate ecosystems, *Advances in Ecological Research,* 15,133-302.

Jochner, M., J. M. Turowski, A. Badoux, M. Stoffel, and C. Rickli (2015), The role of log jams and exceptional flood events in mobilizing coarse particulate organic matter in a steep headwater stream, *Earth Surface Dynamics Discussions,* 3, 173–196. doi,10.5194/esurfd-3-173-2015.

Johnson, J. W., "The Importance of Side-Wall Friction in Bed-Load Investigations" (1942). Civil Eng., Vol. 12, No. 6, June 1942, pp. 329- 331.

Johnson, P.A. and Sheeder, S.A. (2011). Controlling debris at bridges. Pages 385-397 in Simon A., S.J. Bennett, J.M. Castro, eds. Stream Restoration in Dynamic Fluvial Systems: Scientific Approaches, Analyses, and Tools. American Geophysical Union Kattell, J., & Eriksson, M. (1998). Bridge Scour Evaluation : Screening , Analysis , & Countermeasures, (September), 41.

Kattell, J., and Eriksson, M. (1998). "Bridge Scour Evaluation: Screening, Analysis, and Countermeasures." Pub. Rep. No.9877, USDA Forest Service, Washington, D.C.

Koch, A., and Carstanjen, M. (1926). "Von der Bewegung des Wassers und den dabei auftretenden Kraeften." Springer-Verlag KG, Berlin, Germany.

Kramer, N., & Wohl, E. (2014). Estimating fluvial wood discharge using time-lapse photography with varying sampling intervals. Earth Surface Processes and Landforms, 39(6), 844–852. http://doi.org/10.1002/esp.3540

Kundu, P.K., Cohen, I.M., (2008). *Fluid Mechanics*, 4th Edition, Academic, San Diego, USA.

Lagasse, P. F., P. E. Clopper, L. W. Zevenbergen, W. J. Spitz, and L. G. Girard (2010), Effects of debris on bridge pier scour, NCHRP Rep. 653, Transp. Res. Board, Washington, D. C (Available at http://onlinepubs.trb.org/onlinepubs/nchrp/nchrp_rpt_653.pdf).

Lange, D., Bezzola, G.R., (2006). Schwemmholz. Probleme und Lösungsansätze. Laboratory of Hydraulics, Hydrology and Glaciology (VAW), ETHZ, Zürich, Mitteilungen, 188, p. 125 (in German).

Lassettre, N.S., Kondolf, G.M., (2012). Large woody debris in urban stream channels: redefining the problem. River Res. Appl. 28 (9), 1477–1487. http://dx.doi.org/10. 1002/rra.1538.

Laursen, E. M., and Toch, A. (1956). Scour around bridge piers and abutments. Bull. No. 4, Iowa Highways Research Board, Ames, Iowa.

Le Lay, Y.-F., Piégay, H., Moulin, B., (2013). Wood entrance, deposition, transfer and effects on fluvial forms and processes: problem statements and challenging issues. In: Shroder, J. (Editor in Chief), Butler, D.R., Hupp, C.R. (Eds.), Treatise on Geomorphology. Academic Press, San Diego, CA, vol. 12, Ecogeomorphology, pp. 20–36.

Lucía, F., M. Comiti, M. Borga, and M. Cavalli (2014), Large wood recruitment and transport during a severe flash flood in North-western Italy, *Engineering Geology for Society and Territory,* 3, 159-162.

Lucía, A., Comiti, F., Borga, M., Cavalli, M., & Marchi, L. (2015). Dynamics of large wood during a flash flood in two mountain catchments, 1741–1755. http://doi.org/10.5194/nhess-15-1741-2015

Lyn D.A., T. Cooper, Y. K. Yi, R. N. Sinha, and A.R. Rao (2003), Debris Accumulation at Bridge Crossings, Laboratory and Field Studies, TRB Subject Code: 25-1 Publication No.: FHWA/IN/JTRP-2003/10, SPR-2478.

Lyn, D., T. Cooper, D. Condon, and L. Gan (2007), Factors in debris accumulation at bridge piers, Washington, U.S. Department of Transportation, Federal Highway Administration Research and Development, Turner-Fairbank Highway Research Center.

MacVicar, B., and H. Piégay (2012), Implementation and validation of video monitoring for wood budgeting in a wandering piedmont river, the Ain River (France), *Earth Surface Processes and Landforms,* 37(12), 1272–1289. doi,10.1002/esp.3240.

Manners, R.B., Doyle, M.W., Small, M.J., (2007). Structure and hydraulics of natural woody debris jams. Water Resources Research 43 (6), 17

Mao, L., A. Andreoli, A. Iroumé, F. Comiti, and M. A. Lenzi (2013), Dynamics and management alternatives of in-channel large wood in mountain basins of the southern Andes, *Bosque (Valdivia)*, 34(3), 15–16. doi,10.4067/S0717-92002013000300008.

Mazzorana, B., A. Zischg, A. Largiader, and J. Hubl (2009), Hazard index maps for woody material recruitment and transport in alpine catchments, *Nat. Hazards Earth Syst. Sci.,* 9, 197–209.

Mazzorana, B., J. Hübl, A. Zischg, and A. Largiader (2011), Modelling Woody Material Transport and Deposition in Alpine Rivers, *Natural Hazards,* 56 (2), 425–49. doi,10.1007/s11069-009-9492-y.

McLelland, S. J. (2013) Coherent Secondary Flows Over a Water-Worked Rough Bed in a Straight Channel, in Coherent Flow Structures at Earth's Surface (eds J. G. Venditti, J. L. Best, M. Church and R. J. Hardy), John Wiley & Sons, Ltd, Chichester, UK. doi: 10.1002/9781118527221.ch18

Melville, B. and Dongol, D. (1992). Bridge Pier Scour with Debris Accumulation. J. Hydraul. Eng., , 10.1061/ (ASCE) 0733- 9429(1992)118:9(1306), 1306-1310.

Merten, E., J. Finlay, L. Johnson, R. Newman, H. Stefan, and B. Vondracek (2010), Factors influencing wood mobilization in streams, Water Resour. Res., 46, W10514, doi:10.1029/2009WR008772.

Montgomery, D.R., Collins, B.D., Buffington, K.M., Abbe, T.B., (2003). Geomorphic effects of wood in rivers. In: Gregory, S., Boyer, K., Gurnell, A. (Eds.), The Ecology and Management of Wood in World Rivers. American Fisheries Society Symposium, Bethesda, Maryland, pp. 21–47.

Montgomery, D. R., & Piégay, H. (2003). Wood in rivers: interactions with channel morphology and processes. Geomorphology, 51, 1–5. http://doi.org/10.1016/S0169-555X(02)00322-7

Moulin B., and H. Piégay (2004), Characteristics and temporal variability of large woody debris trapped in a reservoir on the river Rhône (Rhône), implications for river basin management, *River Research and Applications*, 20, 79-97.

_____

Mutz,M., Piégay, H., Gregory, K.J., Borchardt, D., Reich, M., Schmieder, K., (2006). Perception and evaluation of dead wood in streams and rivers by German students. Limnologica-Ecology and Management of Inland Waters 36 (2), 110–118. http://dx.doi.org/10.1016/j.limno.2006.01.001.

Nakamura F, Swanson FJ. (1993). Effects of coarse woody debris on morphology and sediment storage of a mountain stream system in western Oregon. Earth Surf Proc. Landforms 18:43-61

Nezu, I., and Nakagawa, H. (1993). "Turbulence in open-channel flows." IAHR monograph, Balkema, Rotterdam, The Netherlands.

Pagliara, S., & Carnacina, I. (2010). Temporal scour evolution at bridge piers: effect of wood debris roughness and porosity. Journal of Hydraulic Research, 48 , 3–13.

Pagliara, S., and I. Carnacina (2011), Influence of large woody debris on sediment scour at bridge piers, Int. J. Sediment Res., 26(2), 121–136, doi:10.1016/S1001-6279(11)60081-4.

Parola, A.C., Apelt, C.J., Jempson, M.A. (2000). Debris forces on highway bridges. NCHRP Report No. 445. Transportation Research Board, Washington, DC.

Petaccia, G., Soares-Frazão, S., Savi, F., Natale, L. & Zech, Y. (2010). Simplified versus Detailed Two-Dimensional Approaches to Transient Flow Modeling in Urban Areas, Journal of Hydraulic Engineering, 136(4), 262–266.

Persi, E., Petaccia, G., Manenti, S., Ghilardi, P., Sibilla, S. (2016). Il trasporto di detriti galleggianti: modellazione bidimensionale e misure idrodinamiche. Atti del XXXV Convegno Nazionale di Idraulica e Costruzioni Idrauliche, 15-16 Settembre 2016, Bologna (Italy).

Piégay, H. (1993). Nature, Mass and Preferential Sites of Coarse Woody Debris Deposits in the Lower Ain Valley (Mollon Reach), France. Regulated Rivers-Research & Management, 8(4), 359–372. http://doi.org/DOI 10.1002/rrr.3450080406

Piégay, H., & Gurnell, A. M. (1997). Large woody debris and river geomorphological pattern: examples from S.E. France and S. England. Geomorphology, 19(1–2), 99–116. http://doi.org/http://dx.doi.org/10.1016/S0169-555X(96)00045-1

Piégay, H., Gregory, K.J., Bondarev, V. et al. Environmental Management (2005) 36: 665. doi:10.1007/s00267-004-0092-z.

Piton, G., and A. Recking (2015), Design of sediment traps with open check dams: a review-Part II: Woody Debris, Journal of Hydraulic Engineering, 1-13, doi:10.1061/(ASCE)HY.1943-7900.0001049

Plate, E., and Goodwin, C. (1965). The influence of wind on open channel flow. Coastal Engg, Santa Barbara Specialty Conference (ASCE), 391-423.

Powell, D. M. (2014), Flow resistance in gravel-bed rivers: Progress in research, Earth Sci. Rev., 136, 301–338.

Rickenmann, D., Waldner, P., Usbeck, T., Köchil, D., Sutter, F., Rickli, C., Badoux, A. (2015). Large wood transport during the 2005 flood events in Switzerland. Proceedings of the Wood in World Rivers Conference, Padova, Italy, July 2015.

Rickenmann D, Badoux A, Hunzinger L (2016) Significance of sediment transport processes during piedmont floods: the 2005 flood events in Switzerland. Earth Surface Processes and Landforms 41(2): 224-230, doi:10.1002/esp.3835.

Rinaldi, M., Amponsah, W., Benvenuti,M., Borga, M., Comiti, F., Lucìa, A., Marchi, L., Nardi, L., Righini, M., Surian, N., (2016). An integrated approach for investigating geomorphic response to an extreme flood event: the case of the Magra River. Earth Surf. Process. Landf. 41, 835–846. http://dx.doi.org/10.1002/esp.3902.

Rosholt, Malcolm (1980). The Wisconsin Logging Book - 1839-1939 (PDF). Rosholt, Wisconsin: Rosholt House. p. 190. ISBN 0-910417-05-9.

Ruiz-Villanueva, V., Bladé Castellet, E., Díez-Herrero, A., Bodoque, J. M., & Sánchez-Juny, M. (2013a). Two-dimensional modelling of large wood transport during flash floods. Earth Surface Processes and Landforms, 39(4), 438–449. http://doi.org/10.1002/esp.3456

Ruiz-Villanueva, V., Bodoque, J. M., Díez-Herrero, A., Eguibar, M. a., & Pardo-Igúzquiza, E. (2013b). Reconstruction of a flash flood with large wood transport and its influence on hazard patterns in an ungauged mountain basin. Hydrological Processes, 27(24), 3424–3437. http://doi.org/10.1002/hyp.9433

Ruiz-Villanueva, V., Bladé Castellet, E., Sánchez-Juny, M., Marti-Cardona, B., Díez-Herrero, A., & Bodoque, J. M. (2014a). Two-dimensional numerical modeling of wood transport. Journal of Hydroinformatics, 16(5), 1077. http://doi.org/10.2166/hydro.2014.026

Ruiz-Villanueva, V., Bodoque, J. M., Díez-Herrero, A., & Bladé Castellet, E. (2014b). Large wood transport as significant influence on flood risk in a mountain village. Natural Hazards. http://doi.org/10.1007/s11069-014-1222-4

Ruiz-Villanueva, V., Díez-Herrero, A., Ballesteros, J. A., & Bodoque, J. M. (2014c). Potential large woody debris recruitment due to landslides, bank erosion and floods in mountain basins: A quantitative estimation approach. River Research and Applications, 30(1), 81–97. http://doi.org/10.1002/rra.2614

Ruiz-Villanueva, V., Wyzga, B., Hajdukiewicz, H., & Stoffel, M. (2015). Exploring large wood retention and deposition in contrasting river morphologies linking numerical modelling and field observations. Earth Surface Processes and Landforms, 41(4), 446–459. http://doi.org/10.1002/esp.3832

Ruiz-Villanueva, V., Miku, P., Hajdukiewiczd, M., Stoffel, M., (2016a). Potential large wood-related hazards at bridges : the Długopole bridge in the Czarny Dunajec River, Polish Carpathians, in: Interpraevent 2016. pp. 610–618.

Ruiz-Villanueva, V., Piégay, H., Gurnell, A.A., Marston, R.A., Stoffel, M., (2016b). Recent advances quantifying the large wood dynamics in river basins: New methods and remaining challenges. Rev. Geophys. 1–42. doi:10.1002/2015RG000514.

Ruiz-Villanueva, V., Wyżga, B., Mikuś, P., Hajdukiewicz, H., Stoffel, M., (2016c). The role of flood hydrograph in the remobilization of large wood in a wide mountain river. J. Hydrol. doi:10.1016/j.jhydrol.2016.02.060

Rusyda, I. M. (2015). Log jams at a bridge with a pier and a bridge without pier. Procedia Engineering, 125, 277–283. http://doi.org/10.1016/j.proeng.2015.11.040

Schmocker, L., and W. H. Hager (2010), Drift Accumulation at River Bridges. River Flow 2010 - Dittrich, Koll, Aberle & Geisenhainer (eds).

Schmocker, L., Hager, W. H., & Asce, F. (2011). Probability of Drift Blockage at Bridge Decks, 470–479. http://doi.org/10.1061/(ASCE)HY.1943-7900.0000319.

Schmocker, L., & Hager, W. H. (2013a). Scale Modeling of Wooden Debris Accumulation at a Debris Rack. Journal of Hydraulic Engineering, 139(8), 827–836. http://doi.org/10.1061/(ASCE)HY.1943-7900.0000714.

Schmocker, L., and V. Weitbrecht (2013b), Driftwood , Risk Analysis and Engineering Measures, *Journal of Hydraulic Engineering*, 683–695. doi,10.1061/(ASCE)HY.1943-7900.0000728.

Schmocker L., Brändli D., Weitbrecht V., Boes R.M. (2015). Backwater rise due to driftwood accumulations. Proc. 36th IAHR World Congress. The Hague, the Netherlands.

Schalko, I., Schmocker, L., Weitbrecht, V., and Boes, R.M., (2016). Modeling the effect of organic fine material in a driftwood accumulation on backwater rise. Proc. River Flow 2016, St. Louis, USA, Constantinescu, Garcia & Hanes (Eds.), ISBN 978-1-315-64447-9: 2326-2332.

Shields, F. D., Jr., and C. V. Alonso (2012). Assessment of flow forces on large wood in rivers, Water Resour. Res., 48, W04516, doi:10.1029/2011WR011547

Seo, Jung Il et al. (2015). "Precipitation Patterns Control the Distribution and Export of Large Wood at the Catchment Scale." *Hydrological Processes*: n/a – n/a. http://doi.wiley.com/10.1002/hyp.10473.

Seo, Jung Il, and Futoshi Nakamura. (2009). "Scale-Dependent Controls upon the Fluvial Export of Large Wood from River Catchments." 800(February): 786–800.

Shields, F. D., Jr., and C. V. Alonso (2012), Assessment of flow forces on large wood in rivers, Water Resour. Res., 48, W04516, doi:10.1029/2011WR011547.

Shrestha, B. B., Nakagawa, H., Kawaike, K., Baba, Y., & Zhang, H. (2012). Driftwood deposition from debris flows at slit-check dams and fans. Natural Hazards, 61(2), 577–602. http://doi.org/10.1007/s11069-011-9939-9

_____

Solari L, Van Oorschot M, Hendriks D, Rinaldi M, Vargas-Luna A. (2015). Advances on modelling riparian vegetation-hydromorphology interactions. River Research and Applications 32: 164–178. DOI: 10.1002/rra.2910

Solari, L., Van Oorschot, M., Belletti, B., Hendriks, D., Rinaldi, M., and Vargas-Luna, A. (2016) Advances on Modelling Riparian Vegetation—Hydromorphology Interactions. River Res. Applic., 32: 164–178. doi: 10.1002/rra.2910.

Thévenet, A., A. Citterio, and H. Piégay (1998), A new methodology for the assessment of large woody debris accumulations on highly modified rivers (example of two French piedmont rivers), Regulat. Rivers, 14, 467–483.

Tominaga, A., Nezu, I., Ezaki, K., and Nakagawa, H. (1989). "Threedimensional turbulent structure in straight open channel flows." J. Hydraul. Res., 27(1), 159–173.

Tyler, R.N. (2011). River Debris: Causes, Impacts, and Mitigation Techniques. Alaska Center for Energy and Power, p1 - 33.

Vanoni, V. A., and Brooks, N. H., (1957). "Laboratory Studies of the Roughness and Suspended Load of Alluvial Streams," Sedimentation Laboratory, California Institute of Technology, Report E-68, Pasadena, Calif.

Waldner, P., et al. (2010). Schwemmholz des Hochwassers 2005 [Driftwood during the 2005 flood event]. Final Report. Federal Office for the Environment FOEN, Swiss Federal Institute for Forest, Snow, and Landscape Research, WSL, Birmensdorf (in German).

Wallerstein, N., & Thorne, C. R. (1997). Impacts of woody debris on fluvial processes and channel morphology in stable and unstable streams. U.S. Army Research Development and Standardization Group, London.

Wallerstein, N., Alonso, C. V., Bennett, S. J., and Throne, C. R.(2002). "Surface wave forces acting on submerged logs." J. Hydraul. Eng., **128**(**3**), 349–353.9fn

Wohl, E. (2011). Threshold-induced complex behavior of wood in mountain streams. Geology, 39(6), 587–590. doi:10.1130/G32105.1

Wohl, E. (2013). Floodplains and wood. Earth-Science Reviews, 123, 194–212.

Wohl, E. (2014). "A Legacy of Absence: Wood Removal in US Rivers." Progress in Physical Geography 38(5): 637–63. http://ppg.sagepub.com/cgi/doi/10.1177/0309133314548091.

Wohl, E., Cenderelli, D. a., Dwire, K. a., Ryan-Burkett, S. E., Young, M. K., & Fausch, K. D. (2010). Large in-stream wood studies: a call for common metrics. Earth Surface Processes and Landforms, 625(March), n/a–n/a. http://doi.org/10.1002/esp.1966

Wohl, E., Bledsoe, B. P., Fausch, K. D., Kramer, N., Bestgen, K. R., & Gooseff, M. N. (2015). Management of Large Wood in Streams: An Overview and Proposed Framework for Hazard Evaluation. American Water Resources Association, 1482(In Press). http://doi.org/10.1017/CBO9781107415324.004

Xu, Y., Liu,X. (2016). 3D computational modeling of stream flow resistance due to large woody debris. Proc. River Flow 2016, St. Louis, USA, Constantinescu, Garcia & Hanes (Eds.), ISBN 978-1-315-64447-9: 2346-2353.

Yen, B. (2002). "Open Channel Flow Resistance." *J. Hydraul. Eng.*, 10.1061/(ASCE)0733-9429(2002)128:1(20), 20-39.

_____

Appendix

A. Description of the 2D numerical model Iber

The two dimensional numerical model for wood transport was developed and proposed by Ruiz-Villanueva et al (2014a) and it was implemented as a new module (*Iber-Wood*) into the 2D hydrodynamic software *Iber* (Corestein et al., 2010; Bladè et al., 2012). The software *Iber* was developed by the Flumen Research Institute (Universitat Politècnica de Catalunya (UPC), the International Center of Numerical Methods in Engineering (CIMNE), and the Water and Environment Engineering Group (GEAMA).

The model has three main computational modules: hydrodynamic, turbulence and sediment transport modules. It solves the 2D shallow water equations coupled with Exner sediment conservation equations and bed/suspended load transport equations. The transport of wood was implemented in the model by means of Lagrangian discretization, the hydraulic variables calculated with the hydrodynamic module are used to update the position and velocity of the logs at every time step. The logs are modelled as cylinder with no roots and no branches.

The solving method is the finite volume method (FVM) with high-resolution (second order) extension of Roe's upwind scheme. The *Iber* interface is based on the pre-process and post-process software GID, developed by CIMNE. The entire workflow for the numerical simulation can be defined as:

- define the geometry of the domain: it can be done by generating the geometry using GiD or importing it from another software (e.g., CAD or GIS);
- define initial and boundary conditions to the geometry and or calculation mesh model generate the calculation mesh;
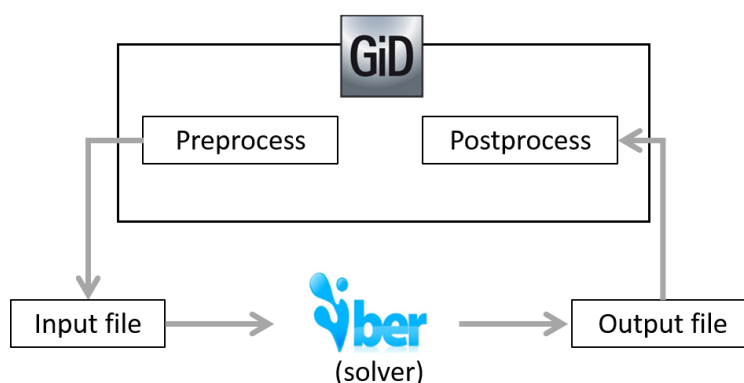- run the calculation;
- analyse the results.

Figure A.1 Scheme of the interface Iber-Gid

A1. The governing equations for wood transport

From the balance of the forces acting on a wood in water, as described in Chapter 3 , derives the threshold velocity for wood incipient motion (U_{lim}).

Ruiz-Villanueva et al. (2014a) used the definition of Mazzorana et al. (2011) for the moving log velocity:

$$U_{log} = (1 - C^*) \cdot U$$

<div align="right">(A-1)</div>

In which C^* is the transport inhibition parameter ($C^*= 0$ for log floating condition; $C^*= 1$ for resting condition; $C^* = 1 - (h/D_{log})$ for sliding/rolling condition).

The authors modified the parameter C^* introducing the relative flow velocity U_r:

$$U_r = (U - U_{log})$$

<div align="right">(A-2)</div>

The   (A-2) becomes:

$$U_{log} = U - U_{lim}$$

<div align="right">(A-3)</div>

In floating conditions, when the log density is about the water density and the water depth is higher than the log diameter and the submerged log diameter, $U_{lim}=0$ and $U_{log} = U$ and the log is transported with the same velocity of the flow (Haga et al., 2002; Bladè et al., 2016). The assumption is confirmed also by field measurements in the Ain River in France during a flood event by MacVicar and Piegay (2012). They compared the surface flow velocity, both measured using the Large Scale Particle Image Velocimetry (LSPIV) and computed with numerical model, with the floating wood velocity, measured with the video monitoring technique, showing that wood velocity and surface water velocity are very close.

In this case, the assumption $U_{log} = U$ is valid for the log centre because if this condition was applied also to both extremities of the log, the log orientation would not change (Bladè et al., 2016).

Determined the log velocity and the water velocity is possible to calculate the position of the log centre at every time step $x_{log}^{cm} = (x_{log\_t1}^{cm}, x_{log\_t2}^{cm})$, and the final position:

$$x_{log}'^{cm} = x_{log}^{cm} + \Delta t \cdot u_{log}^{cm}$$

<div align="right">(A-4)</div>

in which $u_{log}^{cm} = (u_{log\_t1}^{cm}, u_{log\_t2}^{cm})$ is the log center velocity in flow direction with value U_{log}.

The log centre velocity allows the calculation of flow velocity at the ends of log (1 and 2) as follows:

$$u^{1,2} = u^{cm} + \frac{\partial u}{\partial x} \cdot (x_{log}^{1,2} - x_{log}^{cm})$$

<div align="right">(A-5)</div>

in which u^{cm} is the flow velocity at the log center, $\frac{\partial u}{\partial x}$ is the flow velocity gradient and $(x_{log}^{1,2} - x_{log}^{cm})$ is the position of the log centre (x_{log}^{cm}) respect to the log ends ($x_{log}^{1,2}$).

Then the model calculates the new position of the log ends:

_____

$$x'^{1,2}_{log} = x^{1,2}_{log} + \Delta t \cdot u^{1,2}$$

$$(A\text{-}6)$$

and the new value of the log orientation:

$$\theta' = \tan^{-1}\left(\frac{x'^2_{log\_t2} - x'^1_{log\_t2}}{x'^2_{log\_t1} - x'^1_{log\_t1}}\right)$$

$$(A\text{-}7)$$

Figure A.2 contains all the steps and equations involved in the wood transport module developed by Ruiz-Villanueva et al. (2014a) and implemented in the two-dimensional numerical model "*Iber*".
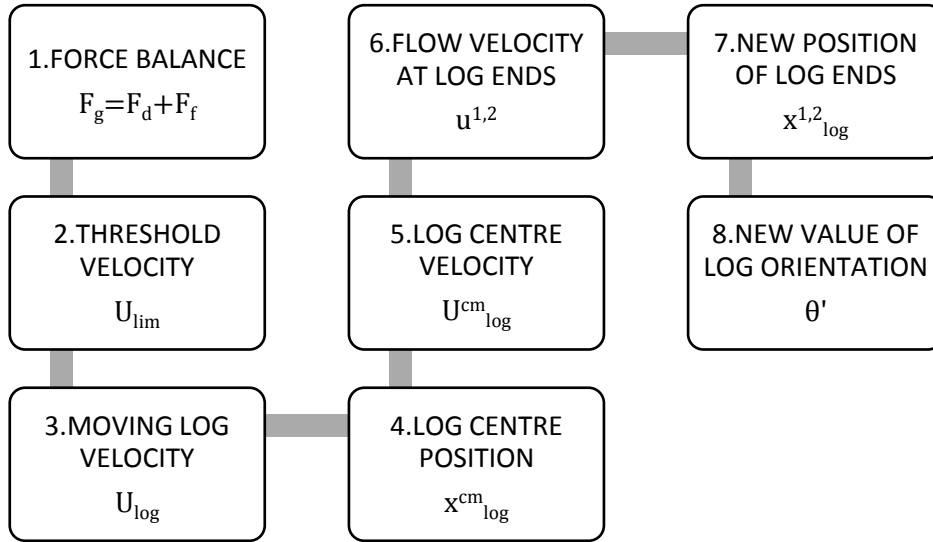
Figure A.2 Scheme of the governing equation of the wood transport module implemented in the hydrodynamic software "Iber".

The dynamic approach is based on Newton's second law and takes into account, in the calculation of log velocity, the log acceleration (based on acting forces on a piece of wood in waterstream; Bladè et al., 2016):

$$a_{log} = \frac{F_g + F_d + F_f}{\rho_{log} \cdot L_{log} \cdot A_{log}}$$

$$(A\text{-}8)$$

And then the log centre velocity and position at time step n+1 are:

$$U^{n+1}_{log} = U^n_{log} + \Delta t \cdot a_{log}$$

$$(A\text{-}9)$$

$$x^{n+1}_{log} = x^n_{log} + \Delta t \cdot U^n_{log} + \frac{1}{2} a_{log} \cdot \Delta t^2$$

$$(A\text{-}10)$$

In order to take into account the effect that wood has on hydrodynamics, the drag force is introduced as an additional shear stress term at every finite volume in the Saint Venant equations:

$$\tau_{wood,i} = \frac{\sum_{\log s} F_d}{A_i}$$
(A-11)

F_d is the drag force obtained from (3-8), A_i is the area of the mesh element i.

The model calculates the interaction between logs and between the log and the channel boundaries, as well. In the first case when two pieces of wood i and j collide, they move with a different velocity calculated from the initial velocity of each piece of wood.

The velocity of the mass centre of the collided logs is:

$$\left(u_{log}\right)_{i+j}^{cm} = \frac{m_i\left(u_{log}\right)^i + m_j\left(u_{log}\right)^j}{m_i + m_j}$$
(A-12)

m_i and m_j are the mass of logs i and j.

After collapse each log acquires a different velocity calculated as:

$$\left(u'_{log}\right)^{i,j} = (1 + e) \cdot \left(u_{log}\right)_{i+j}^{cm} - e \cdot \left(u_{log}\right)^{i,j}$$
(A-13)

in which $\left(u_{log}\right)^{i,j}$ is the initial log velocity, and e is the restitution coefficient that the model assumes to be equal to 1 for elastic interaction.

When a log bumps into the bank or channel boundary, its movement depends on incidence angle between the log and the boundary (σ_{cr}). This angle is fixed by modeller equal to 0.78 radians: when the incidence angle is higher than the fixed value, the log bounces off and changes his direction (Figure A.3, b); when the incidence angle is lower than the fixed value, the log floats parallel to the flow direction (Figure A.3, a). In addition to floating and bouncing a log may be also anchored to a bank, in this case the submerged area is lower and the driving forces acting on the log decrease.

The model calculates the log ends position at every time step and when a log end is outside the channel, it is positioned inside.
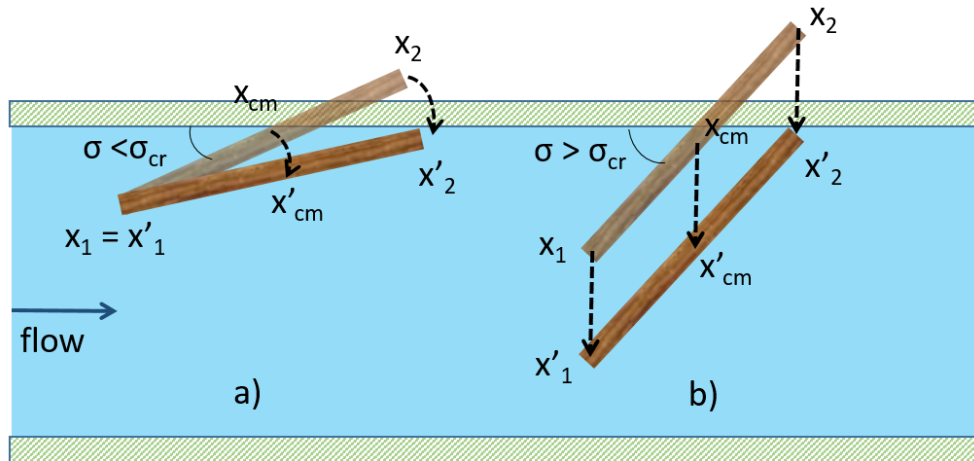
_____

Figure A.3 Schematization of the interaction between the log and the channel wall in case of sliding (a) and bouncing (b) and recalculation of log centre position as computed in 2D numerical model Iber.

The numerical model has been validated through flume experiments (Ruiz-Villanueva et al., 2014a) in a rectangular channel 20 m long and 0.6 m wide, with lateral constrictions and central obstacles and horizontal slope. The results showed a correlation higher than 70% between observed and simulated log trajectories and velocities, for all the channel geometries reproduced. The model was also tested in combination with field observations for analysing the preferential sites for wood deposition in the Czarny Dunajec River, Polish Carpathians (Ruiz-Villanueva et al., 2015), and the most critical wood transport condition for the arch bridge clogging in the Arroyo Cabrera stream, in the Spanish Central System (Ruiz-Villanueva et al., 2013).

B. Description of the numerical model Flow-3D

Flow-3D is a Computation Fluid Dynamics software (CFD) based on Finite Volume Method (FVM) to solve the full Reynolds Averaged Navier-Stokes (RANS) equations of fluid motion in Cartesian coordinates (Flow Science, Inc., 2014). The FVM guarantees the conservation of the mass and the energy. FLOW-3D discretizes the space with a grid of rectangular elements in which average values of flow variables can be defined. The scalar quantities are calculated at the centre of each cell whereas vectors and tensors are calculated at the faces of each cell, as shown in Figure B.1.

The turbulence closure model for the RANS equations selected for the current tests was the RNG model that is known to describe the low intensities turbulent flow and flow having strong shear regions (Flow Science, Inc. 2014).
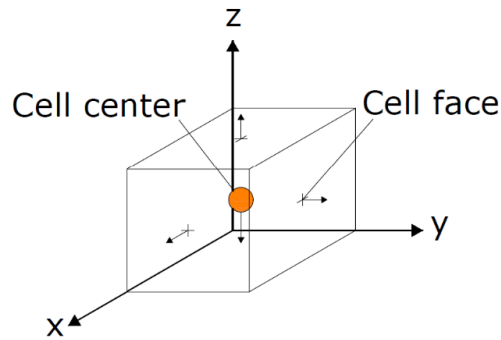
Figure B.1 Location of variables in a grid cell.

B1. Geometry: FAVOR^{TM} Technique

The space is discretized with a grid of rectangular elements in which the flow variables are calculated.

Flow 3D uses a particular technique for modelling solid geometric objects called FAVOR^{TM} (Fractional Area/Volume Obstacle Representation) that consists in incorporating the effects of geometry into the governing equations through the fractional areas (A_x, A_y, A_z) and the fractional volume (V_F) open to flow. The fractional areas are defined as the ratio between the area of the faces open to flow and the area of the cell faces. The fractional volume is the ratio between the portion of the cell volume occupied by the flow and the total volume of the cell.

A zero value of the volume fraction or the area fractions indicates a region defining an obstacle, while a value of one indicates a fluid region.

The preprocessor generates area fractions for each cell face in the grid by determining which corners of the face are inside of a defined geometry. If all four corners of a cell face are inside the geometry, then the entire face is defined to be within the geometry.

Similarly, if all corners lie outside, then the entire face is assumed to be outside the geometry. When some face corners are inside a geometry and some are outside, the intersection of the geometry with face edges are computed. Area fractions are then computed from these intersection points assuming straight-line connections between intersection points within the face. The straight-line assumption introduces a small error in the fractional area when the geometry boundary is curved inside the cell. The approximation is consistent with the other assumptions in the development of the equations and improves, as the grid resolution is refined.
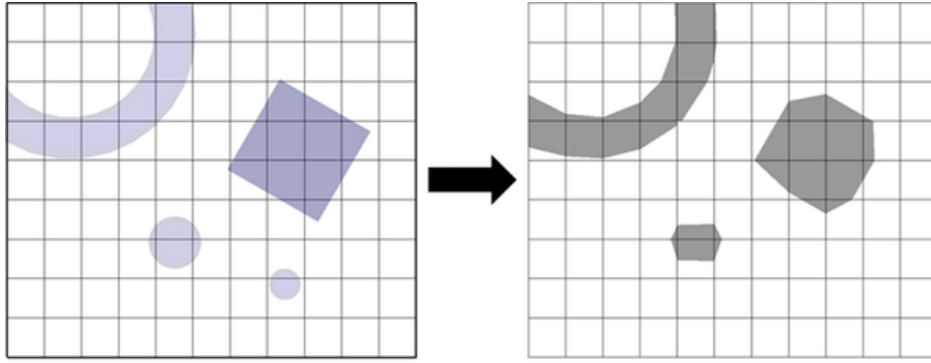
_____

Figure B.2 Real geometry (on the left) and the same geometry created by the model with the FAVOR^{TM} function (on the right) (source: Flow Science, Inc. 2014).

An object that is smaller than the cell size or that does not include a corner is not determined (as the small circle in Figure B.2 B.2). For this reason, the mesh size is fundamental for improving the geometric representation and the solution of the flow governing equations.

For modelling the free surface, Flow-3D implements a technique called TruVOF that consists in defining a function F whose value is unity at any point occupied by fluid and zero otherwise. In particular, a unit value of F would correspond to a cell full of fluid, while a zero value indicates that the cell contains no fluid; cells with value between zero and one must then contain a free surface (Hirt et al., 1981) (Figure B.3, on left).
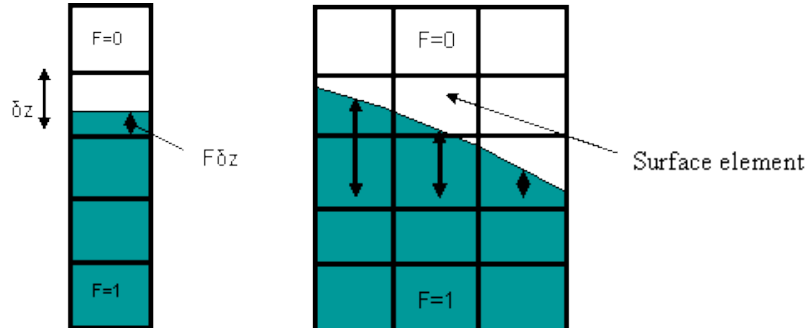

Figure B.3 Surface tracking in 1D column of elements (on left) and 2D grid of elements (on right) (source: Flow Science, Inc. 2014).

In 2D and 3D cases, the computation of the location of the surface is a little more complicated than the 1D case because there is a continuous range of possible surface orientations but the basic idea is the same. In two-dimensions, it is first necessary to find the approximate orientation of the surface by testing the neighbouring elements. Local heights of the surface are computed in element columns that lie in the approximate normal direction. For the two-dimensional case in Figure B.3 these heights are indicated by arrows. Finally, the height in the column containing the surface element gives the location of the surface in that element, while the other two heights can be used to compute the local surface slope and surface curvature. In three-dimensions, the same procedure is used although column heights must be evaluated for nine columns around the surface element.

B2. Wood modelling: General Moving Object (GMO)

A piece of wood is modelled as a General Moving Object (GMO). The description of the main characteristics and equations for GMO are provided in the FLOW-3D User Manual Release 11.0.3.

A general moving object (GMO) is a rigid body under any type of physical motion, which is either dynamically coupled with fluid flow or user-prescribed. It can move with six degrees of freedom (DOF) or rotate about a fixed point or a fixed axis. The GMO model allows users to have multiple moving objects in one problem, and each moving object can have any independently defined type of motion.

At each time step, the hydraulic force and torque due to pressure and shear stress are calculated, and equations of motion are solved for the moving objects under coupled motion with consideration of hydraulic, gravitational and control forces and torques. Source terms are added in the continuity equation to account for the effect of moving objects to displace fluid.

Two numerical options for the coupling of fluid flow and GMO motion are available: an explicit and an implicit method. In the former, fluid and GMO motions of each time step are calculated using the force and velocity data from the previous time step. In the implicit method these are calculated iteratively.

The GMO model also includes the capability to simulate rigid body collisions. Collisions are assumed instantaneous.

They are allowed to occur between rigid bodies (one of which must be moving) and between rigid bodies and wall/symmetry boundaries of the computational domain. Depending on the value of Stronge's restitution coefficient, a collision can be perfectly elastic, partially elastic or completely plastic. Friction at the point of contact is also allowed to exist during collision. There can be relative sliding between two colliding bodies at their contact point and the speed and direction of sliding can vary throughout the collision process.

A body system (x0, y0, z0) is set up for each moving object with its coordinate axes parallel to those of the space system at time t=0. If an object motion has six DOF, the origin of the body system is set at the object mass centre G. The body system is fixed on the moving object and experiences the same translation and rotation as the moving object. Coordinate transformation between the space system (x, y, z) and the body system (x', y', z') is:

$$x_S = [R] \cdot x_b + x_G \qquad\qquad (B\text{-}1)$$

in which:
- x_S and x_b are position vectors of a point in space and body systems, respectively;
- x_G is position vector of mass centre in space system;
- $[R]$ is an orthogonal coordinate transformation tensor.

For a space vector A, transformation between space and body systems is:

$$A_S = [R] \cdot A_b \qquad\qquad (B\text{-}2)$$

_____

in which:
- A_S and A_b denote expressions of A in space and body systems, respectively;
- $[R]$ is calculated by solving:

$$\frac{d[R]}{dt} = [\Omega] \cdot [R] \tag{B-3}$$

in which:

$$[\Omega] = \begin{bmatrix} 0 & -\Omega_z & \Omega_y \\ \Omega_z & 0 & -\Omega_x \\ -\Omega_y & \Omega_x & 0 \end{bmatrix} \tag{B-4}$$

$\Omega_x, \Omega_y, \Omega_z$ are x, y and z components, respectively, of the object's angular velocity in space system.

Velocity of any point on a rigid body (V_P) is equal to the velocity of an arbitrarily selected base point on the object (it is convenient to select the object mass centre V_G) plus velocity due to rotation about the base point:

$$V_P = V_G + \omega \times r_{P/G} \tag{B-5}$$

in which $r_{P/G}$ is the distance vector from G to P. The first term on the right-hand side of Eq. (B-5) represents translation of the mass centre, and the second term represents rotation about the mass centre.

Equations of motion governing the two separate motions are:

$$F = m\frac{dV_G}{dt} \tag{B-6}$$

And

$$T_G = [J] \cdot \frac{d\omega}{dt} + \omega \times ([J] \cdot \omega) \tag{B-7}$$

respectively, where:
- F is the total force;
- m is rigid body mass;
- T_G is the total torque about G;
- $[J]$ is moment of inertia tensor in the body system ("inertia tensor").

B3. Wall effects

Depending on the non-dimensional normal distance from the solid surface (y^+) (sometime called viscous length) in relation to dimensionless velocity u^+ is possible to estimate the height (thickness) of the boundary layer regions normal to the solid surface (Figure B.4). These quantities are represented through the following equations:

$$y^+ = \frac{u_\tau \cdot y \cdot \rho_f}{\mu_f} \qquad\qquad (B\text{-}8)$$

$$u_\tau = \sqrt{\frac{\tau_w}{\rho_f}} \qquad\qquad (B\text{-}9)$$

$$u^+ = \frac{u}{u_\tau} \qquad\qquad (B\text{-}10)$$

in which u_τ is the shear velocity, y is the normal distance from the solid, ρ_f is the fluid density, μ_f is the fluid dynamic viscosity, u is the flow velocity, τ_w is the shear stress velocity of the fluid.

Roughness has the dimensions of length, and is incorporated into the shear stress calculations by adding to the molecular viscosity the product of ($fluid\ density \cdot roughness \cdot relative\ velocity$), where $relative\ velocity$ means the difference between the local fluid velocity and the wall velocity (which is zero for stationary walls and components) (Flow Science, Inc. 2014). Flow-3D considers the solid surface as smooth by default that is the current case of the smooth surface of gravel particles. This methodology allows to account for the hydraulic resistance without changing the Manning's coefficient.
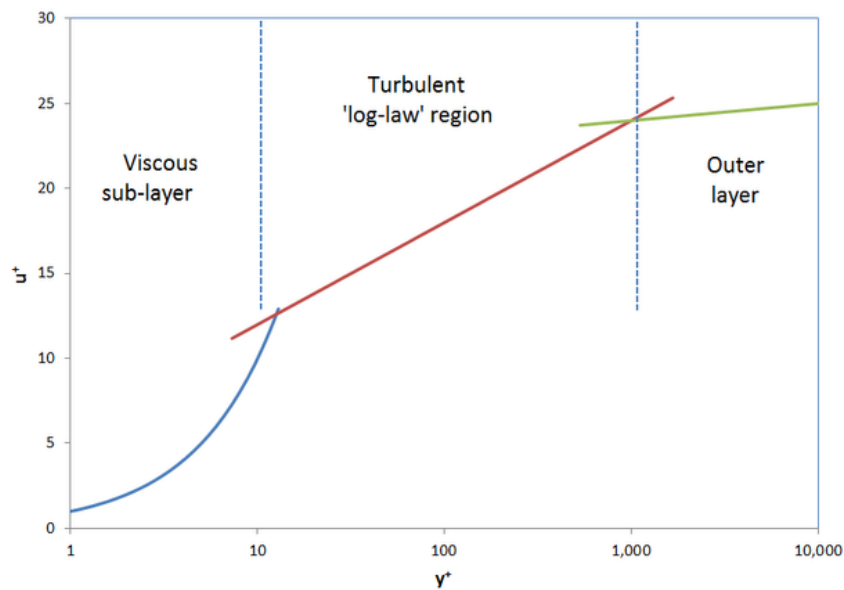

Figure B.4 Relationship that exists between the non-dimension normal distance from the wall (y+) and the dimensionless velocity (u+). Three zones are highlight: the viscous sub-layer, the turbulent log-law region and outer layer (source: Flow Science, Inc. 2014).